



TECH BRIEFS

NATIONAL AERONAUTICS AND SPACE ADMINISTRATION

-  **Technology Focus**
-  **Electronics/Computers**
-  **Software**
-  **Materials**
-  **Mechanics/Machinery**
-  **Manufacturing**
-  **Bio-Medical**
-  **Physical Sciences**
-  **Information Sciences**
-  **Books and Reports**

INTRODUCTION

Tech Briefs are short announcements of innovations originating from research and development activities of the National Aeronautics and Space Administration. They emphasize information considered likely to be transferable across industrial, regional, or disciplinary lines and are issued to encourage commercial application.

Availability of NASA Tech Briefs and TSPs

Requests for individual Tech Briefs or for Technical Support Packages (TSPs) announced herein should be addressed to

National Technology Transfer Center

Telephone No. (800) 678-6882 or via World Wide Web at www.nttc.edu

Please reference the control numbers appearing at the end of each Tech Brief. Information on NASA's Innovative Partnerships Program (IPP), its documents, and services is also available at the same facility or on the World Wide Web at <http://ipp.nasa.gov>.

Innovative Partnerships Offices are located at NASA field centers to provide technology-transfer access to industrial users. Inquiries can be made by contacting NASA field centers listed below.

NASA Field Centers and Program Offices

Ames Research Center

Lisa L. Lockyer
(650) 604-1754
lisa.l.lockyer@nasa.gov

Dryden Flight Research Center

Gregory Poteat
(661) 276-3872
greg.poteat@dfrc.nasa.gov

Glenn Research Center

Kathy Needham
(216) 433-2802
kathleen.k.needham@nasa.gov

Goddard Space Flight Center

Nona Cheeks
(301) 286-5810
nona.k.cheeks@nasa.gov

Jet Propulsion Laboratory

Ken Wolfenbarger
(818) 354-3821
james.k.wolfenbarger@jpl.nasa.gov

Johnson Space Center

Michele Brekke
(281) 483-4614
michele.a.brekke@nasa.gov

Kennedy Space Center

David R. Makufka
(321) 867-6227
david.r.makufka@nasa.gov

Langley Research Center

Martin Waszak
(757) 864-4015
martin.r.waszak@nasa.gov

Marshall Space Flight Center

Jim Dowdy
(256) 544-7604
jim.dowdy@msfc.nasa.gov

Stennis Space Center

John Bailey
(228) 688-1660
john.w.bailey@nasa.gov

Carl Ray, Program Executive

Small Business Innovation
Research (SBIR) & Small
Business Technology
Transfer (STTR) Programs
(202) 358-4652
carl.g.ray@nasa.gov

Doug Comstock, Director

Innovative Partnerships
Program Office
(202) 358-2560
doug.comstock@nasa.gov



TECH BRIEFS

NATIONAL AERONAUTICS AND SPACE ADMINISTRATION



5 Technology Focus: Composites & Coating

- 5 Nanotip Carpets as Antireflection Surfaces
- 6 Nano-Engineered Catalysts for Direct Methanol Fuel Cells
- 7 Capillography of Mats of Nanofibers
- 8 Directed Growth of Carbon Nanotubes Across Gaps



9 Electronics/Computers

- 9 High-Voltage, Asymmetric-Waveform Generator
- 9 Magic-T Junction Using Microstrip/Slotline Transitions
- 11 On-Wafer Measurement of a Silicon-Based CMOS VCO at 324 GHz
- 11 Group-III Nitride Field Emitters
- 12 HEMT Amplifiers and Equipment for Their On-Wafer Testing



15 Manufacturing & Prototyping

- 15 Thermal Spray Formation of Polymer Coatings
- 15 Improved Gas Filling and Sealing of an HC-PCF

17 Materials

- 17 Making More-Complex Molecules Using Superthermal Atom/Molecule Collisions
- 17 Nematic Cells for Digital Light Deflection
- 18 Improved Silica Aerogel Composite Materials



21 Mechanics/Machinery

- 21 Microgravity, Mesh-Crawling Legged Robots
- 21 Advanced Active-Magnetic-Bearing Thrust-Measurement System
- 22 Thermally Actuated Hydraulic Pumps
- 23 A New, Highly Improved Two-Cycle Engine
- 24 Flexible Structural-Health-Monitoring Sheets
- 24 Alignment Pins for Assembling and Disassembling Structures



27 Bio-Medical

- 27 Purifying Nucleic Acids From Samples of Extremely Low Biomass
- 27 Adjustable-Viewing-Angle Endoscopic Tool for Skull Base and Brain Surgery
- 28 UV-Resistant Non-Spore-Forming Bacteria From Spacecraft-Assembly Facilities



29 Physical Sciences

- 29 Hard-X-Ray/Soft- γ -Ray Imaging Sensor Assembly for Astronomy
- 29 Simplified Modeling of Oxidation of Hydrocarbons
- 30 Near-Field Spectroscopy With Nanoparticles Deposited by AFM
- 31 Light Collimator and Monitor for a Spectroradiometer
- 32 Hyperspectral Fluorescence and Reflectance Imaging Instrument
- 32 Improving the Optical Quality Factor of the WGM Resonator
- 33 Ultra-Stable Beacon Source for Laboratory Testing of Optical Tracking
- 34 Transmissive Diffractive Optical Element Solar Concentrators
- 35 Delaying Trains of Short Light Pulses in WGM Resonators



37 Information Sciences

- 37 Toward Better Modeling of Supercritical Turbulent Mixing
- 37 JPEG 2000 Encoding With Perceptual Distortion Control
- 38 Intelligent Integrated Health Management for a System of Systems
- 39 Delay Banking for Managing Air Traffic
- 40 Spline-Based Smoothing of Airfoil Curvatures
- 41 Reducing Spaceborne-Doppler-Radar Rainfall-Velocity Error



43 Books and Reports

- 43 Progress in Acoustic Transmission of Power Through Walls

- 43 Lightweight Carbon-Carbon High-Temperature Space Radiator
- 43 Stochastic Analysis of Orbital Lifetimes of Spacecraft



45 Software

- 45 Displaying CFD Solution Parameters on Arbitrary Cut Planes
- 45 Flow Solver for Incompressible 2-D Drive Cavity
- 45 Flow Solver for Incompressible Rectangular Domains
- 45 Simulating Avionics Upgrades to the Space Shuttles
- 46 Simulating the Phoenix Landing Radar System
- 46 Injecting Artificial Memory Errors Into a Running Computer Program
- 47 Fault-Tolerant, Multiple-Zone Temperature Control
- 47 Implementing a Digital Phasemeter in an FPGA
- 48 Post-Flight Estimation of Motion of Space Structures: Part 1
- 48 Post-Flight Estimation of Motion of Space Structures: Part 2
- 48 Simulating Operation of a Large Turbofan Engine
- 49 Automated Assistance for Designing Active Magnetic Bearings
- 49 Computational Simulation of a Water-Cooled Heat Pump
- 49 Computational Model of Heat Transfer on the ISS
- 50 Optimization of Angular-Momentum Biases of Reaction Wheels
- 50 Short- and Long-Term Propagation of Spacecraft Orbits
- 50 Monte Carlo Simulation To Estimate Likelihood of Direct Lightning Strikes
- 51 Adaptive MGS Phase Retrieval
- 51 Simulating the Gradually Deteriorating Performance of an RTG
- 52 Calculations for Calibration of a Mass Spectrometer
- 52 Predicting Boundary-Layer Transition on Space-Shuttle Re-Entry
- 53 2D/3D Synthetic Vision Navigation Display
- 54 Automated Camera Array Fine Calibration
- 54 Multichannel Networked Phasemeter Readout and Analysis
- 54 MISR Instrument Data Visualization
- 55 Platform for Postprocessing Waveform-Based NDE
- 56 Automatic Rock Detection and Mapping from HiRISE Imagery
- 56 Parallel Computing for the Computed-Tomography Imaging Spectrometer
- 56 Rock Segmentation Through Edge Regrouping
- 57 System for Continuous Delivery of MODIS Imagery to Internet Mapping Applications
- 58 Processing LiDAR Data To Predict Natural Hazards
- 58 Estimating Software-Development Costs With Greater Accuracy
- 59 DSN Array Simulator
- 59 Parametric-Studies and Data-Plotting Modules for the SOAP
- 60 Testing of Error-Correcting Sparse Permutation Channel Codes
- 60 Visual Target Tracking on the Mars Exploration Rovers
- 61 SPICE Module for the Satellite Orbit Analysis Program (SOAP)
- 62 Facilitating Analysis of Multiple Partial Data Streams
- 63 Mars Reconnaissance Orbiter Wrapper Script
- 63 Service-Oriented Architecture for NVO and TeraGrid Computing
- 64 Enhanced Reporting of Mars Exploration Rover Telemetry

This document was prepared under the sponsorship of the National Aeronautics and Space Administration. Neither the United States Government nor any person acting on behalf of the United States Government assumes any liability resulting from the use of the information contained in this document, or warrants that such use will be free from privately owned rights.



Technology Focus: Nano Materials & Manufacturing

Nanotip Carpets as Antireflection Surfaces

Reflectance less than 10^{-3} is readily achieved.

NASA's Jet Propulsion Laboratory, Pasadena, California

Carpetlike random arrays of metal-coated silicon nanotips have been shown to be effective as antireflection surfaces. Now undergoing development for incorporation into Sun sensors that would provide guidance for robotic exploratory vehicles on Mars, nanotip carpets of this type could also have many uses on Earth as antireflection surfaces in instruments that handle or detect ultraviolet, visible, or infrared light.

In the original Sun-sensor application, what is required is an array of 50- μm -diameter apertures on what is otherwise an opaque, minimally reflective surface, as needed to implement a miniature multiple-pinhole camera. The process for fabrication of an antireflection nanotip carpet for this application (see Figure 1) includes, and goes somewhat beyond, the process described in "A New Process for Fabricating Random Silicon Nanotips" (NPO-40123), *NASA Tech Briefs*, Vol. 28, No. 1 (November 2004), page 62. In the first step, which is not part of the previously reported process, photolithography is performed to deposit

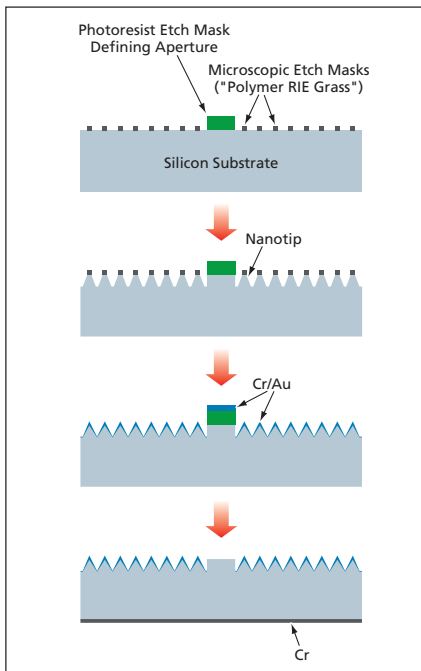
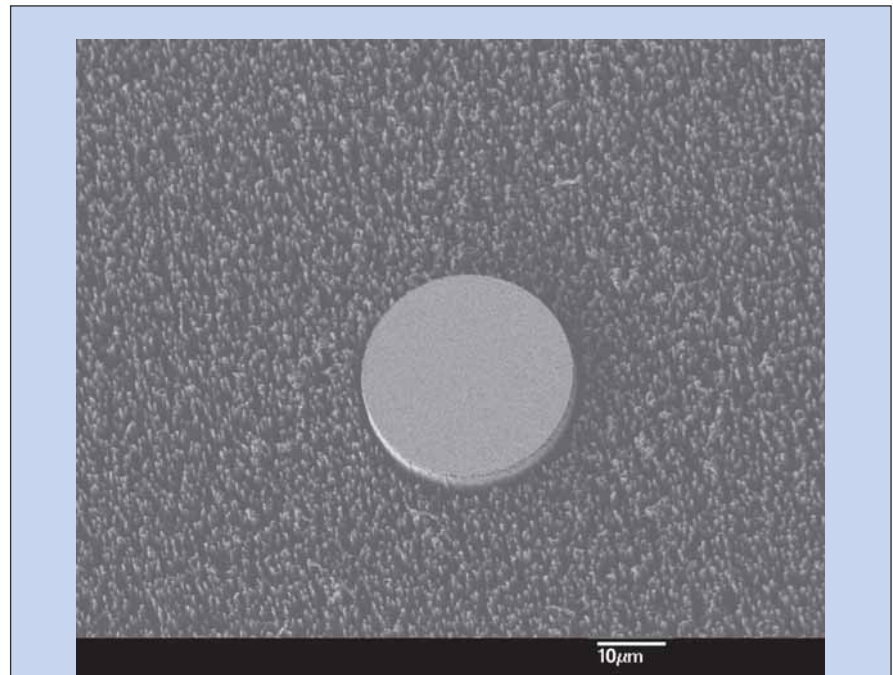
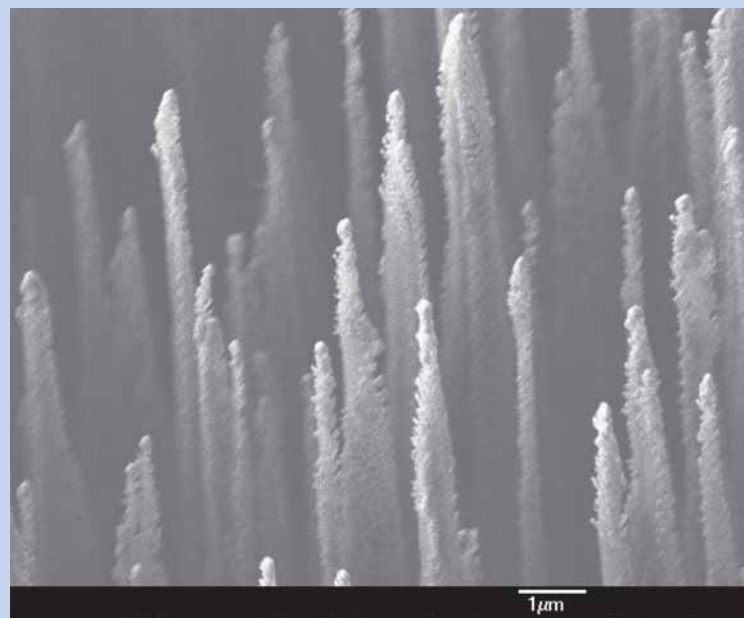


Figure 1. A Random Array of Nanotips is formed on the flat substrate surface surrounding an aperture. The nanotips are coated with Cr/Au to enhance absorption of light. The Cr layer on the rear surface serves as a light attenuator.



Nanotip Carpet Surrounding an Aperture



Enlarged Detail Showing Nanotips

Figure 2. The Antireflection Nanotip Carpet surrounding the aperture absorbs most of the incident light. The reflectance of the carpet at a wavelength of 1 μm was found to be 0.06 percent of that of an aluminum mirror.

etch masks to define the 50- μm apertures on a silicon substrate. In the second step, which is part of the previously reported process, the non-masked silicon area between the apertures is subjected to reactive ion etching (RIE) under a special combination of conditions that results in the growth of fluorine-based compounds in randomly distributed formations, known in the art as "polymer RIE grass," that have dimensions of the order of microns.

The polymer RIE grass formations serve as microscopic etch masks during the next step, in which deep reactive ion etching (DRIE) is performed. What remains after DRIE is the carpet of nano-

tips, which are high-aspect-ratio peaks, the tips of which have radii of the order of nanometers. Next, the nanotip array is evaporatively coated with Cr/Au to enhance the absorption of light (more specifically, infrared light in the Sun-sensor application). The photoresist etch masks protecting the apertures are then removed by dipping the substrate into acetone. Finally, for the Sun-sensor application, the back surface of the substrate is coated with a 57-nm-thick layer of Cr for attenuation of sunlight.

This work was done by Youngsam Bae, Sohrab Mobasser, Harish Manohara, and Choonsup Lee of Caltech for NASA's Jet

Propulsion Laboratory. Further information is contained in a TSP (see page 1).

In accordance with Public Law 96-517, the contractor has elected to retain title to this invention. Inquiries concerning rights for its commercial use should be addressed to:

*Innovative Technology Assets Management
JPL*

*Mail Stop 202-233
4800 Oak Grove Drive
Pasadena, CA 91109-8099
(818) 354-2240*

E-mail: iaoffice@jpl.nasa.gov

Refer to NPO-42592, volume and number of this NASA Tech Briefs issue, and the page number.

Nano-Engineered Catalysts for Direct Methanol Fuel Cells

Small particle sizes and large surface areas can be produced economically and consistently.

NASA's Jet Propulsion Laboratory, Pasadena, California

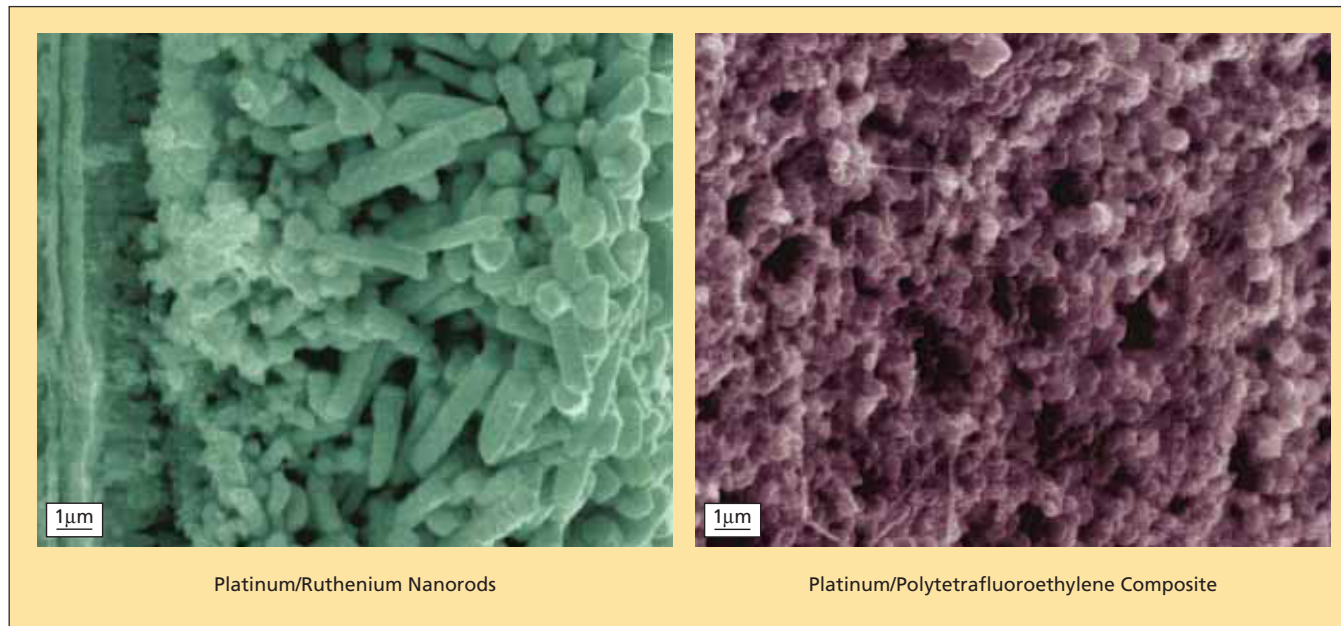
Nano-engineered catalysts, and a method of fabricating them, have been developed in a continuing effort to improve the performances of direct methanol fuel cells as candidate power sources to supplant primary and secondary batteries in a variety of portable electronic products. In order to realize the potential for high energy densities (as much as 1.5 W·h/g) of direct methanol fuel cells, it will be necessary to optimize the chemical compositions and geometric configurations of catalyst layers and electrode structures. High performance

can be achieved when catalyst particles and electrode structures have the necessary small feature sizes (typically of the order of nanometers), large surface areas, optimal metal compositions, high porosity, and hydrophobicity.

The present method involves electrodeposition of one or more catalytic metal(s) or a catalytic-metal/polytetrafluoroethylene nanocomposite on an alumina nanotemplate. The alumina nanotemplate is then dissolved, leaving the desired metal or metal/polytetrafluoroethylene-composite catalyst layer. Unlike some prior methods

of making fine metal catalysts, this method does not involve processing at elevated temperature; all processing can be done at room temperature. In addition, this method involves fewer steps and is more amenable to scaling up for mass production.

Alumina nanotemplates are porous alumina membranes that have been fabricated, variously, by anodizing either pure aluminum or aluminum that has been deposited on silicon by electron-beam evaporation. The diameters of the pores (7 to 300 nm), areal densities of



These Are Scanning Electron Micrographs of catalysts fabricated by the method described in the text. The platinum/ruthenium rods, about 0.2 μm wide and 1 μm long, were electrodeposited from a plating bath containing H_2PtCl_6 , K_2RuCl_5 , and H_2SO_4 . The platinum/polytetrafluoroethylene composite was electrodeposited from a solution containing H_2PtCl_6 , H_2SO_4 , CH_3OH , and suspended polytetrafluoroethylene nanoparticles having sizes from 0.1 to 0.2 μm .

pores (as much as $7 \times 10^{10} \text{ cm}^{-2}$), and lengths of pores (up to about 100 nm) can be tailored by selection of fabrication conditions.

In a given case, the catalytic metal, catalytic metal alloy, or catalytic-metal/polytetrafluoroethylene composite is electrodeposited in the pores of the alumina nanotemplate. The dimensions of the pores, together with the electrodeposition conditions, determine the sizes and surface areas of the catalytic particles. Hence, the small features and large surface areas of the porosity translate to the desired small particle size and large surface area of the catalyst (see figure).

When polytetrafluoroethylene is included, it is for the purpose of imparting hydrophobicity in order to prevent water from impeding the desired diffusion of gases through the catalyst layer. To incorporate polytetrafluoroethylene into a catalytic-metal/polytetrafluoroethylene nanocomposite, one suspends polytetrafluoroethylene nanoparticles in the electrodeposition solution. The polytetrafluoroethylene content can be varied to obtain the desired degree of hydrophobicity and permeability by gas.

This work was done by Nosang Myung, Sekharipuram Narayanan, and Dean Wiberg of Caltech for NASA's Jet Propulsion Labora-

tory. Further information is contained in a TSP (see page 1).

In accordance with Public Law 96-517, the contractor has elected to retain title to this invention. Inquiries concerning rights for its commercial use should be addressed to:

*Innovative Technology Assets Management
JPL*

*Mail Stop 202-233
4800 Oak Grove Drive
Pasadena, CA 91109-8099
(818) 354-2240*

E-mail: iaoffice@jpl.nasa.gov

Refer to NPO-30840, volume and number of this NASA Tech Briefs issue, and the page number.

Capillography of Mats of Nanofibers

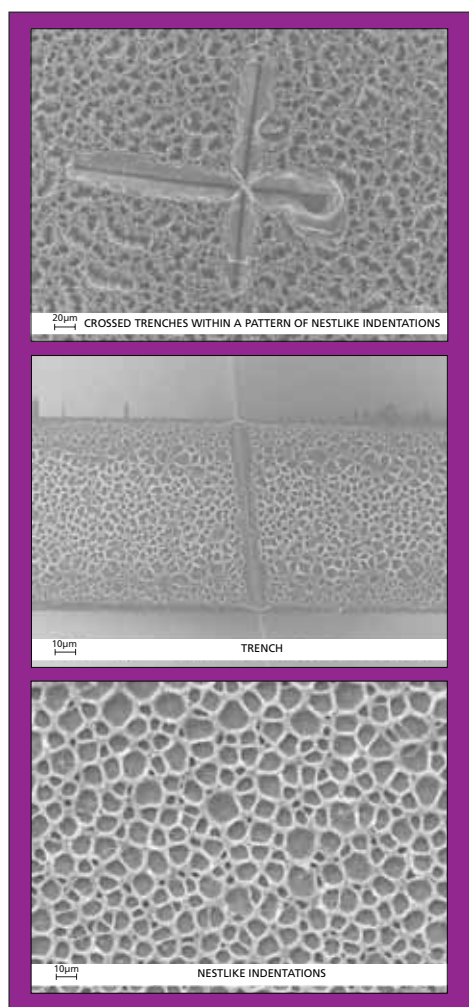
These mats can be the basis of small devices and instruments.

NASA's Jet Propulsion Laboratory, Pasadena, California

Capillography (from the Latin capillus, "hair", and the Greek graphein, "to write") is a recently conceived technique for forming mats of nanofibers into useful patterns. The concept was inspired by experiments on carpetlike mats of multiwalled carbon nanotubes. Capillography may have the potential to be a less-expensive, less-time-consuming alternative to electron-beam lithography as a means of nanoscale patterning for the fabrication of small devices and instruments.

In capillography, one exploits the lateral capillary forces exerted on small objects that pierce the surface of a liquid. If the small objects are identical, then the forces are always attractive. Two examples of the effects of such forces are the agglomeration of small particles floating on the surface of a pond and the drawing together of hairs of a wet paintbrush upon removal of the brush from water. Because nanoscale objects brought into contact remain stuck together indefinitely due to Van der Waals forces, patterns formed by capillography remain even upon removal of the liquid.

For the experiments on the mats of carbon nanotubes, a surfactant solution capable of wetting carbon nanotubes (which are ultra-hydrophobic) was prepared. The mats were wetted with the solution, then dried. Once the mats were dry, it was found that the nanotubes had become ordered into various patterns, including nestlike in-



These **Scanning Electron Micrographs** show representative patterns formed in mats of multiwalled carbon nanotubes that were wetted with a surfactant solution and then dried.

dentations, trenches, and various combinations thereof (see figure).

It may be possible to exploit such ordering effects through controlled wetting and drying of designated portions of mats of carbon nanotubes (and, perhaps, mats of nanofibers of other materials) to obtain patterns similar to those heretofore formed by use of electron-beam lithography. For making patterns that include nestlike indentations, it has been conjectured that it could be possible to control the nesting processes by use of electrostatic fields. Further research is needed to understand the physics of the patterning processes in order to develop capabilities to control patterns formed in capillography.

This work was done by Flavio Noca, Elijah Sansom, Jijie Zhou, and Mory Gharib of Caltech for NASA's Jet Propulsion Laboratory. For further information is contained in a TSP (see page 1).

In accordance with Public Law 96-517, the contractor has elected to retain title to this invention. Inquiries concerning rights for its commercial use should be addressed to:

*Innovative Technology Assets Management
JPL*

*Mail Stop 202-233
4800 Oak Grove Drive
Pasadena, CA 91109-8099
(818) 354-2240*

E-mail: iaoffice@jpl.nasa.gov

Refer to NPO-40980, volume and number of this NASA Tech Briefs issue, and the page number.

Directed Growth of Carbon Nanotubes Across Gaps

Single-walled carbon nanotubes grow aligned along applied electric fields.

Ames Research Center, Moffett Field, California

An experiment has shown that when single-walled carbon nanotubes (SWNTs) are grown by chemical vapor deposition in the presence of an electric field of suitable strength, the nanotubes become aligned along the electric field. In an important class of contemplated applications, one would exploit this finding in fabricating nanotube transistors; one would grow SWNTs across gaps between electrodes that would serve, subsequently, as source and drain contacts during operation of the transistors.

In preparation for the experiment, a multilayer catalyst comprising a 20-nm-thick underlayer of iridium (platinum group), a 1-nm-thick middle layer of iron, and a 0.2-nm-thick outer layer of

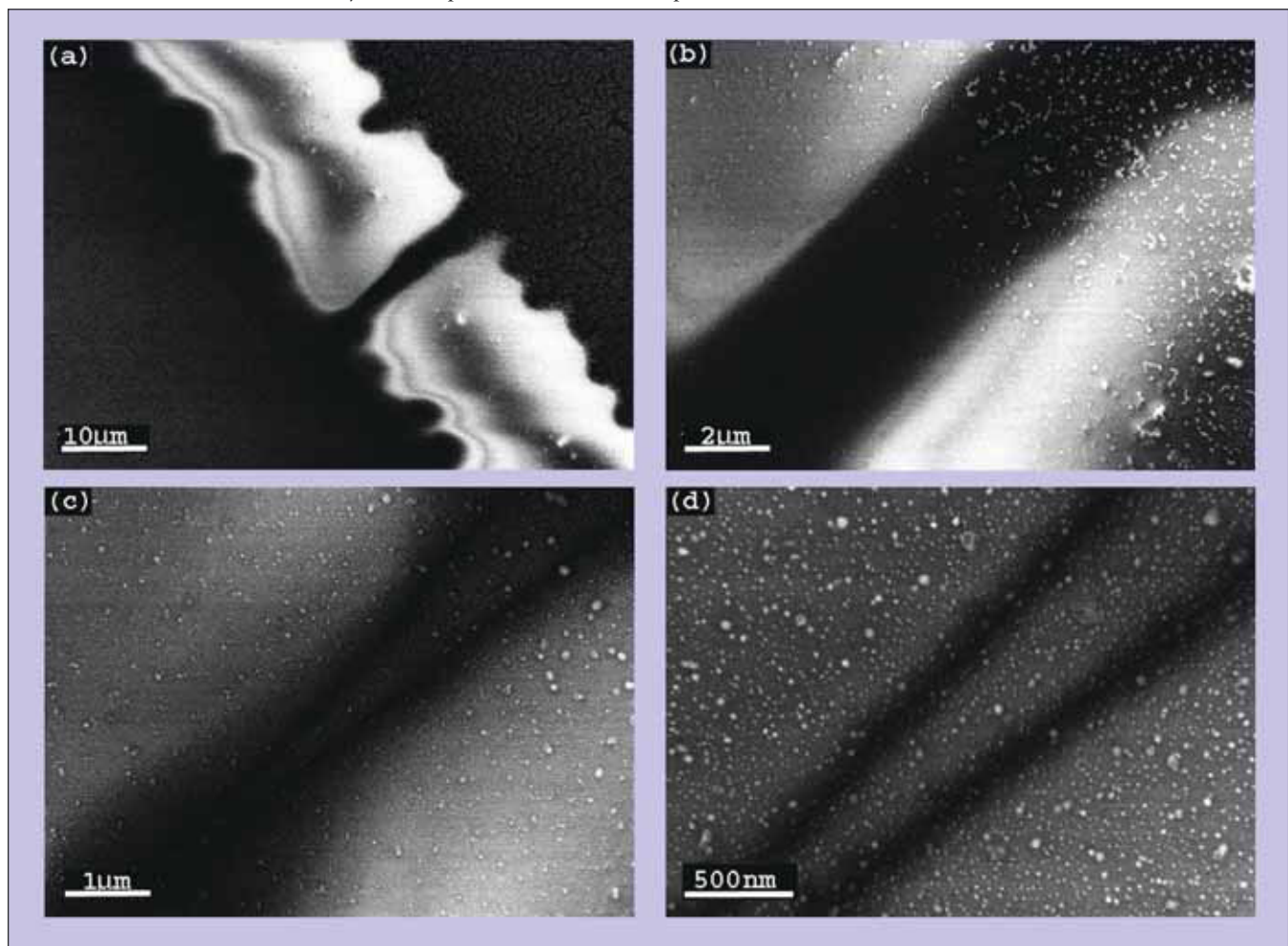
molybdenum was ion-beam sputtered onto a quartz substrate. A 25- μm -diameter iron wire was used as a shadow mask during the sputtering to create a 25- μm gap in the catalyst. Then electrical leads were connected to the catalyst areas separated by the gap so that these catalyst areas would also serve as electrodes.

The substrate as thus prepared was placed in a growth chamber that consisted of a quartz tube of 1-in. (2.54-cm) diameter enclosed in a furnace. SWNTs of acceptably high quantity and quality were grown in 10 minutes with methane at atmospheric pressure flowing through the chamber at a rate of 1,000 standard cubic centimeters per minute at a temperature of 900°C. To prevent oxidation

of the SWNTs, the chamber was purged with 99.999-percent pure argon before and after growth, and the chamber was cooled to <300°C before opening it to the atmosphere after growth.

When no voltage was applied across the gap, the SWNTs grew in random directions extending out from the edges of the catalyst at the gap. When a potential of 10 V was applied between the catalyst/electrode areas to create an electric field across the gap, the SWNTs grew across the gap, as shown in the figure.

This work was done by Lance DeZeit and Meyya Meyyapan of Ames Research Center and Ramsey Stevens and Cathien Nguyen of Elovit Corporation. Further information is contained in a TSP (see page 1). ARC-14985-1



These Scanning Electron Micrographs show SWNTs that were grown to bridge a 25- μm gap between two catalyst/electrode areas. Progressively higher magnification of one of the bridges reveals that it consists of two closely spaced SWNTs.



High-Voltage, Asymmetric-Waveform Generator

This circuit would be optimized for a capacitive load.

NASA's Jet Propulsion Laboratory, Pasadena, California

The shapes of waveforms generated by commercially available analytical separation devices, such as some types of mass spectrometers and differential mobility spectrometers are, in general, inadequate and result in resolution degradation in output spectra. A waveform generator was designed that would be able to circumvent these shortcomings. It is capable of generating an asymmetric waveform, having a peak amplitude as large as 2 kV and frequency of several megahertz, which can be applied to a capacitive load. In the original intended application, the capacitive load would consist of the drift plates in a differential-mobility spectrometer. The main advantage to be gained by developing the proposed generator is that the shape of the waveform is made nearly optimum for various analytical devices requiring asymmetric-waveform such as differential-mobility spectrometers. In addition, this waveform generator could easily be adjusted to modify the waveform in accordance with changed operational requirements for differential-mobility spectrometers.

The capacitive nature of the load is an important consideration in the de-

sign of the proposed waveform generator. For example, the design provision for shaping the output waveform is based partly on the principle that (1) the potential (V) on a capacitor is given by $V = q/C$, where C is the capacitance

The proposed waveform generator would comprise four functional blocks: a sine-wave generator, a buffer, a voltage shifter, and a high-voltage switch (see Figure 1). The sine-wave generator would include a pair of operational amplifiers in a feedback configuration, the parameters of which would be chosen to obtain a sinusoidal timing signal of the desired frequency. The buffer would introduce a slight delay (≈ 20 ns) but would otherwise leave the fundamental timing signal unchanged. The buffered timing signal would be fed as input to the level shifter. The output of the level shifter would serve as a timing and control signal for the high-voltage switch, causing the switch to alternately be (1) opened, allowing the capacitive load to be charged from a high-voltage DC power supply; then (2) closed to discharge the capacitive load to ground. Hence, the output waveform would closely approximate a series of exponential charging and discharging curves (see Figure 2).

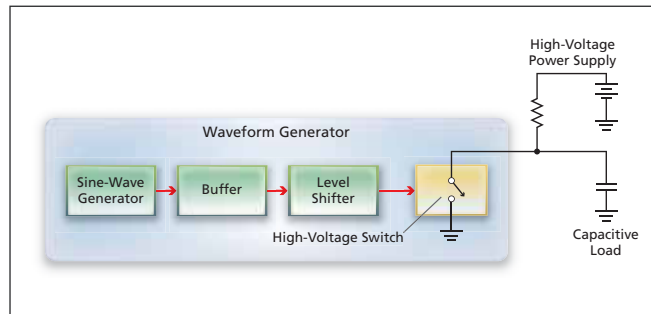


Figure 1. The **Waveform Generator** would cause the capacitive load to be alternately (1) charged from the high-voltage power supply, then (2) discharged to ground.

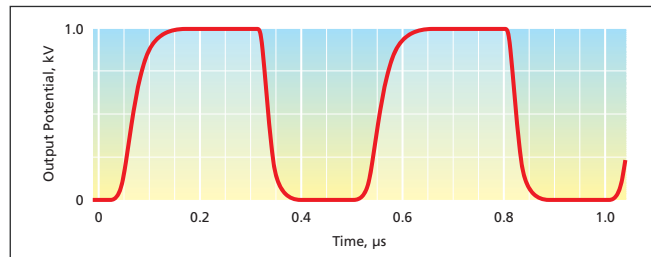


Figure 2. This **Typical Output Waveform** of the proposed waveform generator was simulated, assuming a design supply potential of 1 kV and a design frequency of 2 MHz.

and q is the charge stored in the capacitor; and, hence (2) the rate of increase or decrease of the potential is similarly proportional to the charging or discharging current.

This work was done by Luther W. Beegle, Tuan A. Duong, Vu A. Duong, and Isik Kanik of Caltech for NASA's Jet Propulsion Laboratory. Further information is contained in a TSP (see page 1). NPO-45665

Magic-T Junction Using Microstrip/Slotline Transitions

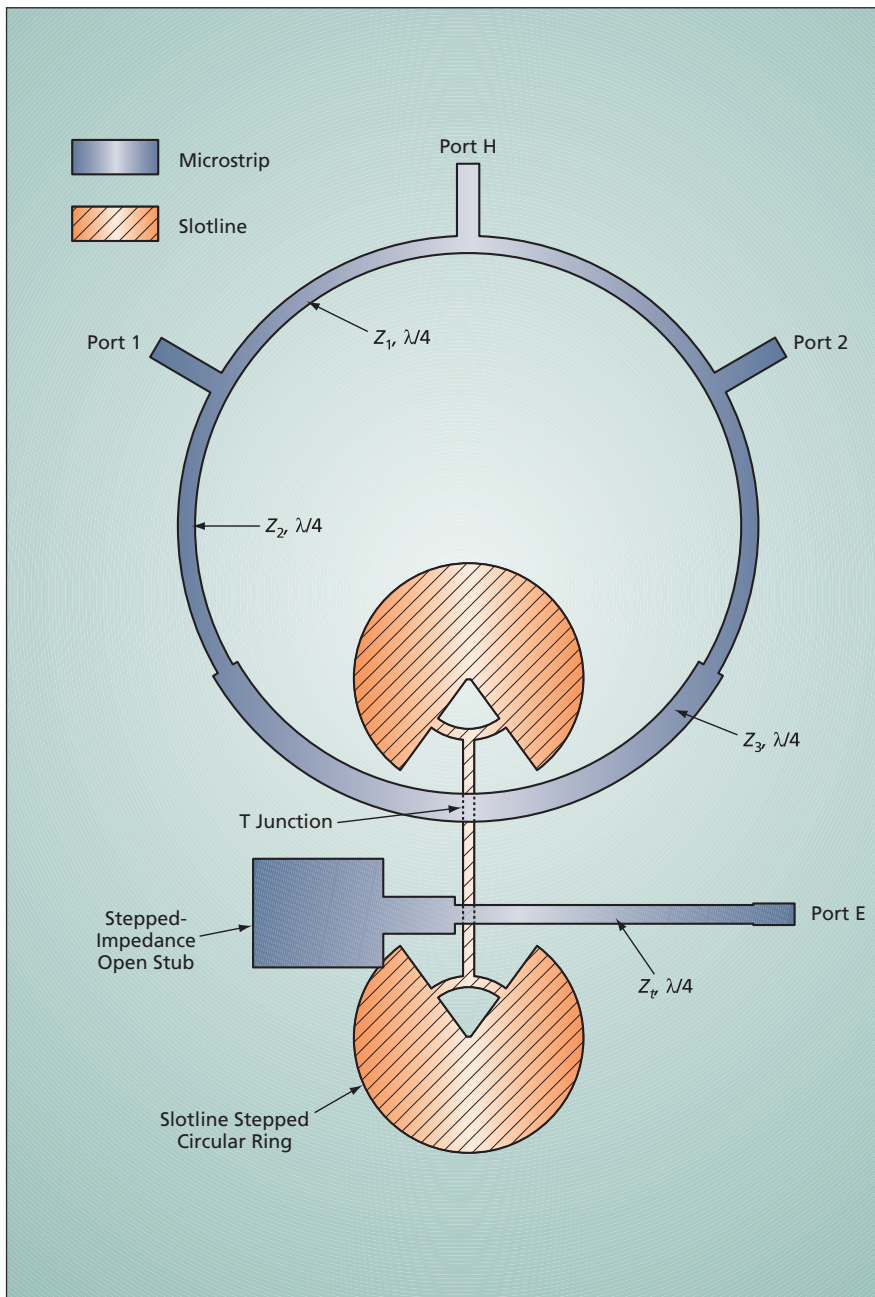
Economical broadband junctions have potential utility in diverse microwave systems.

Goddard Space Flight Center, Greenbelt, Maryland

An improved broadband planar magic-T junction that incorporates microstrip/slotline transitions has been developed. In comparison with a prior broadband magic-T junction incorporating microstrip/slotline transitions,

this junction offers superior broadband performance. In addition, because this junction is geometrically simpler and its performance is less affected by fabrication tolerances, the benefits of the improved design can be

realized at lower fabrication cost. There are potential uses for junctions like this one in commercial microwave communication receivers, radar and polarimeter systems, and industrial microwave instrumentation.



The Improved Broad-Band Planar Magic-T Junction incorporates a unique microstrip ring structure, microstrip/slotline transitions, and impedance-matching $\lambda/4$ transmission-line sections.

A magic-T junction is a four-port waveguide junction consisting of a combination of an H-type and an E-type junction. An E-type junction is so named because it includes a junction arm that extends from a main waveguide in the same direction as that of the electric (E) field in the waveguide. An H-type junction is so named because it includes a junction arm parallel to the magnetic (H) field in a main waveguide. A magic-T junction includes two input ports (here labeled 1 and 2, respectively) and two output ports (here labeled E and H, respectively). In an ideal case, (1) a magic-T

junction is lossless, (2) the input signals add (that is, they combine in phase with each other) at port H, and (3) the input signals subtract (that is, they combine in opposite phase) at port E.

The prior junction over which the present junction is an improvement affords in-phase-combining characterized by a broadband frequency response, and features a small slotline area to minimize in-band loss. However, with respect to isolation between ports 1 and 2 and return loss at port E, it exhibits narrow-band frequency responses. In addition, its performance is sensitive to misalign-

ment of microstrip and slotline components: this sensitivity is attributable to a limited number of quarter-wavelength ($\lambda/4$) transmission-line sections for matching impedances among all four ports, and to strong parasitic couplings at the microstrip/slotline T junction, where four microstrip lines and a slotline are combined.

The present improved broadband magic-T junction (see figure) includes a microstrip ring structure and two microstrip-to-slotline transitions. One of the microstrip/slotline transitions is a small T junction between the ring and a slotline; the other microstrip/slotline transition effects coupling between the slotline and port E. The smallness of the T junction and the use of minimum-size slotline terminations help to minimize radiation loss. An impedance-transformation network that includes multiple quarter-wavelength sections is used to increase the operating bandwidth and minimize the parasitic coupling around the microstrip/slotline T junction. As a result, the improved junction has greater bandwidth and lower phase imbalance at the sum and difference ports than did the prior junction.

The upper portion of the ring between ports 1 and 2, consisting of two $\lambda/4$ transmission-line sections that have a characteristic impedance of Z_1 and meet at port H, serves as an in-phase combiner. The portion of the ring below ports 1 and 2 consists of two pairs of $\lambda/4$ transmission-line sections having characteristic impedances of Z_2 and Z_3 connected in series and meeting at the T junction. These sections are used to transform between the microstrip and the slotline, which has a characteristic impedance of Z_4 . The slotline is terminated at both ends with stepped circular rings to provide a broadband virtual open circuit. Finally, the slotline output is transformed to a microstrip output at port E by use of a microstrip-slotline transition.

An experimental version of this junction, optimized for operation at a nominal frequency of 10 GHz, was built and tested. The experimental results show that this junction functions over the frequency band from 6.6 to 13.6 GHz (as defined by falloff of 1 dB) with an insertion loss of less than 0.6 dB, phase imbalance of less than 1° , and amplitude imbalance of less than 0.25 dB.

This work was done by Kongpob U-yen, Edward J Wollack, and Terence Doiron of Goddard Space Flight Center. Further information is contained in a TSP (see page 1). GSC-15470-1

On-Wafer Measurement of a Silicon-Based CMOS VCO at 324 GHz

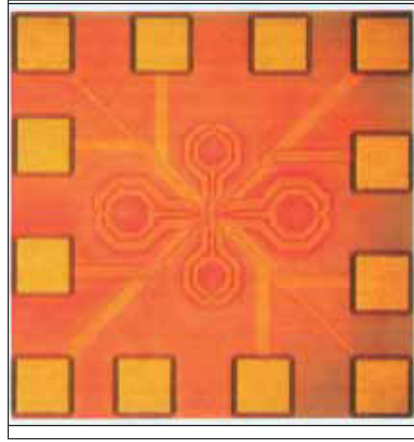
Compact, low-power, electronically tunable submillimeter-wave local oscillators are now feasible.

NASA's Jet Propulsion Laboratory, Pasadena, California

The world's first silicon-based complementary metal oxide/semiconductor (CMOS) integrated-circuit voltage-controlled oscillator (VCO) operating in a frequency range around 324 GHz has been built and tested. Concomitantly, equipment for measuring the performance of this oscillator has been built and tested. These accomplishments are intermediate steps in a continuing effort to develop low-power-consumption, low-phase-noise, electronically tunable signal generators as local oscillators for heterodyne receivers in submillimeter-wavelength (frequency > 300 GHz) scientific instruments and imaging systems. Submillimeter-wavelength imaging systems are of special interest for military and law-enforcement use because they could, potentially, be used to detect weapons hidden behind clothing and other opaque dielectric materials. In comparison with prior submillimeter-wavelength signal generators, CMOS VCOs offer significant potential advantages, including great reductions in power consumption, mass, size, and complexity. In addition, there is potential for on-chip integration of CMOS VCOs with other CMOS integrated circuitry, including phase-lock loops, analog-to-digital converters, and advanced microprocessors.

The 324-GHz CMOS VCO (see figure) was designed and fabricated according

to the design rules of 90-nm-gate-length CMOS technology. However, it was nec-



This CMOS Integrated Circuit includes a VCO that generates four signals in phase quadrature at a fundamental frequency of about 81 GHz. The four 81-GHz signals are rectified and superposed to obtain a signal at 324 GHz.

essary to follow a somewhat unconventional approach because it is impossible to make a 90-nm-gate-length CMOS circuit oscillate at a frequency greater than about 170 GHz. The essence of the approach followed here is to generate a 324-GHz signal as a fourth-harmonic signal through linear superposition of four phase-delayed, rectified 81-GHz fundamental signals: Two cross-coupled 81-GHz VCO cores generate quadrature outputs at relative phases of 0°, 90°,

180°, and 270°. These four signals are rectified by class-B amplifiers, and the outputs of the amplifiers are combined. The fundamental-to-harmonic power-conversion efficiency is significantly greater than that of traditional harmonic generation through exploitation of nonlinear circuit characteristics. Moreover, the phase noise of the output signal is less than that of traditional harmonic generation because the phase noise is limited to that of the fundamental signal.

A custom on-wafer probe was developed for measuring the performance of the 324-GHz CMOS VCO. The probe includes a unique coplanar-waveguide/coaxial-cable/waveguide transition. The probe contacts are spaced at 100 μm — a distance chosen to match the pitch of the contact pads on the CMOS VCO chip. The probe has been used to measure the phase noise, frequency of oscillation, and scattering parameters of the VCO at frequencies up to 340 GHz.

This work was done by Lorene Samoska, King Man Fung, and Todd Gaier of Caltech; Daquan Huang, Tim Larocca, and M. F. Chang of the University of California, Los Angeles; Richard Campbell of Portland State University; and Michael Andrews of Cascade Microtech for NASA's Jet Propulsion Laboratory. Further information is contained in a TSP (see page 1). NPO-45494

Group-III Nitride Field Emitters

Growing group-III nitride films spontaneously split into columns.

Marshall Space Flight Center, Alabama

Field-emission devices (cold cathodes) having low electron affinities can be fabricated through lattice-mismatched epitaxial growth of nitrides of elements from group III of the periodic table. Field emission of electrons from solid surfaces is typically utilized in vacuum microelectronic devices, including some display devices. The present field-emission devices and the method of fabricating them were developed to satisfy needs to reduce the cost of fabricating field emitters, make them compatible

with established techniques for deposition of and on silicon, and enable monolithic integration of field emitters with silicon-based driving circuitry.

In fabricating a device of this type, one deposits a nitride of one or more group-III elements on a substrate of (111) silicon or other suitable material. One example of a suitable deposition process is chemical vapor deposition in a reactor that contains plasma generated by use of electron cyclotron resonance. Under properly chosen growth condi-

tions, the large mismatch between the crystal lattices of the substrate and the nitride causes strains to accumulate in the growing nitride film, such that the associated stresses cause the film to crack. The cracks lie in planes parallel to the direction of growth, so that the growing nitride film becomes divided into microscopic growing single-crystal columns. The outer ends of the fully-grown columns can serve as field-emission tips. By virtue of their chemical compositions and crystalline structures,

the columns have low work functions and high electrical conductivities, both of which are desirable for field emission of electrons.

From examination of transmission electron micrographs of a prototype device, the average column width was determined to be about 100 nm and the sharpness of the tips was determined to be characterized by a dimension somewhat less than 100 nm. The areal density of the columns was found to be about $5 \times 10^9 \text{ cm}^{-2}$ — about 4 to 5 orders of magnitude greater than the areal density of tips in prior field-emission devices. The electric field necessary to turn on the emission current and the current per tip in this device are both lower than in prior field-emission devices, such that it becomes possible to achieve longer operational

lifetime. Moreover, notwithstanding the lower current per tip, because of the greater areal density of tips, it becomes possible to achieve greater current density averaged over the cathode area.

The thickness of the grown nitride film (equivalently, the length of the columns) could lie between about 0.5 μm and a few microns; in any event, a thickness of about 1 μm is sufficient and costs less than do greater thicknesses.

It may be possible to grow nitride emitter columns on glass or other substrate materials that cost less than silicon does. What is important in the choice of substrate material is the difference between the substrate and nitride crystalline structures. Inasmuch as the deposition process is nondestructive, an

ability to grow emitter columns on a variety of materials would be advantageous in that it would facilitate the integration of field-emitter structures onto previously processed integrated circuits.

Doping seems to play an important role in the field-emission properties of the columns. The nitride in the prototype device was doped with silicon at a concentration of $5 \times 10^{19} \text{ cm}^{-3}$. Other elements from groups II, IV, and VI of the periodic table could be used as alternative or additional dopants. Doping levels could range from about 10^{16} to 10^{21} cm^{-3} .

This work was done by Abdelhak Bensaoula and Igor Berishev of the University of Houston for Marshall Space Flight Center. For more information, contact Sammy Nabors, MSFC Commercialization Lead at sammy.a.nabors@nasa.gov. MFS-32514-1

HEMT Amplifiers and Equipment for Their On-Wafer Testing

Power levels in CPW circuits can be measured without packaging.

NASA's Jet Propulsion Laboratory, Pasadena, California

Power amplifiers comprising InP-based high-electron-mobility transistors (HEMTs) in coplanar-waveguide (CPW) circuits designed for operation at frequencies of hundreds of gigahertz, and a test set for on-wafer measurement of their power levels have been developed. These amplifiers utilize an advanced 35-nm HEMT monolithic microwave integrated-circuit (MMIC) technology and have potential utility as local-oscillator drivers and power sources in future submillimeter-wavelength heterodyne receivers and imaging systems. The test set can reduce development time by enabling rapid output power characterization, not only of these and similar amplifiers, but also of other coplanar-waveguide power circuits, without the necessity of packaging the circuits.

One of the amplifiers designed and tested at 330 GHz is shown in Figure 1. It is a three-stage unit containing one HEMT in the first stage, two HEMTs in the second stage, and four HEMTs in the third stage, with 1:2 CPW power splitters between the HEMT

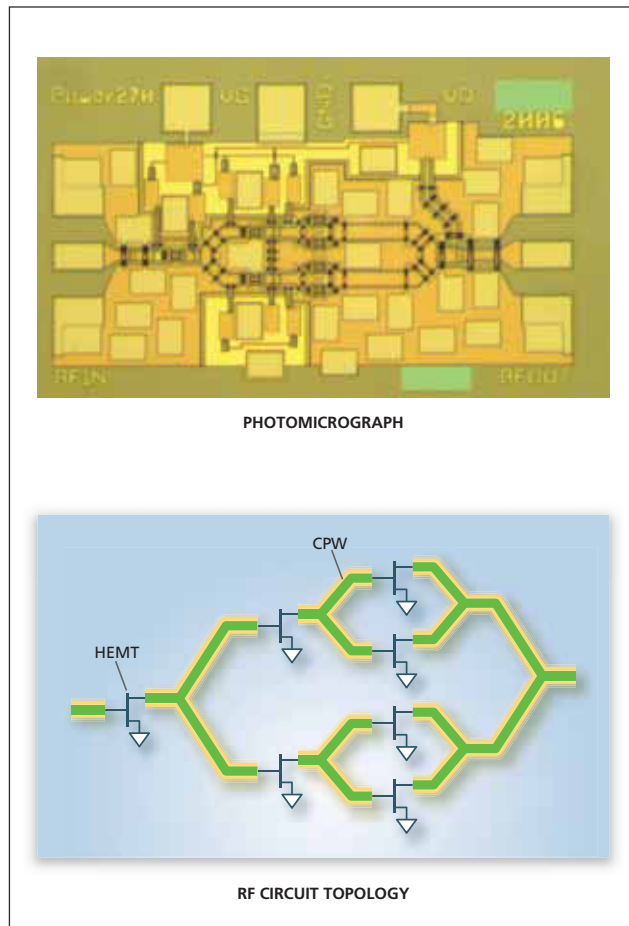


Figure 1. This Three-Stage Amplifier contains HEMTs with RF coupling via CPW structures.

stages. The outputs of the third-stage HEMTs are coupled via a 4:1 CPW power combiner. Each HEMT is a two-finger device having an output periphery of 10 μm per finger, so that the total output periphery per HEMT is 20 μm . Hence, the total output periphery of all four third-stage HEMTs is 80 μm . Because the layout is so extremely compact that individual biasing of each stage cannot be accommodated, the gate and drain bias conductors of all seven transistors are tied together.

Figure 2 schematically depicts the power test set as configured for characterizing this amplifier or another device at 330 GHz at different input power levels. A Gunn oscillator generates a 110-GHz signal, which is then fed via a W-band amplifier and a variable attenuator to a frequency tripler. The output of the frequency tripler is a 330-GHz power source used as the input signal for the amplifier or other device under test (DUT). A calorimeter measures the power output of the DUT. Input and output cou-

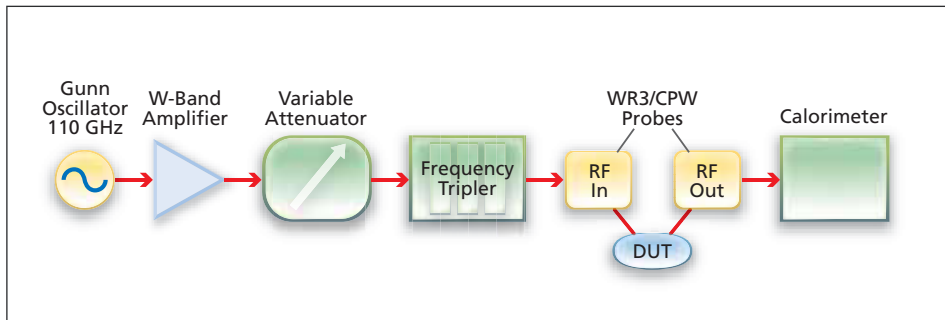


Figure 2. The Test Set feeds a 330-GHz signal to the DUT and measures the output power of the DUT. Standard sections of CPW can be substituted for the DUT for calibration measurements.

pling of the 330-GHz signals between the test set and the DUT is effected by means of commercially available waveguide probes of WR3 cross section (a

standard rectangular cross section for a nominal frequency range of 220 to 325 GHz) with transitions to CPW contacts at one end. For measurement of the

DUT-input 330-GHz power, the output of the frequency tripler is coupled directly via a waveguide to the calorimeter. For measurement of power levels used to correct for losses in the probes, a standard section of CPW is substituted for the DUT. In tests performed thus far, the amplifier exhibited an output power of 1.6 dB, with a maximum low power level gain of 7 dB.

This work was done by King Man Fung, Todd Gaier, Lorene Samoska, William Deal, Vesna Radisic, Xiaobing Mei, and Richard Lai of Caltech for NASA's Jet Propulsion Laboratory. For more information, contact iaoffice@jpl.nasa.gov. NPO-45022



Thermal Spray Formation of Polymer Coatings

John Glenn Research Center, Cleveland, Ohio

This innovation forms a sprayable polymer film using powdered precursor materials and an in-process heating method. This device directly applies a powdered polymer onto a substrate to form an adherent, mechanically-sound, and thickness-regulated film. The process can be used to lay down both fully dense and porous, e.g., foam, coatings. This system is field-deployable and includes power distribution, heater controls, polymer constituent material

bins, flow controls, material transportation functions, and a thermal spray apparatus.

The only thing required for operation in the field is a power source. Because this method does not require solvents, it does not release the toxic, volatile organic compounds of previous methods. Also, the sprayed polymer material is not degraded because this method does not use hot combustion gas or hot plasma gas. This keeps

the polymer from becoming rough, porous, or poorly bonded.

This work was done by Scott Cogull, Stephen L. Galbraith, Darren L. Tuss, Milan Ivosevic, and Lawrence Farrar of Resodyn Corporation for Glenn Research Center.

Inquiries concerning rights for the commercial use of this invention should be addressed to NASA Glenn Research Center, Innovative Partnerships Office, Attn: Steve Fedor, Mail Stop 4-8, 21000 Brookpark Road, Cleveland, Ohio 44135. Refer to LEW-18246-1.

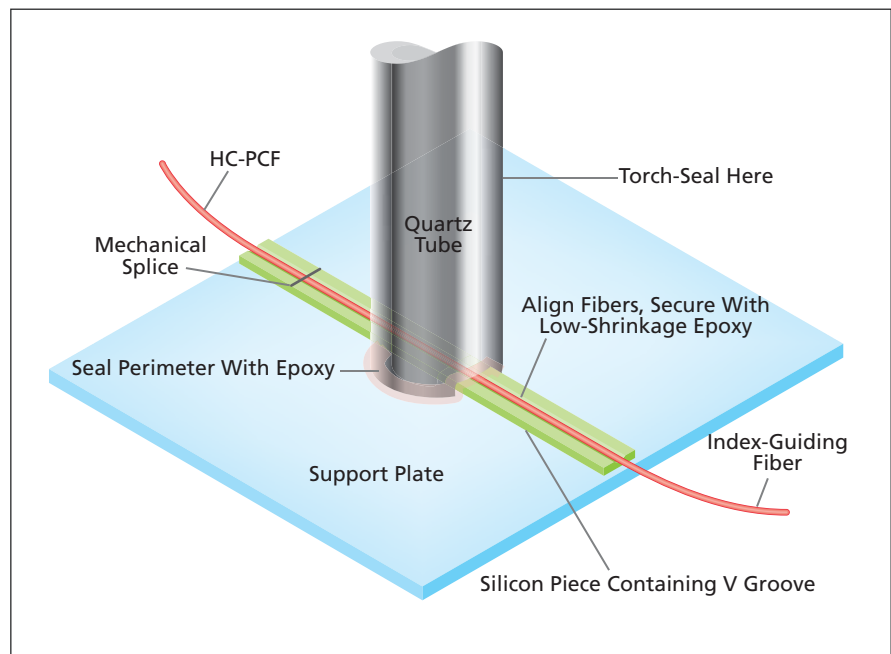
Improved Gas Filling and Sealing of an HC-PCF

Compact hermetic joint is formed to seal connectorized all-fiber gas reference cell.

NASA's Jet Propulsion Laboratory, Pasadena, California

An improved packaging approach has been devised for filling a hollow-core photonic-crystal fiber (HC-PCF) with a gas, sealing the HC-PCF to retain the gas, and providing for optical connections and, optionally, a plumbing fitting for changing or augmenting the gas filling. Gas-filled HC-PCFs can be many meters long and have been found to be attractive as relatively compact, lightweight, rugged alternatives to conventional gas-filled glass cells for use as molecular-resonance frequency references for stabilization of lasers in some optical-metrology, lidar, optical-communication, and other advanced applications. Prior approaches to gas filling and sealing of HC-PCFs have involved, variously, omission of any attempt to connectorize the PCF, connectorization inside a vacuum chamber (an awkward and expensive process), or temporary exposure of one end of an HC-PCF to the atmosphere, potentially resulting in contamination of the gas filling. Prior approaches have also involved, variously, fusion splicing of HC-PCFs with other optical fibers or other termination techniques that give rise to Fresnel reflections of about 4 percent, which results in output intensity noise.

In the improved approach (see figure), at first, one end of an HC-PCF is



A Quartz Tube Is Attached and Sealed With Epoxy to an assembly that includes a mechanical splice between an HC-PCF and a solid-core optical fiber. The tube is used for evacuation and gas filling of the HC-PCF.

mechanically spliced to one end of an index-guiding optical fiber, the end face of which has been cleaved at an angle to suppress Fresnel reflections. The fibers are placed in a V-cross-section groove in a piece of silicon with a gap of 30 to 100

μm between their end faces. The fibers are fixed in place in the groove by use of a low-shrinkage epoxy. The gap between the end faces of the fibers is small enough to ensure adequate optical coupling, yet it accommodates flow of gas

into and out of the HC-PCF.

The V-groove silicon piece that supports the mechanical splice rests on a support plate. One end of a quartz tube is prepared by contouring it to fit over the V-groove silicon piece and support plate. This end of the tube is put in place to cover the splice region, and an epoxy is used to seal the tube to the V-groove silicon piece, the optical fibers, and the support plate.

The other end of the quartz tube is inserted into a plumbing fitting of a vacuum chamber, which is equipped with valves and connected to a vacuum pump for removal of air from the interior of the HC-PCF, and to a gas cylinder and pressure gauge for filling the interior of the HC-PCF with the desired gas. In a typical application, once the HC-PCF has been filled with the gas, the quartz tube is torch-sealed, forming a relatively

compact hermetic junction. Alternatively, if the plumbing fitting includes a valve, it can be left in place to enable re-evacuation and/or refilling of the HC-PCF without the necessity of breaking and remaking the splice.

This work was done by Ilya Poberezhskiy, Patrick Meras, Daniel Chang, and Gary Spiers of Caltech for NASA's Jet Propulsion Laboratory. Further information is contained in a TSP (see page 1). NPO-45193



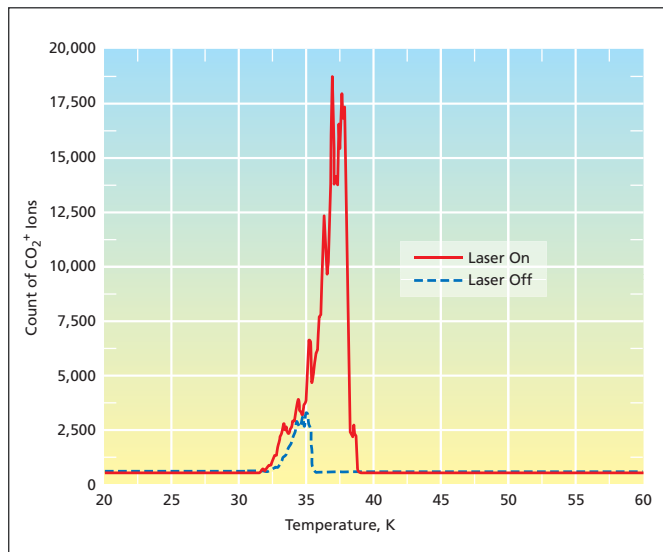
Making More-Complex Molecules Using Superthermal Atom/Molecule Collisions

Atoms adsorbed on cold surfaces react with energetic impinging atoms.

NASA's Jet Propulsion Laboratory, Pasadena, California

A method of making more-complex molecules from simpler ones has emerged as a by-product of an experimental study in outer-space atom/surface collision physics. The subject of the study was the formation of CO₂ molecules as a result of impingement of O atoms at controlled kinetic energies upon cold surfaces onto which CO molecules had been adsorbed. In this study, the O/CO system served as a laboratory model, not only for the formation of CO₂ but also for the formation of other compounds through impingement of rapidly moving atoms upon molecules adsorbed on such cold interstellar surfaces as those of dust grains or comets. By contributing to the formation of increasingly complex molecules, including organic ones, this study and related other studies may eventually contribute to understanding of the origins of life.

In the study, CO was adsorbed onto a cryo-cooled surface, then the surface was exposed to a beam of ground-state O atoms at a kinetic energy of 10 eV per



These Plots of the CO₂⁺ Reading of the mass spectrometer versus desorption temperature have been interpreted as signifying that CO₂ had been adsorbed on the surface in the reaction O + CO → CO₂. The plot labeled "Laser Off" is that of a background reading that must be subtracted from the total-reading "Laser On" reading to obtain the net CO₂⁺-ion count from the superthermal reaction.

atom. After an exposure time of 135 minutes, the surface was retracted from the O-atom beam into the field of view of a quadrupole mass spectrometer. The reaction products were desorbed by heating the cold surface according to a defined temperature-vs.-time schedule (temperature-programmed

desorption). Desorbed molecules were ionized, then detected in the mass spectrometer. The temperature dependence of the CO₂ peak in the mass-spectrometer readout (see figure) indicated that large quantities of CO₂ were desorbed; this observation was taken to be evidence for the reaction O + CO(s) → CO₂(s).

Generalizing the method used in this study, it may be possible, for example, to make simple and more-complex amines, even amino acids by reacting ice mixtures of CH₄ and NH₃ with superthermal O and H beams. In general, by choice of atomic projectiles, kinetic energies, atomic quantum states, surfaces, and exposure times, it may be possible

to create new molecular species and stabilize them on the solid surfaces on which they were created.

This work was done by Brian Shortt, Ara Chutjian, and Otto Orient of Caltech for NASA's Jet Propulsion Laboratory. Further information is contained in a TSP (see page 1). NPO-41300

Nematic Cells for Digital Light Deflection

Smectic A (SmA) prisms can be made in a variety of shapes and are useful for visible spectrum and infrared beam steering.

John H. Glenn Research Center, Cleveland, Ohio

Smectic A (SmA) materials can be used in non-mechanical, digital beam deflectors (DBDs) as fillers for passive birefringent prisms based on decoupled pairs of electrically controlled, liquid crystalline polarization rotators, like twisted nematic (TN) cells and passive deflectors. DBDs are used in free-space

laser communications, optical fiber communications, optical switches, scanners, and *in-situ* wavefront correction.

Depending on the applied voltage, the TN cell rotates the polarization of incident light by $\pi/2$ (no field, OFF state) or leaves the polarization intact (when the applied electric field reorients the

liquid crystal molecules perpendicular to the plates of the cell, ON state). The decoupled pair of a rotator and a deflector has no moving parts, and can be cascaded into N stages, making 2^N addressable beam directions. This approach allows for the separation of time response and beam deflection angles, and

the optimization of these two parameters separately. A 0.5-ms response time of dual-frequency nematic 90° TN cells was achieved by implementing an overdriving scheme of electrical switching, where an electrical signal is a sequence of high-amplitude pulses (64 V RMS, at 2 kHz and 50 kHz) and holding voltages (6 V and 4 V RMS at 1 kHz and 50 kHz, respectively).

Deflection angles can be optimized by the design of the birefringent prisms. SmA-filled prisms are attractive in low-cost applications where one needs large apertures, large angles of deflection, and/or non-trivial geometries. Mixtures of homologues of 4,4'-*n*-dialkylazoxybenzene produce SmA phases with a broad temperature range of SmA existence (from 10–20 °C to 40–50 °C) with a relatively small number of residual defects, such as focal conic domains, and high transmission characteristics. In this innovation, the typical magnetic fields needed to remove director distortions around the mechanical inclusions and focal conic domains have been determined. For the SmA prism, the optical axis (and thus the preferred orientation of the SmA molecules) should be aligned along the edge of the wedge. In this geometry, the director field is uniform everywhere. A passive birefringent prism separates the beam into two channels, depending on the beam polariza-

tion. Inside the prism, the beam propagates as ordinary or extraordinary mode. As the ordinary and extraordinary refractive indices are different, the two modes of propagation through the prism result in a different angle of deflection.

The SmA prisms are easier and cheaper to form than solid birefringent crystals, such as yttrium vanadate (YVO₄) or calcite (CaCO₃). The optical axis of SmA prisms can be controlled by surface alignment. They can be prepared as relatively thick prisms (up to 7 mm) or as arrays of micropisms. Light scattering in SmA birefringent prisms can be reduced by proper alignment to levels that are significantly lower than light scattering at the director fluctuations in the nematic samples of the same thickness. As the light scattering is caused mostly by focal conic domains that have a fixed size, it becomes smaller with the increase of the wavelength of light; the infrared (IR) part of the spectrum is less sensitive to these losses. Thus, the SmA prisms are suitable candidates for beam steering not only in the visible part of the spectrum, but in the IR part as well. While SmA prisms can only be used in the temperature range of the SmA phase, it can be expanded significantly by using mixtures.

The TN cells are used to realize the fast switching of the linearly polarized light. The fast switching is achieved be-

cause the dual-frequency nematic is always driven by the operational voltage. To reorient the director along the field, operational voltage is applied at a frequency of 1 kHz. To reorient the director perpendicular to the field, the operational voltage is applied at the higher frequency of 50 kHz. The amplitude of the driving voltage determines the switching time between the states. In regular liquid crystal cells, the field is applied only to reorient the director in one state; the reverse transition is achieved by simply switching the field OFF; the director relaxation is slow in this case as the active reorienting bulk torque is absent. Finally, with their high birefringence, SmA prisms can be constructed in a variety of shapes, including single prisms and prismatic, blazed gratings of different angles and profiles.

This work was done by Oleg Pishnyak, Andrii Golovin, and Oleg Lavrentovich of Kent State University; Liubov Kremenska of Truman State University; Bruce Winker of Rockwell Scientific Company; and John Pouch and Felix Miranda of Glenn Research Center. Further information is contained in a TSP (see page 1).

Inquiries concerning rights for the commercial use of this invention should be addressed to NASA Glenn Research Center, Innovative Partnerships Office, Attn: Steve Fedor, Mail Stop 4-8, 21000 Brookpark Road, Cleveland, Ohio 44135. Refer to LEW-18215-1.

Improved Silica Aerogel Composite Materials

Shrinkage and cracking are greatly reduced.

NASA's Jet Propulsion Laboratory, Pasadena, California

A family of aerogel-matrix composite materials having thermal-stability and mechanical-integrity properties better than those of neat aerogels has been developed. Aerogels are known to be excellent thermal- and acoustic-insulation materials because of their molecular-scale porosity, but heretofore, the use of aerogels has been inhibited by two factors:

- Their brittleness makes processing and handling difficult.
- They shrink during production and shrink more when heated to high temperatures during use. The shrinkage and the consequent cracking make it difficult to use them to encapsulate objects in thermal-insulation materials.

A material in the present family consists of a silica aerogel matrix reinforced with silica fibers and silica powder. The density

of this composite material is typically only about 10 percent greater than the density of the corresponding neat aerogel. The underlying concept of aerogel-matrix composites is not new; the novelty of the present family of materials lies in formulations and processes that result in superior properties, which include (1) much less shrinkage during a supercritical-drying process employed in producing a typical aerogel, (2) much less shrinkage during exposure to high temperatures, and (3) as a result of the reduction in shrinkage, much less or even no cracking.

Synthesis of a composite aerogel of this type is based on a sol-gel process. The first step is to make a silica sol by refluxing and distilling a mixture of silicon alkoxide (tetramethyl ortho silicate, tetraethyl ortho silicate), a suitable sol-

vent (methanol, ethanol), water, and nitric acid. The resultant concentrated sol is then diluted with acetonitrile. The second step is to prepare a solution for casting the composite aerogel: Fumed silica (325-mesh powder having specific surface area of about 200 m²/g) and silica powder (particle sizes between 1 and 2 μm) are suspended in acetonitrile and then the silica sol, water, and ammonium hydroxide base are added to the acetonitrile/powder suspension. The amount of each component can be adjusted to suit a specific application. After thus preparing the aerogel-casting solution, a piece of silica fiber felt (destined to become the fiber reinforcement in the composite) is placed in a mold. Then the aerogel-casting solution is poured into the mold, where it perme-

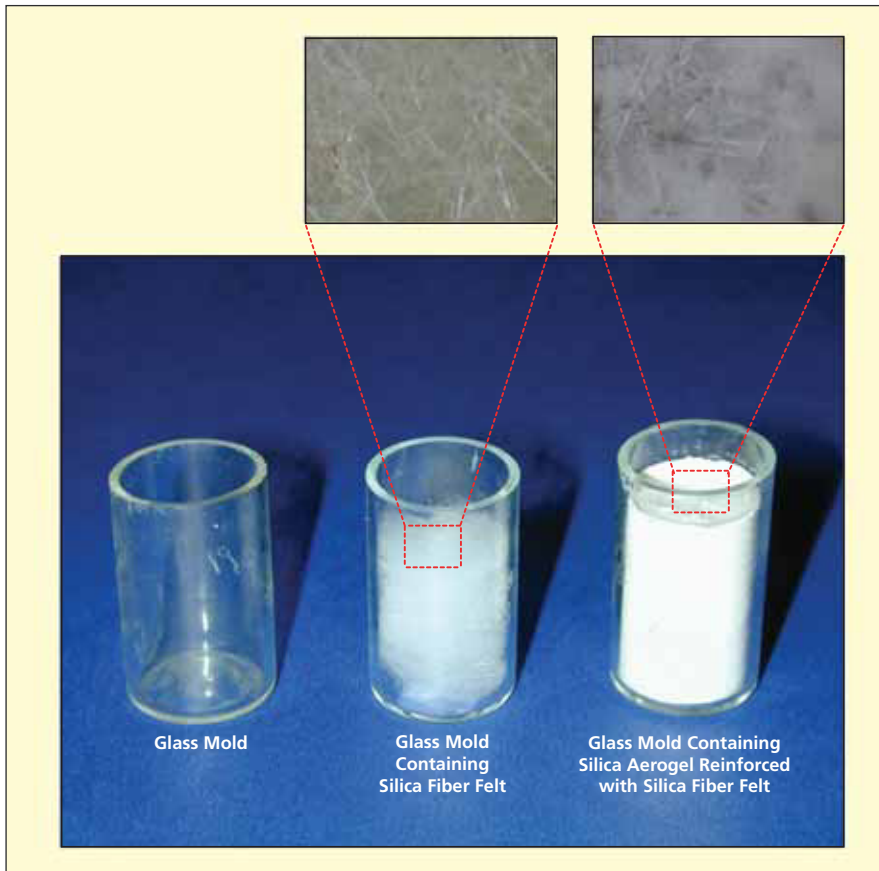


Figure 1. These Images Depict Three Stages in the synthesis of a silica-aerogel/silica-felt/silica-powder composite.

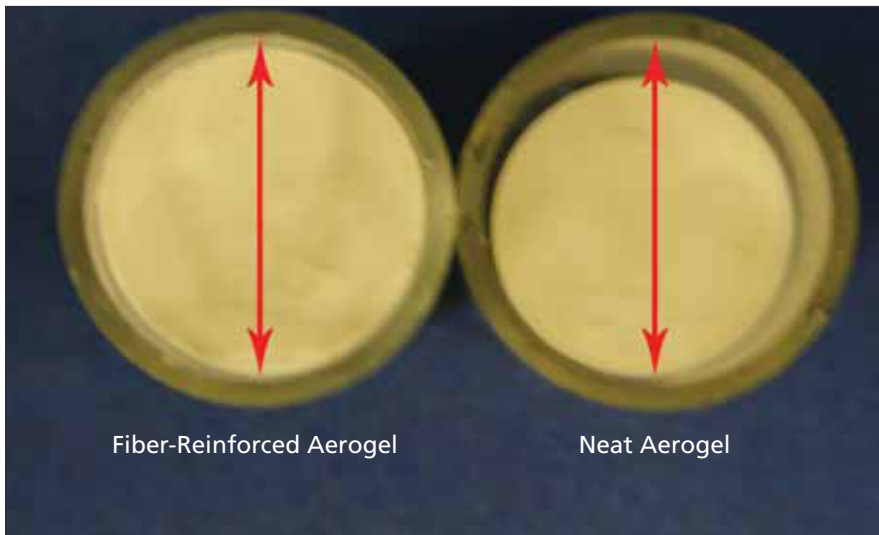


Figure 2. No Apparent Shrinkage was observed in a fiber-reinforced aerogel composite after supercritical drying, whereas a neat aerogel composite exhibited a linear shrinkage of about 5 percent.

ates the silica fiber felt (see Figure 1). After the solution has gelled, the casting is transferred to an autoclave filled with acetonitrile, wherein the casting is subjected to supercritical drying at a temperature of 295 °C and pressure of 5.5 MPa.

Heretofore, neat silica aerogels had been observed to undergo linear shrinkages between 5 and 10 percent upon supercritical drying. In tests of a composite of the present type, the incorporation of the silica fiber felt has been found to reduce the shrinkage to a negligible level (see Figure 2). The silica fiber felt seems to strengthen the aerogel and to serve as rigid framework that prevents shrinkage. It has been conjectured that the silica fiber felt divides the volume of the casting into small subvolumes, thereby confining strain to relatively small unit spaces (between fibers) instead of allowing strain to act over relatively large (millimeter to centimeter) lengths.

In other tests, a neat aerogel exhibited linear shrinkage of about 6 percent after exposure to a temperature of 1,000 °C in a vacuum for four hours, and an even greater shrinkage (about 50 percent) after four hours at 1,000 °C in air. In contrast, a composite aerogel of the present type exhibited no apparent shrinkage after 1 week at 1,000 °C in a vacuum, and a linear shrinkage of only about 2 percent after a week at 1,000 °C in air.

This work was done by Jong-Ah Paik, Jeffrey Sakamoto, and Steven Jones of Caltech for NASA's Jet Propulsion Laboratory. Further information is contained in a TSP (see page 1).

In accordance with Public Law 96-517, the contractor has elected to retain title to this invention. Inquiries concerning rights for its commercial use should be addressed to:

*Innovative Technology Assets Management
JPL*

*Mail Stop 202-233
4800 Oak Grove Drive
Pasadena, CA 91109-8099
(818) 354-2240*

E-mail: iaoffice@jpl.nasa.gov

Refer to NPO-44287, volume and number of this NASA Tech Briefs issue, and the page number.



Microgravity, Mesh-Crawling Legged Robots

These relatively inexpensive robots may be used in search and rescue operations.

NASA's Jet Propulsion Laboratory, Pasadena, California

The design, fabrication, and microgravity flight-testing are part of a continuing development of palm-sized mobile robots that resemble spiders (except that they have six legs apiece, whereas a spider has eight legs). Denoted SpiderBots (see figure), they are prototypes of proposed product line of relatively inexpensive walking robots that could be deployed in large numbers to function cooperatively in construction, repair, exploration, search, and rescue activities in connection with exploration of outer space and remote planets.

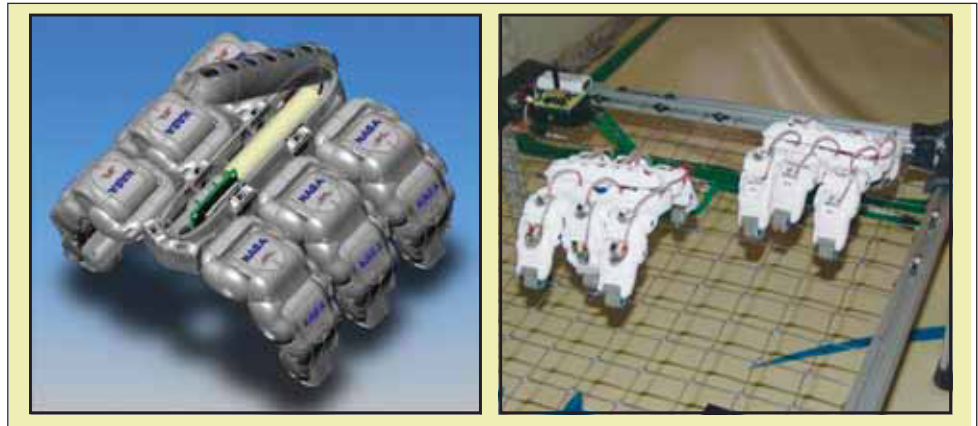
Relative to other legged robots, including ones reported in previous *NASA Tech Briefs* articles, SpiderBots are smaller, less power-hungry, and more specialized. A SpiderBot at the present stage of development is designed primarily to demonstrate that it can crawl on a flexible rectangular mesh (in micro-gravity) and secondarily that it can walk on flat surfaces and assemble simple structures. Each leg includes two spring-compliant joints and a

gripping actuator. The SpiderBot moves in a hard-coded set of tripod gaits involving alternating motions of legs variously anchored or not anchored to a mesh.

The robots were recently tested on a reduced gravity aircraft and were able to demonstrate crawling along the mesh during the microgravity portion of the parabolic flight. In one contemplated improvement, feedback from sensors on the feet would provide indications of success or the lack

thereof in gripping a mesh, thereby contributing to robust, fault-tolerant operation.

This work was done by Alberto Behar, Neville Marzwell, Jaret Matthews, and Krandalyn Richardson of Caltech; Jonathan Wall and Michael Poole of Blue Sky Robotics; David Foor of Texas A&M University; and Damian Rodgers of ISU (International Space University) for NASA's Jet Propulsion Laboratory. Further information is contained in a TSP (see page 1). NPO-42672



Photos of SpiderBots show a prototype and one crawling on a mesh.

Advanced Active-Magnetic-Bearing Thrust-Measurement System

Automatic multipoint calibration and a fringing model are used to increase accuracy.

Stennis Space Center, Mississippi

An advanced thrust-measurement system utilizes active magnetic bearings to both (1) levitate a floating frame in all six degrees of freedom and (2) measure the levitation forces between the floating frame and a grounded frame. This system was developed for original use in measuring the thrust exerted by a rocket engine mounted on the floating frame, but can just as well be used in other force-measurement applications.

This system offers several advantages over prior thrust-measurement systems

based on mechanical support by flexures and/or load cells:

- The system includes multiple active magnetic bearings for each degree of freedom, so that by selective use of one, some, or all of these bearings, it is possible to test a given article over a wide force range in the same fixture, eliminating the need to transfer the article to different test fixtures to obtain the benefit of full-scale accuracy of different force-measurement devices for different force ranges.

- Like other active magnetic bearings, the active magnetic bearings of this system include closed-loop control subsystems, through which the stiffness and damping characteristics of the magnetic bearings can be modified electronically.
- The design of the system minimizes or eliminates cross-axis force-measurement errors. The active magnetic bearings are configured to provide support against movement along all three orthogonal Cartesian axes, and such that the support along a given axis does not

produce force along any other axis. Moreover, by eliminating the need for such mechanical connections as flexures used in prior thrust-measurement systems, magnetic levitation of the floating frame eliminates what would otherwise be major sources of cross-axis forces and the associated measurement errors.

Overall, relative to prior mechanical-support thrust-measurement systems, this system offers greater versatility for adaptation to a variety of test conditions and requirements.

The basic idea of most prior active-magnetic-bearing force-measurement systems is to calculate levitation forces on the basis of simple proportionalities between changes in those forces and changes in feedback-controlled currents

applied to levitating electromagnetic coils. In the prior systems, the effects of gap lengths on fringing magnetic fields and the concomitant effects on magnetic forces were neglected. In the present system, the control subsystems of the active magnetic bearings are coupled with a computer-based automatic calibration system running special-purpose software wherein gap-length-dependent fringing factors are applied to current- and magnetic-flux-based force equations and combined with a multipoint calibration method to obtain greater accuracy. All of the inputs required for calibration can be obtained from the control subsystems of the active magnetic bearings (and from magnetic-flux sensors if they are used). Tests have verified that force accuracies characterized by errors or <5

percent of full-scale readings are achievable when using current-based force equations or by errors <0.5 percent of full-scale readings when using flux-based equations.

This work was done by Joseph Imlach of Innovative Concepts In Engineering LLC and Mary Kasarda and Eric Blumber of Virginia Polytechnic Institute and State University for Stennis Space Center.

Inquiries concerning rights for the commercial use of this invention should be addressed to:

*Innovative Concepts In Engineering LLC
2142 Tributary Circle
Anchorage, AK 99516
(907) 337-8954*

Refer to SSC-00177-1/8-1, volume and number of this NASA Tech Briefs issue, and the page number.

⚙️ Thermally Actuated Hydraulic Pumps

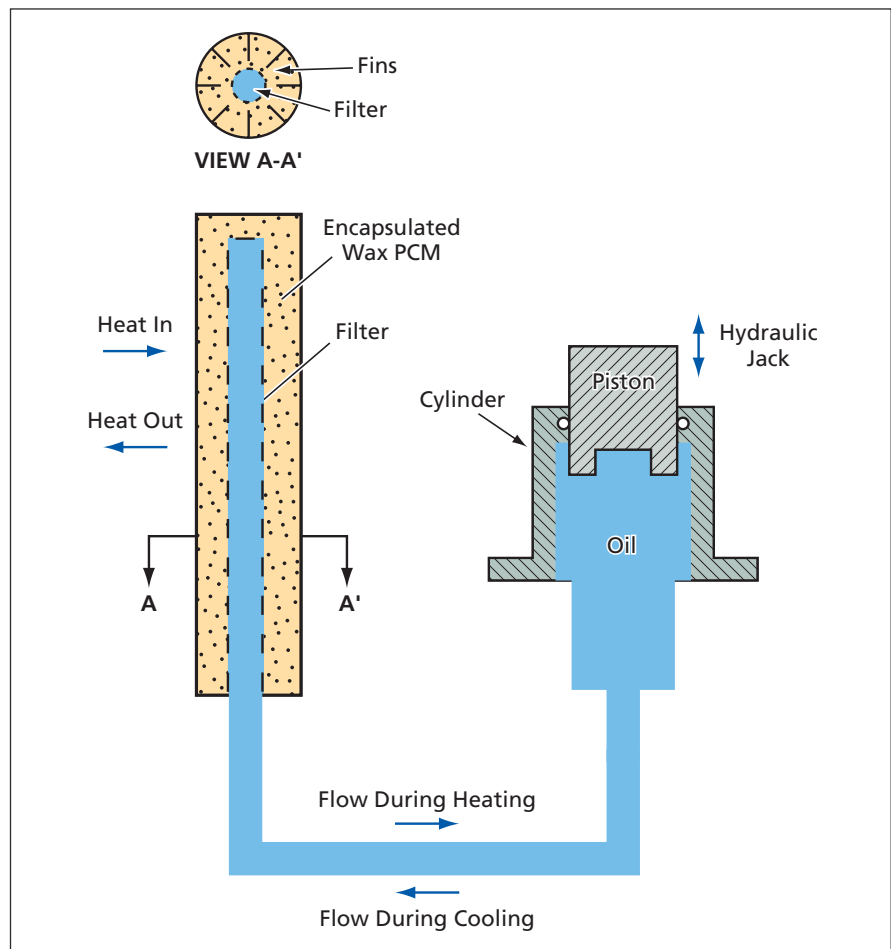
These pumps would contain no sliding (wearing) parts.

NASA's Jet Propulsion Laboratory, Pasadena, California

Thermally actuated hydraulic pumps have been proposed for diverse applications in which direct electrical or mechanical actuation is undesirable and the relative slowness of thermal actuation can be tolerated. The proposed pumps would not contain any sliding (wearing) parts in their compressors and, hence, could have long operational lifetimes.

The basic principle of a pump according to the proposal is to utilize the thermal expansion and contraction of a wax or other phase-change material in contact with a hydraulic fluid in a rigid chamber. Heating the chamber and its contents from below to above the melting temperature of the phase-change material would cause the material to expand significantly, thus causing a substantial increase in hydraulic pressure and/or a substantial displacement of hydraulic fluid out of the chamber. Similarly, cooling the chamber and its contents from above to below the melting temperature of the phase-change material would cause the material to contract significantly, thus causing a substantial decrease in hydraulic pressure and/or a substantial displacement of hydraulic fluid into the chamber. The displacement of the hydraulic fluid could be used to drive a piston.

The figure illustrates a simple example of a hydraulic jack driven by a thermally actuated hydraulic pump. The pump chamber would be a cylinder con-



A Thermally Actuated Hydraulic Pump would displace oil, which would displace a piston in a hydraulic jack.

taining encapsulated wax pellets and containing radial fins to facilitate transfer of heat to and from the wax.

The plastic encapsulation would serve as an oil/wax barrier and the remaining interior space could be filled with hydraulic oil. A filter would retain the encapsulated wax particles in the pump chamber while allowing the hydraulic oil to flow into and out of the chamber.

In one important class of potential applications, thermally actuated hydraulic pumps, exploiting vertical ocean temperature gradients for heating and cooling as needed, would be used to vary hy-

draulic pressures to control buoyancy in undersea research vessels. Heretofore, electrically actuated hydraulic pumps have been used for this purpose. By eliminating the demand for electrical energy for pumping, the use of the thermally actuated hydraulic pumps could prolong the intervals between battery charges, thus making it possible to greatly increase the durations of undersea exploratory missions.

This work was done by Jack Jones, Ronald Ross, and Yi Chao of Caltech for NASA's Jet Propulsion Laboratory. Further information is contained in a TSP (see page 1).

In accordance with Public Law 96-517, the contractor has elected to retain title to this invention. Inquiries concerning rights for its commercial use should be addressed to:

*Innovative Technology Assets Management
JPL*

*Mail Stop 202-233
4800 Oak Grove Drive
Pasadena, CA 91109-8099
(818) 354-2240*

*E-mail: iaoffice@jpl.nasa.gov
Refer to NPO-40844, volume and number of this NASA Tech Briefs issue, and the page number.*

⚙️ A New, Highly Improved Two-Cycle Engine

Performance is improved while mechanical complexity is reduced.

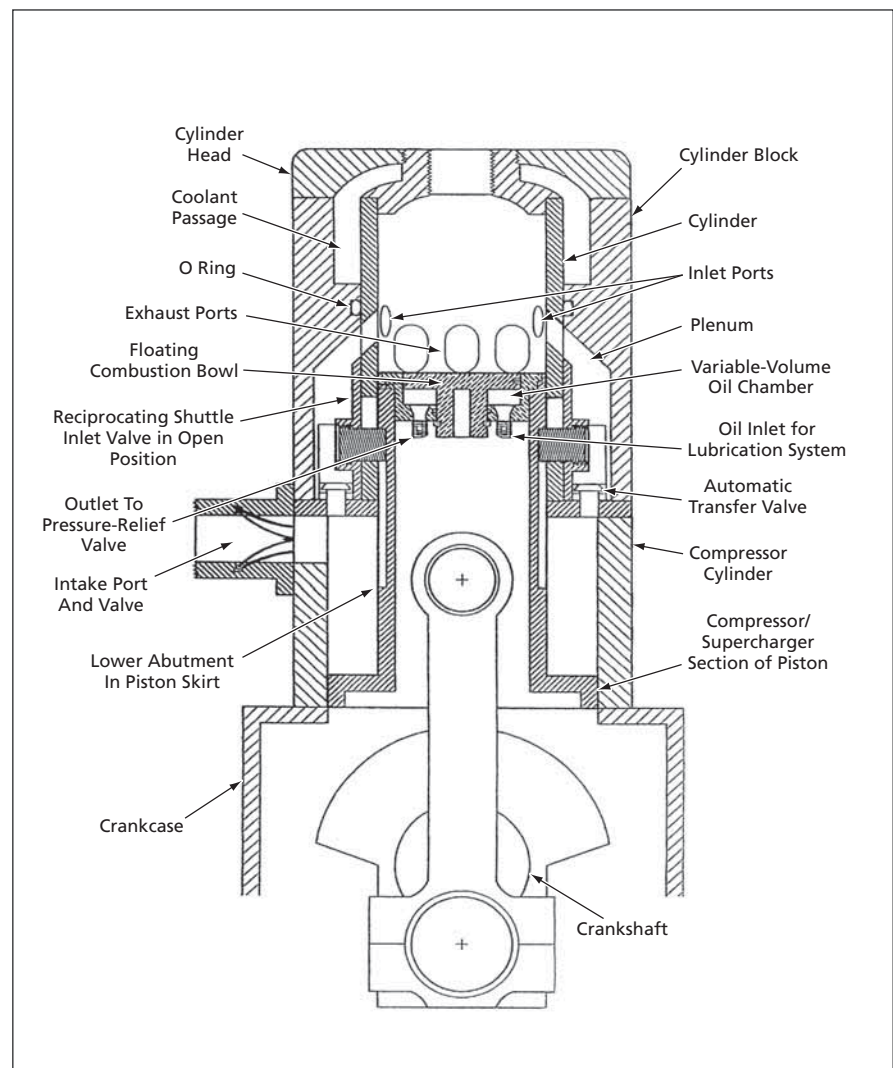
John H. Glenn Research Center, Cleveland, Ohio

The figure presents a cross-sectional view of a supercharged, variable-compression, two-cycle, internal-combustion engine that offers significant advantages over prior such engines. The improvements are embodied in a combination of design changes that contribute synergistically to improvements in performance and economy. Although the combination of design changes and the principles underlying them are complex, one of the main effects of the changes on the overall engine design is reduced (relative to prior two-cycle designs) mechanical complexity, which translates directly to reduced manufacturing cost and increased reliability. Other benefits include increases in the efficiency of both scavenging and supercharging. The improvements retain the simplicity and other advantages of two-cycle engines while affording increases in volumetric efficiency and performance across a wide range of operating conditions that, heretofore have been accessible to four-cycle engines but not to conventionally scavenged two-cycle ones, thereby increasing the range of usefulness of the two-cycle engine into all areas now dominated by the four-cycle engine.

The design changes and benefits are too numerous to describe here in detail, but it is possible to summarize the major improvements:

- *Reciprocating Shuttle Inlet Valve*

The entire reciprocating shuttle inlet valve and its operating gear is constructed as a single member. The shuttle valve is actuated in a lost-motion arrangement in which, at the ends of its stroke, projections on the shuttle valve



This **Internal Combustion Engine Design** features improved performance and reduced mechanical complexity.

come to rest against abutments at the ends of grooves in a piston skirt. This shuttle-valve design obviates the customary complex valve mechanism, actuated from an engine crankshaft or camshaft, yet it is effective with every type of two-cycle engine, from small high-speed single cylinder model engines, to large low-speed multiple cylinder engines.

- *Variable Compression Ratio*

The piston has a stepped configuration: It includes a narrower power section (the upper portion in the figure) and a wider compressor/supercharger section (the lower portion in the figure). The variable-compression-ratio mechanism includes a high-pressure oil lubrication circuit acting in unison with the pulsating flow and pressure of the air caused by the reciprocation of the compressor/supercharger section of the piston. In terms that are necessarily oversimplified for the sake of brevity, the operation of this mechanism involves interactions among pressures and flows of air, oil, and combustion gases, to vary the axial position of a floating combus-

tion bowl in the power section of the piston and thereby vary the compression ratio. The design of the mechanism is such that when the throttle opening is suddenly changed, the compression ratio becomes adjusted relatively quickly to the value at which the engine operates most efficiently.

- *Supercharging*

The stepped-piston arrangement obviates the complication and high cost of "add-on" supercharging mechanisms like those used on prior engines. During the compression stroke, the motion of the compressor/supercharger section of the piston gives rise to a flow of air at high pressure from the compressor cylinder through one-way transfer valves, through a plenum, into the power cylinder. This flow contributes to scavenging and cooling of the power cylinder. The highly compressed air continues to enter the plenum and power cylinder after the exhaust ports are closed and the supercharging of the cylinder has been completed. The compressed air that continues to enter the plenum after

the inlet ports are covered by the rising power piston is retained in the plenum under pressure until the end of the expansion stroke, when the lowering power piston opens the exhaust ports. Soon after this, the abutments in the piston skirt make contact with the projections on the reciprocating shuttle inlet valve, forcing the valve to the open position, in which the compressed air rushes from the plenum into the power cylinder, thereby effecting the initial scavenging. An additional benefit of the stepped-piston arrangement is that the blow-by gases and particulate matter that escape past the power-piston rings are isolated from the crankcase and returned to the power cylinder on the following stroke.

This work was done by Bernard Wiesen of Wiesen Engine for Glenn Research Center.

Inquiries concerning rights for the commercial use of this invention should be addressed to NASA Glenn Research Center, Innovative Partnerships Office, Attn: Steve Fedor, Mail Stop 4-8, 21000 Brookpark Road, Cleveland, Ohio 44135. Refer to LEW-18043-1.

✿ Flexible Structural-Health-Monitoring Sheets

Marshall Space Flight Center, Alabama

A generic design for a type of flexible structural-health-monitoring sheet with multiple sensor/actuator types and a method of manufacturing such sheets has been developed. A sheet of this type contains an array of sensing and/or actuation elements, associated wires, and any other associated circuit elements incorporated into various flexible layers on a thin, flexible substrate. The sheet can be affixed to a structure so that the array of sensing and/or actuation elements can be used to analyze the structure in accordance with structural-

health-monitoring techniques. Alternatively, the sheet can be designed to be incorporated into the body of the structure, especially if the structure is made of a composite material.

Customarily, structural-health monitoring is accomplished by use of sensors and actuators arrayed at various locations on a structure. In contrast, a sheet of the present type can contain an entire sensor/actuator array, making it unnecessary to install each sensor and actuator individually on or in a structure. Sensors of different types such as piezoelectric

and fiber-optic can be embedded in the sheet to form a hybrid sensor network. Similarly, the traces for electric communication can be deposited on one or two layers as required, and an entirely separate layer can be employed to shield the sensor elements and traces.

This work was done by Xinlin Qing and Fuo Kuo Chang of Acellent Technologies for Marshall Space Flight Center. For further information, contact Sammy Nabors, MSFC Commercialization Assistance Lead, at sammy.a.nabors@nasa.gov. Refer to MFS-32510-1.

✿ Alignment Pins for Assembling and Disassembling Structures

Simple tooling prevents damage to structures.

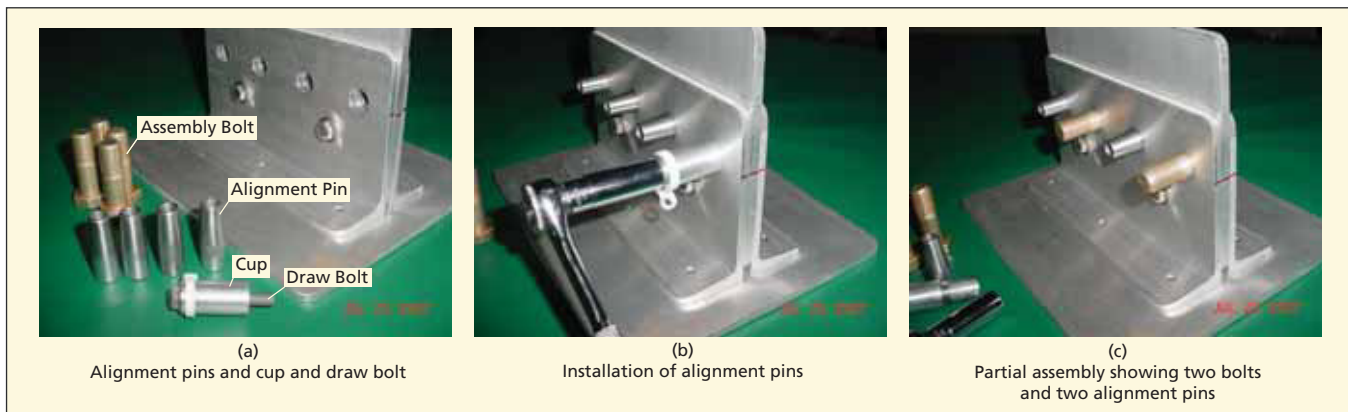
John F. Kennedy Space Center, Florida

Simple, easy-to-use, highly effective tooling has been devised for maintaining alignment of bolt holes in mating structures during assembly and disassembly of the structures. The tooling was originally used during removal of a body flap from

the space shuttle Atlantis, in which misalignments during removal of the last few bolts could cause the bolts to bind in their holes. By suitably modifying the dimensions of the tooling components, the basic design of the tooling can readily be

adapted to other structures that must be maintained in alignment.

The tooling includes tapered, internally threaded alignment pins designed to fit in the bolt holes in one of the mating structures, plus a draw bolt and a



A Tapered Alignment Pin is easily installed or removed by use of a cup and draw bolt.

cup that are used to install or remove each alignment pin. In preparation for disassembly of two mating structures, external supports are provided to prevent unintended movement of the structures. During disassembly of the structures, as each bolt that joins the structures is removed, an alignment pin is installed in its place. Once all the bolts have been removed and replaced with pins, the pins maintain alignment as the structures are gently pushed or pulled apart on the supports. In assembling the two structures, one reverses

the procedure described above: pins are installed in the bolt holes, the structures are pulled or pushed together on the supports, then the pins are removed and replaced with bolts.

The figure depicts the tooling and its use. To install an alignment pin in a bolt hole in a structural panel, the tapered end of the pin is inserted from one side of the panel, the cup is placed over the pin on the opposite side of the panel, the draw bolt is inserted through the cup and threaded into the pin, the draw bolt is tightened to pull the pin until the

pin is seated firmly in the hole, then the draw bolt and cup are removed, leaving the pin in place. To remove an alignment pin, the cup is placed over the pin on the first-mentioned side of the panel, the draw bolt is inserted through the cup and threaded into the pin, then the draw bolt is tightened to pull the pin out of the hole.

This work was done by Oliver C. Campbell of United Space Alliance for Kennedy Space Center. For further information, contact Oliver C. Campbell at (321) 861-5080. KSC-12785



Purifying Nucleic Acids From Samples of Extremely Low Biomass

NASA's Jet Propulsion Laboratory, Pasadena, California

A new method is able to circumvent the bias to which one commercial DNA extraction method falls prey with regard to the lysing of certain types of microbial cells, resulting in a truncated spectrum of microbial diversity. By prefacing the protocol with glass-bead-beating agitation (mechanically lysing a much more encompassing array of cell types and spores), the resulting microbial diversity detection is greatly enhanced.

In preliminary studies, a commercially available automated DNA extraction method is effective at delivering total DNA yield, but only the non-hardy members of the bacterial bisque were

represented in clone libraries, suggesting that this method was ineffective at lysing the harder cell types. To circumvent such a bias in cells, yet another extraction method was devised. In this technique, samples are first subjected to a stringent bead-beating step, and then are processed via standard protocols. Prior to being loaded into extraction vials, samples are placed in microcentrifuge bead tubes containing 50 μL of commercially produced lysis solution. After inverting several times, tubes are agitated at maximum speed for two minutes. Following agitation, tubes are centrifuged at 10,000 \times g for one minute. At this time, the aqueous

volumes are removed from the bead tubes and are loaded into extraction vials to be further processed via extraction regime.

The new method couples two independent methodologies in such a way as to yield the highest concentration of PCR-amplifiable DNA with consistent and reproducible results and with the most accurate and encompassing report of species richness.

This work was done by Myron La Duc, Shariff Osman, and Kasthuri Venkateswaran of Caltech for NASA's Jet Propulsion Laboratory. For more information, contact iaoffice@jpl.nasa.gov. NPO-45740

Adjustable-Viewing-Angle Endoscopic Tool for Skull Base and Brain Surgery

Surgeons could operate more precisely.

NASA's Jet Propulsion Laboratory, Pasadena, California

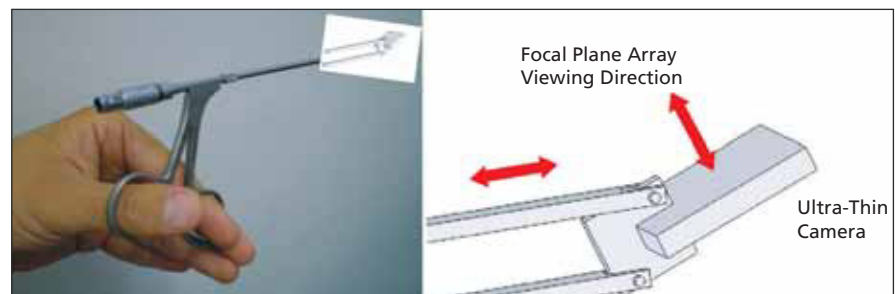
The term "Multi-Angle and Rear Viewing Endoscopic tool" (MARVEL) denotes an auxiliary endoscope, now undergoing development, that a surgeon would use in conjunction with a conventional endoscope to obtain additional perspective. The role of the MARVEL in endoscopic brain surgery would be similar to the role of a mouth mirror in dentistry. Such a tool is potentially useful for *in-situ* planetary geology applications for the close-up imaging of unexposed rock surfaces in cracks or those not in the direct line of sight.

A conventional endoscope provides mostly a frontal view — that is, a view along its longitudinal axis and, hence, along a straight line extending from an opening through which it is inserted. The MARVEL could be inserted through the same opening as that of the conventional endoscope, but could be adjusted to provide a view from almost any desired angle. The MARVEL cam-

era image would be displayed, on the same monitor as that of the conventional endoscopic image, as an inset within the conventional endoscopic image. For example, while viewing a tumor from the front in the conventional endoscopic image, the surgeon could simultaneously view the tumor from the side or the rear in the MARVEL image, and could thereby gain additional visual cues that would aid in

precise three-dimensional positioning of surgical tools to excise the tumor. Indeed, a side or rear view through the MARVEL could be essential in a case in which the object of surgical interest was not visible from the front.

The conceptual design of the MARVEL exploits the surgeon's familiarity with endoscopic surgical tools. The MARVEL would include a miniature electronic camera and miniature radio



The MARVEL would include part of the mechanism of an endo-scissor. The scissor linkage would be modified for use in adjusting the camera angle instead of actuating a scissor blade.

transmitter mounted on the tip of a surgical tool derived from an endo-scissor (see figure). The inclusion of the radio transmitter would eliminate the need for wires, which could interfere with manipulation of this and other surgical tools. The handgrip of the tool would be connected to a linkage similar to that of an endo-scissor, but the linkage would be configured to enable adjustment of the camera angle instead of actuation of a scissor blade.

It is envisioned that thicknesses of the tool shaft and the camera would be less than 4 mm, so that the camera-tipped tool could be swiftly inserted and with-

drawn through a dime-size opening. Electronic cameras having dimensions of the order of millimeters are already commercially available, but their designs are not optimized for use in endoscopic brain surgery. The variety of potential endoscopic, thoracoscopic, and laparoscopic applications can be expected to increase as further development of electronic cameras yields further miniaturization and improvements in imaging performance.

This work was done by Youngsam Bae, Anna Liao, and Harish Manohara of Caltech and Hrayr Shahinian from Skull Base Institute for NASA's Jet Propulsion Labora-

tory. Further information is contained in a TSP (see page 1).

In accordance with Public Law 96-517, the contractor has elected to retain title to this invention. Inquiries concerning rights for its commercial use should be addressed to:

*Innovative Technology Assets Management
JPL*

Mail Stop 202-233

4800 Oak Grove Drive

Pasadena, CA 91109-8099

E-mail: iaoffice@jpl.nasa.gov

Refer to NPO-45579, volume and number of this NASA Tech Briefs issue, and the page number.

UV-Resistant Non-Spore-Forming Bacteria From Spacecraft-Assembly Facilities

NASA's Jet Propulsion Laboratory, Pasadena, California

Four species of non-spore-forming bacteria collected from clean-room surfaces in spacecraft-assembly facilities could survive doses of ultraviolet (UV) radiation that would suffice to kill most known cultivable bacterial species. In a previous study, high UV resistance was found in spores of the SAFR-032 strain of *Bacillus pumilus*, as reported in "Ultraviolet-Resistant Bacterial Spores," *NASA Tech Briefs*, Vol. 31, No. 9 (September 2007), page 94. These studies are parts of a continuing effort to understand the

survival of hardy species of bacteria under harsh conditions, and develop means of sterilizing spacecraft to prevent biocontamination of Mars that could in turn interfere with future life detection missions.

The four species investigated were *Arthrobacter* sp. KSC_Ak2i, *Microbacterium schleiferi* LMA_AkK1, *Brevundimonas diminuta* KSC_Ak3a, and *Sphingomonas trueperi* JSC_Ak7-3. In the study, cells of these species were mixed into Atacama Desert soil (to elucidate the shadowing

effect of soil particles) and the resulting mixtures were tested both in solution and in a desiccated state under simulated Martian atmospheric and UV conditions. The UV-survival indices of *Arthrobacter* sp. and *Microbacterium schleiferi* were found to be comparable to those of *Bacillus pumilus* spores.

This work was done by Kasthuri Venkateswaran and Shariff Osman of Caltech for NASA's Jet Propulsion Laboratory. For more information, contact iaoffice@jpl.nasa.gov. NPO-45739



Hard-X-Ray/Soft-γ-Ray Imaging Sensor Assembly for Astronomy

A pixilated scintillator is coupled with an array of avalanche photodiodes.

Goddard Space Flight Center, Greenbelt, Maryland

An improved sensor assembly has been developed for astronomical imaging at photon energies ranging from 1 to 100 keV. The assembly includes a thallium-doped cesium iodide scintillator divided into pixels and coupled to an array of high-gain avalanche photodiodes (APDs). Optionally, the array of APDs can be operated without the scintillator to detect photons at energies below 15 keV. The array of APDs is connected to compact electronic readout circuitry that includes, among other things, 64 independent channels for detection of photons in various energy ranges, up to a maximum energy of 100

keV, at a count rate up to 3 kHz. The readout signals are digitized and processed by imaging software that performs “on-the-fly” analysis.

The sensor assembly has been integrated into an imaging spectrometer, along with a pair of coded apertures (Fresnel zone plates) that are used in conjunction with the pixel layout to implement a shadow-masking technique to obtain relatively high spatial resolution without having to use extremely small pixels. Angular resolutions of about 20 arc-seconds have been measured. Thus, for example, the imaging spectrometer can be used to (1) deter-

mine both the energy spectrum of a distant x-ray source and the angular deviation of the source from the nominal line of sight of an x-ray telescope in which the spectrometer is mounted or (2) study the spatial and temporal development of solar flares, repeating γ-ray bursters, and other phenomena that emit transient radiation in the hard-x-ray/soft-γ-ray region of the electromagnetic spectrum.

This work was done by Richard A. Myers of Radiation Monitoring Devices, Inc. for Goddard Space Flight Center. Further information is contained in a TSP (see page 1). GSC-14853-1

Simplified Modeling of Oxidation of Hydrocarbons

Only a few dozen molecular and radical species are included in calculations.

NASA's Jet Propulsion Laboratory, Pasadena, California

A method of simplified computational modeling of oxidation of hydrocarbons is undergoing development. This is one of several developments needed to enable accurate computational simulation of turbulent, chemically reacting flows. At present, accurate computational simulation of such flows is difficult or impossible in most cases because (1) the numbers of grid points needed for adequate spatial resolution of turbulent flows in realistically complex geometries are beyond the capabilities of typical supercomputers now in use and (2) the combustion of typical hydrocarbons proceeds through decomposition into hundreds of molecular species interacting through thousands of reactions. Hence, the combination of detailed reaction-rate models with the fundamental flow equations yields flow models that are computationally prohibitive. Hence, further, a reduction of at least an order of magnitude in the dimension of reaction kinetics is one of the prerequisites for feasibility of computational simulation of turbulent, chemically reacting flows.

In the present method of simplified modeling, all molecular species involved

in the oxidation of hydrocarbons are classified as either light or heavy; heavy molecules are those having 3 or more carbon atoms. The light molecules are not subject to meaningful decomposition, and the heavy molecules are considered to decompose into only 13 specified constituent radicals, a few of which are listed in the table. One constructs a reduced-order model, suitable for use in estimating the release of heat and the evolution of temperature in combustion, from a base comprising the 13 constituent radicals plus a total of 26 other species that include the light molecules

and related light free radicals. Then rather than following all possible species through their reaction coordinates, one follows only the reduced set of reaction coordinates of the base.

The behavior of the base was examined in test computational simulations of the combustion of heptane in a stirred reactor at various initial pressures ranging from 0.1 to 6 MPa. Most of the simulations were performed for stoichiometric mixtures; some were performed for fuel/oxygen mole ratios of 1/2 and 2. The following are among the conclusions drawn from the results of these simulations:

Constituent Radical	δh^0	δh^c	δh^f
CH ₃ (methyl)	-42.0	714	188
CH ₂ (methylene)	-20.8	614.3	411
CH (methylidyne)	≈ -7	≈ 507	≈ 603
C ₂ H ₃ (vinyl)	62.5	1212	237

Some of the Constituent Radicals included in the simplified model are listed with some of their pertinent thermodynamic properties. The listed properties, all in units of kilojoules per mole, are the heat of formation (δh^0), the heat of combustion (δh^c), and the heat of component-to-free transition (δh^f). Other pertinent properties, omitted for the sake of simplicity, are coefficients in an equation for partial molar heat capacity as a function of temperature.

- The release of heat in combustion of heptane is modeled adequately.
- A simplified, low-dimensional chemistry model depends on an adequate representation of a reduced rate set. The net constituent rate is nearly quasi-steady and can be split into an incubation zone of modest temperature rise followed by a fast-reaction zone of high temperature.
- The incubation region is characterized by reaction times of the order of milliseconds — similar to diffusion time scales. Therefore, chemistry is expected to be significantly coupled with flow processes

during incubation. This coupling gives rise to several issues that must be resolved in further development of a simplified model.

- In the fast-reaction zone, the coupling between chemistry and flow processes is weak, and combustion is determined primarily by the mixing rate. The temperature profiles in the fast-reaction zone tend to be independent of the details of behavior during incubation.

The development of the model is not yet complete. To close the model

system of equations, it will be necessary to determine effective mean source strengths for light molecules and light radicals resulting from decomposition of heavy molecules. The final model will thus focus on reactions of the light species; the necessary rates are expected to be well determined insofar as kinetic interactions among light species prevail.

This work was done by Josette Bellan and Kenneth Harstad of Caltech for NASA's Jet Propulsion Laboratory. Further information is contained in a TSP (see page 1). NPO-44750

Near-Field Spectroscopy With Nanoparticles Deposited by AFM

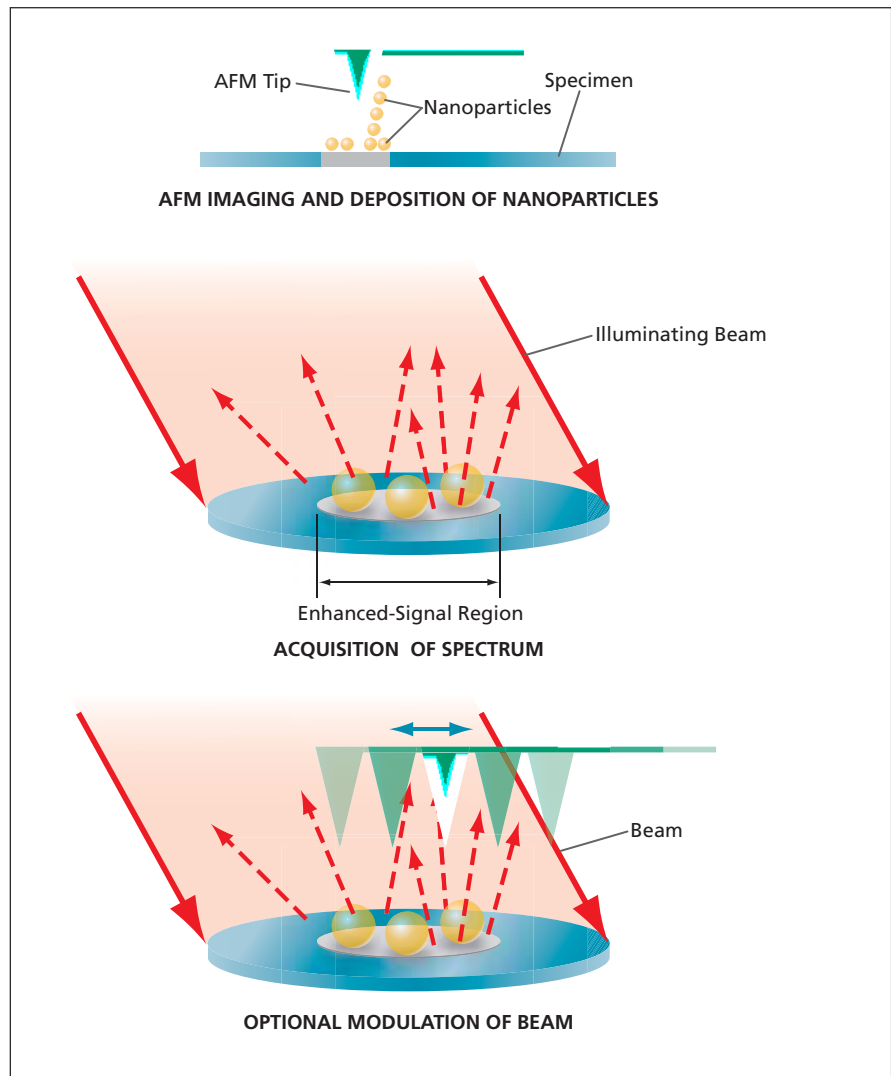
It is not necessary to integrate an AFM with a spectrometer.

NASA's Jet Propulsion Laboratory, Pasadena, California

An alternative approach to apertureless near-field optical spectroscopy involving an atomic-force microscope (AFM) entails less complexity of equipment than does a prior approach. The alternative approach has been demonstrated to be applicable to apertureless near-field optical spectroscopy of the type using an AFM and surface enhanced Raman scattering (SERS), and is expected to be equally applicable in cases in which infrared or fluorescence spectroscopy is used.

Apertureless near-field optical spectroscopy is a means of performing spatially resolved analyses of chemical compositions of surface regions of nanostructured materials. In apertureless near-field spectroscopy, it is common practice to utilize nanostructured probe tips or nanoparticles (usually of gold) having shapes and dimensions chosen to exploit plasmon resonances so as to increase spectroscopic-signal strengths. To implement the particular prior approach to which the present approach is an alternative, it is necessary to integrate a Raman spectrometer with an AFM and to utilize a special SERS-active probe tip. The resulting instrumentation system is complex, and the tasks of designing and constructing the system and using the system to acquire spectro-chemical information from nanometer-scale regions on a surface are correspondingly demanding.

In the present alternative approach, unlike in the prior approach, one does not integrate a spectrometer with the AFM; that is, the spectrometer and the



An AFM Tip Is Used to both image a specimen surface and deposit gold nanoparticles at a location of interest on the surface. Optionally, the tip can be moved through a spectrometer beam to modulate the light.

AFM are separate instruments. Moreover, instead of using a special SERS-active AFM/spectrometer probe tip, one fabricates SERS-active regions at locations of interest on the specimen surface by using an AFM tip to deposit gold nanoparticles at those locations.

The first step is to image the specimen by use of the AFM to establish the locations of interest for high-resolution spectro-chemical analysis. Then SERS-active regions are fabricated at those locations by a form of dip-pen nanolithography: The AFM tip is dipped into a colloidal gold solution and used to de-

posit a single gold nanoparticle or a cluster of gold nanoparticles at each affected location (see figure). Then the AFM is disengaged, the deposited nanoparticles are illuminated in the spectrometer excitation beam, and the locally enhanced spectrum is acquired. Optionally, the AFM tip or the cantilever on which it is mounted can be moved above the deposited nanoparticles to modulate the light to enhance discrimination between the particle-enhanced components of the signal and the components from illuminated areas surrounding the particles.

This work was done by Mark S. Anderson of Caltech for NASA's Jet Propulsion Laboratory.

In accordance with Public Law 96-517, the contractor has elected to retain title to this invention. Inquiries concerning rights for its commercial use should be addressed to:

*Innovative Technology Assets Management
JPL*

Mail Stop 202-233

4800 Oak Grove Drive

Pasadena, CA 91109-8099

E-mail: iaoffice@jpl.nasa.gov

Refer to NPO-44033, volume and number of this NASA Tech Briefs issue, and the page number.

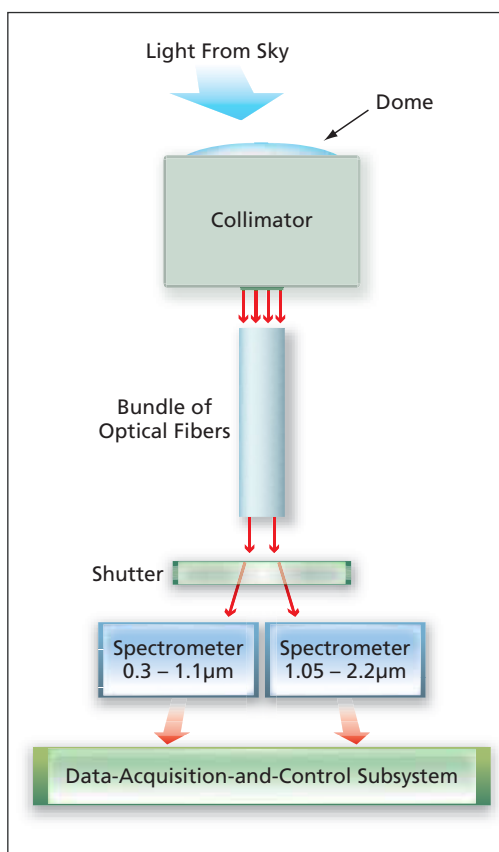
Light Collimator and Monitor for a Spectroradiometer

This system handles the optical input and electronic output of two spectrometers.

Ames Research Center, Moffett Field, California

A system that comprises optical and electronic subsystems has been developed as an infrastructure for a spectroradiometer that measures time-dependent spectral radiance of the daylight sky, in a narrow field of view (having angular width of the order of 1°) centered on the zenith, in several spectral bands in the wavelength range from 0.3 to 2.2 μm . This system is used in conjunction with two commercially available monolithic spectrometers: a silicon-based one for wavelengths from 0.3 to 1.1 μm and a gallium arsenide-based one for wavelengths from 1.05 to 2.2 μm (see figure). The role of this system is to collect the light from the affected region of the sky, collimate the light, deliver the collimated light to the monolithic spectrometers, and process the electronic outputs of the spectrometers.

This system includes a dome that faces the sky. Light collected via the dome passes through a collimator that has an aperture diameter ≈ 22 mm, a focal length ≈ 50 mm, and a field-of-view angular width that is adjustable between 1° and 2° . The collimated light enters a bundle of optical fibers that are chosen to have small numerical apertures so as to further limit the acceptance angle of received light. After propagating along the bundle of optical fibers, the light encounters a shutter that is operated on a controlled cycle, during which the shutter is alternately open for a time t_1 , then closed for a time t_2 . The cycle frequency can be 5 Hz or any suit-



The **Spectroradiometer** comprises optical and electronic subsystems that include two spectrometers operating in conjunction with the system described in the text.

able lower frequency; in practice, the cycle frequency (and, hence, the associated sampling frequency) is typically chosen to be 1 Hz.

When the shutter is open, light enters the monolithic spectrometer, electronic

circuits in the spectrometers pre-process the outputs of photodetectors (one photodetector for each wavelength band), and the outputs of the spectrometer electronic circuits for the various wavelength ranges are sent to a data-acquisition-and-control subsystem that is part of the present system. When the shutter is closed, the same process takes place, for the purpose of collecting dark-current readings from the photodetector of each wavelength band.

The data-acquisition-and-control subsystem digitizes the spectrometer outputs and further processes them to generate any or all of a variety of useful output data. Among other things, this subsystem subtracts shutter-closed (dark-current) readings from shutter-open readings to obtain corrected spectral-radiance readings. In addition to alternately opening and closing the shutter and taking dark-current readings during the t_2 portions of successive cycles, the system can be made to sample dark currents during longer periods (e.g., a dark period of 5 minutes during each hour) to enable identification of anomalies in this system and/or in the spectrometers.

This work was done by Warren Gore of Ames Research Center.

This invention is owned by NASA, and a patent application has been filed. Inquiries concerning rights for the commercial use of this invention should be addressed to the Ames Technology Partnerships Division at (650) 604-2954. Refer to ARC-15714-1.

Hyperspectral Fluorescence and Reflectance Imaging Instrument

A single system contains spatial-scanning, illumination, and spectral-imaging subsystems.

Stennis Space Center, Mississippi

The system is a single hyperspectral imaging instrument that has the unique capability to acquire both fluorescence and reflectance high-spatial-resolution data that is inherently spatially and spectrally registered. Potential uses of this instrument include plant stress monitoring, counterfeit document detection, biomedical imaging, forensic imaging, and general materials identification.

Until now, reflectance and fluorescence spectral imaging have been performed by separate instruments. Neither a reflectance spectral image nor a fluorescence spectral image alone yields as much information about a target surface as does a combination of the two modalities. Before this system was developed, to benefit from this combination, analysts needed to perform time-consuming post-processing efforts to co-register the reflective and fluorescence information. With this instrument, the inherent spatial and spectral registration of the reflectance and fluorescence images minimizes the need for this post-processing step.

The main challenge for this technology is to detect the fluorescence signal in the presence of a much stronger reflectance signal. To meet this challenge, the instrument modulates artificial light sources from ultraviolet through the visible to the near-infrared part of the spectrum; in this way, both the reflective and

fluorescence signals can be measured through differencing processes to optimize fluorescence and reflectance spectra as needed.

The main functional components of the instrument are a hyperspectral imager, an illumination system, and an image-plane scanner. The hyperspectral imager is a one-dimensional (line) imaging spectrometer that includes a spectrally dispersive element and a two-dimensional focal plane detector array. The spectral range of the current imaging spectrometer is between 400 to 1,000 nm, and the wavelength resolution is approximately 3 nm. The illumination system consists of narrowband blue, ultraviolet, and other discrete wavelength light-emitting-diode (LED) sources and white-light LED sources designed to produce consistently spatially stable light. White LEDs provide illumination for the measurement of reflectance spectra, while narrowband blue and UV LEDs are used to excite fluorescence. Each spectral type of LED can be turned on or off depending on the specific remote-sensing process being performed. Uniformity of illumination is achieved by using an array of LEDs and/or an integrating sphere or other diffusing surface. The image plane scanner uses a fore optic with a field of view large enough to provide an entire scan line on the image plane. It builds up a two-dimensional image in

pushbroom fashion as the target is scanned across the image plane either by moving the object or moving the fore optic.

For fluorescence detection, spectral filtering of a narrowband light illumination source is sometimes necessary to minimize the interference of the source spectrum wings with the fluorescence signal. Spectral filtering is achieved with optical interference filters and absorption glasses. This dual spectral imaging capability will enable the optimization of reflective, fluorescence, and fused datasets as well as a cost-effective design for multispectral imaging solutions. This system has been used in plant stress detection studies and in currency analysis.

This work was done by Robert E. Ryan and S. Duane O'Neal of Science Systems and Applications, Inc.; Mark Lanoue of the Institute for Technology Development; and Jeffrey Russell of Computer Sciences Corporation for Stennis Space Center.

Inquiries concerning rights for its commercial use should be addressed to:

*Institute For Technology Development
Stennis Space Center
Bldg. 1103, Suite 118
Stennis Space Center, MS 39529
E-mail: Mark.Lanoue@iftd.org
Phone No.: (228) 688-2509*

Refer to SSC-00254, volume and number of this NASA Tech Briefs issue, and the page number.

Improving the Optical Quality Factor of the WGM Resonator

New iterative annealing and polishing increases the resonator's finesse over the fundamental limit.

NASA's Jet Propulsion Laboratory, Pasadena, California

Resonators usually are characterized with two partially dependent values: finesse (\mathcal{F}) and quality factor (Q). The finesse of an empty Fabry-Perot (FP) resonator is defined solely by the quality of its mirrors and is calculated as

$$\mathcal{F} = \pi R^{1/2} / (1 - R).$$

The maximum up-to-date value of reflectivity $R \approx 1 - 1.6 \times 10^{-6}$ is achieved with dielectric mirrors. An FP resonator made with the mirrors has finesse $\mathcal{F} = 1.9 \times 10^6$. Further practical increase of the finesse of

FP resonators is problematic because of the absorption and the scattering of light in the mirror material through fundamental limit on the reflection losses given by the internal material losses and by thermodynamic density fluctuations on the order of parts in 10^9 . The quality factor of a resonator depends on both its finesse and its geometrical size. A one-dimensional FP resonator has $Q = 2 \mathcal{F} L / \lambda$, where L is the distance between the mirrors and λ is the wavelength. It is easy to see that the quality fac-

tor of the resonator is unlimited because L is unlimited. \mathcal{F} and Q are equally important.

In some cases, finesse is technically more valuable than the quality factor. For instance, buildup of the optical power inside the resonator, as well as the Purcell factor, is proportional to finesse. Sometimes, however, the quality factor is more valuable. For example, inverse threshold power of intracavity hyperparametric oscillation is proportional to Q^2 and efficiency of parametric fre-

quency mixing is proportional to Q^2 . Therefore, it is important to know both the maximally achievable finesse and quality factor values of a resonator.

Whispering gallery mode (WGM) resonators are capable of achieving larger finesse compared to FP resonators. For instance, fused silica resonators with finesse 2.3×10^6 and 2.8×10^6 have been demonstrated. Crystalline WGM resonators reveal even larger finesse values, $\mathcal{F} = 6.3 \times 10^6$, because of low attenuation of light in the transparent optical crystals. The larger values of \mathcal{F} and Q result in the enhancement of various nonlinear processes. Low-threshold Raman lasing, optomechanical oscillations, frequency doubling, and hyper-

parametric oscillations based on these resonators have been recently demonstrated. Theory predicts a possibility of nearly 10^{14} room-temperature optical Q -factors of optical crystalline WGM resonators, which correspond to finesse levels higher than 10^9 . Experiments have shown numbers a thousand times lower than that. The difference occurs due to media imperfections.

To substantially reduce the optical losses caused by the imperfections, a specific, multi-step, asymptotic processing of the resonator is implemented. The technique has been initially developed to reduce microwave absorption in dielectric resonators. One step of the process consists of mechanical polishing

performed after high temperature annealing. Several steps repeat one after another to lead to significant reduction in optical attenuation and, as a result, to the increase of Q -factor as well as finesse of the resonator which demonstrates a CaF_2 WGM resonator with $\mathcal{F} > 10^7$ and $Q > 10^{11}$.

This work was done by Lute Maleki of OE Waves and Anatoliy Savchenkov, Andrey Matsko, and Vladimir Ilchenko of Caltech for NASA's Jet Propulsion Laboratory.

This invention is owned by NASA, and a patent application has been filed. Inquiries concerning nonexclusive or exclusive license for its commercial development should be addressed to the Patent Counsel, NASA Management Office-JPL. Refer to NPO-45053.

Ultra-Stable Beacon Source for Laboratory Testing of Optical Tracking

A prototype laser beacon assembly provides reference for testing tracking and pointing systems.

NASA's Jet Propulsion Laboratory, Pasadena, California

The ultra-stable beacon source (USBS) provides a laser-beam output with a very low angular jitter and can be used as an absolute angular reference to simulate a beacon in the laboratory. The laser is mounted on the top of a very short (≈ 1 m) inverted pendulum (IP) with its optical axis parallel to the carbon fiber pendulum leg. The 85-cm, carbon fiber rods making up the leg are very lightweight and rigid, and are supported by a flex-joint at the bottom (see figure). The gimbal-mounted laser is a weight-adjustable load of about 1.5 kg with its center of rotation co-located with the center of percussion of the inverted pendulum. This reduces the coupling of transverse motion at the base of the pendulum to angular motion of the laser at the top.

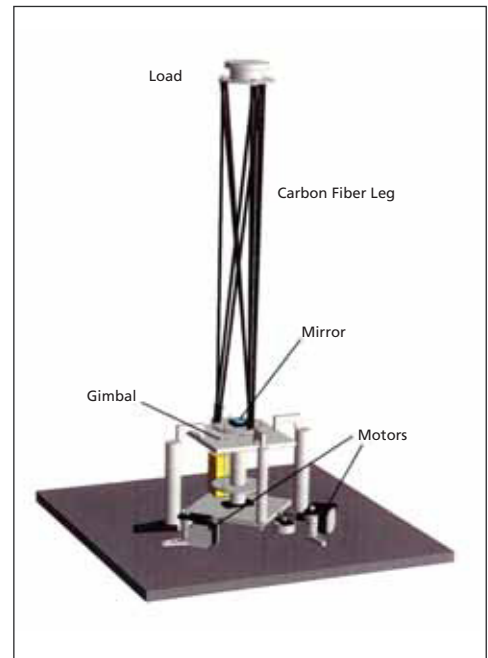
The inverted pendulum is mounted on a gimbal with its center of rotation coinciding with the pivot position of the inverted pendulum flexure joint. This reduces coupling of ground tilt at the inverted pendulum base to motion of the laser mounted at the top. The mass of the top gimbal is adjusted to give the pendulum a very low resonant frequency (≈ 10 mHz) that filters transverse seismic disturbances from the ground where the base is attached.

The motion of the IP is monitored by an optical-lever sensor. The laser light is reflected by the mirror on the IP, and

then is detected by a quadrant photo-detector (QPD). The position of the beam spot on the QPD corresponds to the tilt of the IP. Damping of this motion is provided by two coil and magnet pairs.

The bottom gimbal mount consists of two plates. The IP is mounted on the second plate. The first plate is supported by two posts through needles and can be rotated about the axis connecting the tips of the needles. The second plate hangs from the first plate and can be rotated about the axis perpendicular to the first plate. As a result, the second plate acts as a two-axis rotation stage. Its center of rotation is located at the effective bending point of the flex-joint. The second plate is pressed against two screw actuators by the weight of the IP. The screw actuators are orthogonal to each other and are used to adjust the inclination of the second plate. The actuators are driven by stepper motors.

The whole IP system is housed in a box made of Lexan plastic plates to provide isolation from air currents and temperature variations. The signals from the sensors are processed and recorded with a PC using the xPC Target realtime environment of MathWorks. The control algorithms are writ-



In the **Inverted Pendulum** configuration, an additional gimbal is mounted at the top with a laser at the center of rotation. The laser provides the outgoing beacon source.

ten using the Simulink package from The MathWorks.

This work was done by Yoichi Aso and Szabolcs Marka of Columbia University and Joseph Kovalik of Caltech for NASA's Jet Propulsion Laboratory. Further information is contained in a TSP (see page 1). NPO-45127.

Transmissive Diffractive Optical Element Solar Concentrators

These would weigh and cost less than do mirror-type solar concentrators.

NASA's Jet Propulsion Laboratory, Pasadena, California

Solar-thermal-radiation concentrators in the form of transmissive diffractive optical elements (DOEs) have been proposed as alternatives to mirror-type solar concentrators now in use. In comparison with functionally equivalent mirror-type solar concentrators, the transmissive, diffractive solar concentrators would weigh and cost less, and would be subject to relaxed mechanical tolerances.

A DOE concentrator would be made from a thin, flat disk or membrane of a transmissive material having a suitable index of refraction. By virtue of its thinness, the DOE concentrator would have an areal mass density significantly less than that of a functionally equivalent conventional mirror.

The DOE concentrator would have a relatively wide aperture — characterized by a focal-length/aperture-diameter ratio ("f number") on the order of 1. A

kinofrom (a surface-relief phase hologram) of high diffractive order would be microfabricated onto one face of the disk. The kinofrom (see figure) would be designed to both diffract and refract incident solar radiation onto a desired focal region, without concern for forming an image of the Sun. The high diffractive order of this kinofrom (in contradistinction to the low diffractive orders of some other kinofroms) would be necessary to obtain the desired f number of 1, which, in turn, would be necessary for obtaining a desired concentration ratio of 2,500 or greater.

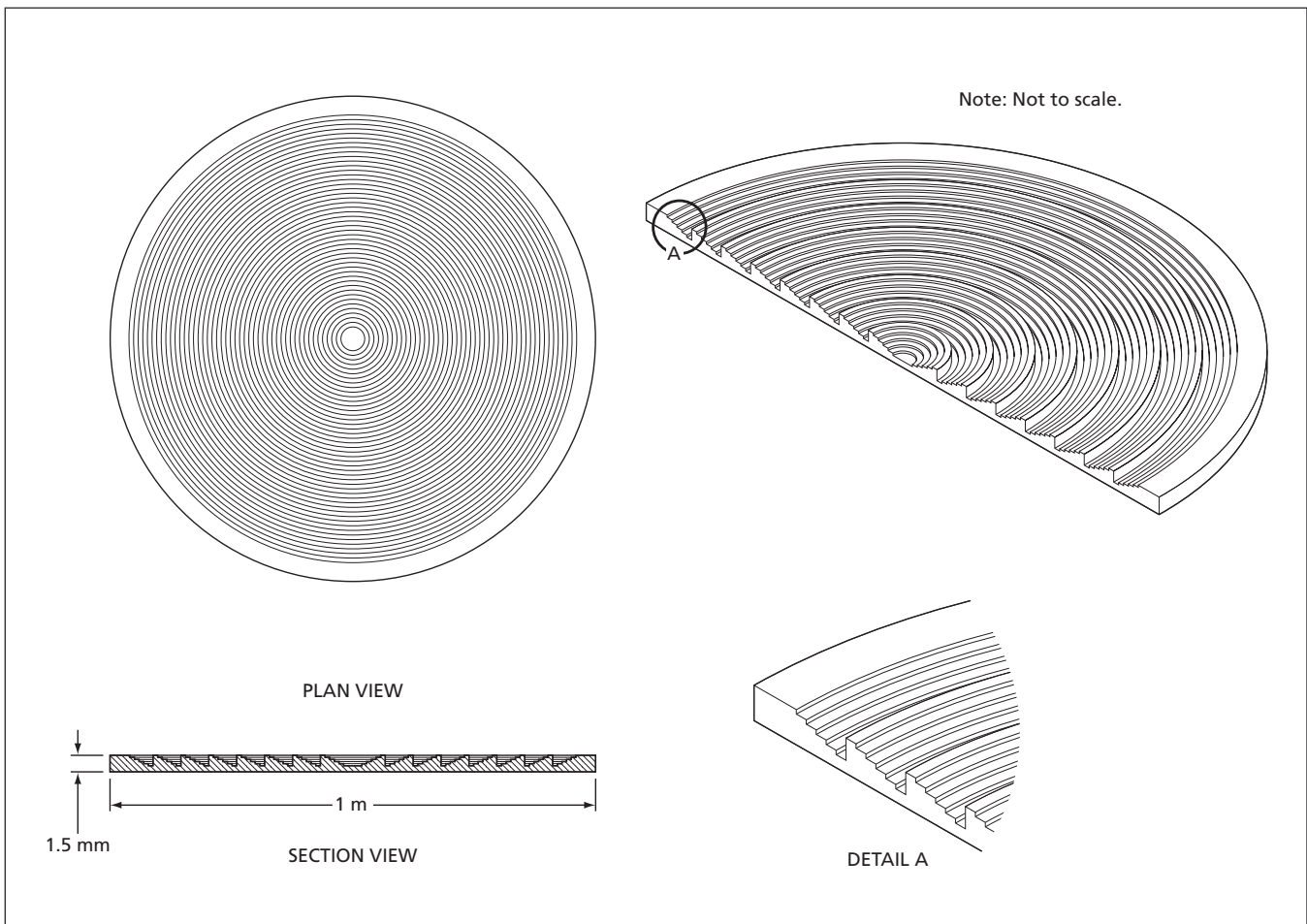
The design process of optimizing the concentration ratio of a proposed DOE solar concentrator includes computing convolutions of the optical bandwidth of the Sun with the optical transmission of the diffractive medium. Because, as in the cases of other non-imaging, light-

concentrating optics, image quality is not a design requirement, the process also includes trading image quality against concentration ratio.

A baseline design for one example calls for an aperture diameter of 1 m. This baseline design would be scalable to a diameter as large as 10 m, or to a smaller diameter for a laboratory test article. Initial calculations have indicated that the characteristics of the test article would be readily scalable to a full-size unit.

This work was done by Richard Baron, Philip Moynihan, and Douglas Price of Caltech for NASA's Jet Propulsion Laboratory. Further information is contained in a TSP (see page 1).

This invention is owned by NASA, and a patent application has been filed. Inquiries concerning nonexclusive or exclusive license for its commercial development should be addressed to the Patent Counsel, NASA Management Office-JPL. Refer to NPO-43801.



A DOE Solar Concentrator should not be confused with a Fresnel lens, which it partly resembles. The DOE is a non-imaging optic designed to exploit both diffraction and refraction to obtain a high concentration ratio.

Delaying Trains of Short Light Pulses in WGM Resonators

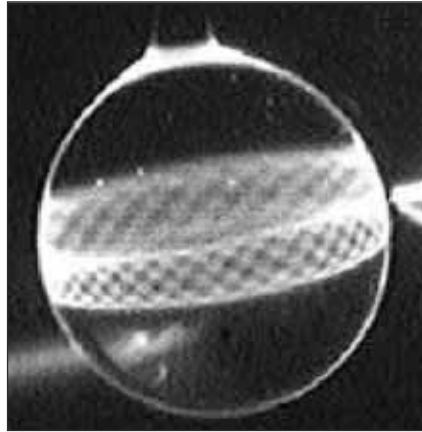
Delays would not be limited by resonator ring-down times.

NASA's Jet Propulsion Laboratory, Pasadena, California

Suitably configured whispering-gallery-mode (WGM) optical resonators have been proposed as delay lines for trains of short light pulses. Until now, it has been common practice to implement an optical delay line as a coiled long optical fiber, which is bulky and tends to be noisy. An alternative has been to implement an optical delay line as a coupled-resonator optical waveguide (a chain of coupled optical resonators), which is compact but limits the width of the pulse spectrum to the width of an optical resonance and thereby places a lower limit on the duration of a pulse. In contrast, a delay line according to the proposal could be implemented as a single WGM resonator, and the pulses delayed by the resonator could be so short that their spectral widths could greatly exceed the spectral width of any single resonance.

The proposal emerged from theoretical and experimental studies of the propagation of a pulse train in a WGM resonator. An important element of the theoretical study was recognition that the traditional definition of group velocity — in effect, the velocity of a single pulse comprising a packet of waves propagating in a medium, the responsivity of which is a monotonous function of frequency — does not necessarily apply in the case of a WGM resonator or other medium having a spectrum consisting of discrete resonance peaks at different frequencies. A new definition of group ve-

locity, applicable to a train of pulses propagating in such a medium, was introduced and found to lead to the discovery of previously unknown features



A **Stationary Fluorescence Pattern** represents the intensity of interfering traveling light waves in a carefully selected combination of WGM modes in a microsphere optical resonator.

of propagation.

Notably, it was found that in a microsphere optical resonator that supports a suitable combination of WGM modes, the group velocity for a train of light pulses could be positive, zero, or negative. A positive group velocity could be so small that the delay could be much longer than the ring-down time of the resonator; a delay of such great length is impossible for a single pulse interacting with either a linearly responding lossless resonator or a coupled-resonator optical waveguide.

The phenomenon of “stopped light,” which corresponds to a group velocity of zero (and, hence, to infinite delay), was demonstrated in experiments on a fused-silica microsphere of 300- μm diameter. Light from a diode laser at a nominal wavelength of 635 nm was swept through a 5-GHz frequency range at a repetition rate of 20 Hz and coupled into the resonator via an angle-cut optical fiber. The resonator was immersed in a solution containing a dye that fluoresces in response to evanescent-wave coupling of light from the WGM surface modes. When the tip of the angle-cut optical fiber was positioned and oriented to excite suitable combinations of WGM modes, stationary fluorescence patterns were observed (see figure).

This work was done by Andrey Matsko, Vladimir Ilchenko, Dmitry Strelakov, Anatoly Savchenkov, and Lute Maleki of Caltech for NASA's Jet Propulsion Laboratory.

In accordance with Public Law 96-517, the contractor has elected to retain title to this invention. Inquiries concerning rights for its commercial use should be addressed to:

*Innovative Technology Assets Management
JPL*

*Mail Stop 202-233
4800 Oak Grove Drive
Pasadena, CA 91109-8099*

E-mail: iaoffice@jpl.nasa.gov

Refer to NPO-44956, volume and number of this NASA Tech Briefs issue, and the page number.



➤ Toward Better Modeling of Supercritical Turbulent Mixing

NASA's Jet Propulsion Laboratory, Pasadena, California

A study was done as part of an effort to develop computational models representing turbulent mixing under thermodynamic supercritical (here, high pressure) conditions. The question was whether the large-eddy simulation (LES) approach, developed previously for atmospheric-pressure compressible-perfect-gas and incompressible flows, can be extended to real-gas non-ideal (including supercritical) fluid mixtures. [In LES, the governing equations are approximated such that the flow field is spatially filtered and subgrid-scale (SGS) phenomena are represented by

models.] The study included analyses of results from direct numerical simulation (DNS) of several such mixing layers based on the Navier-Stokes, total-energy, and conservation-of-chemical-species governing equations.

Comparison of LES and DNS results revealed the need to augment the atmospheric-pressure LES equations with additional SGS momentum and energy terms. These new terms are the direct result of high-density-gradient-magnitude regions found in the DNS and observed experimentally under fully turbulent flow condi-

tions. A model has been derived for the new term in the momentum equation and was found to perform well at small filter size but to deteriorate with increasing filter size. Several alternative models were derived for the new SGS term in the energy equation that would need further investigations to determine if they are too computationally intensive in LES.

This work was done by Laurent Selle, Nora Okong'o, Josette Bellan, and Kenneth Harstad, of Caltech for NASA's Jet Propulsion Laboratory. For more information, contact iaoffice@jpl.nasa.gov. NPO-44402

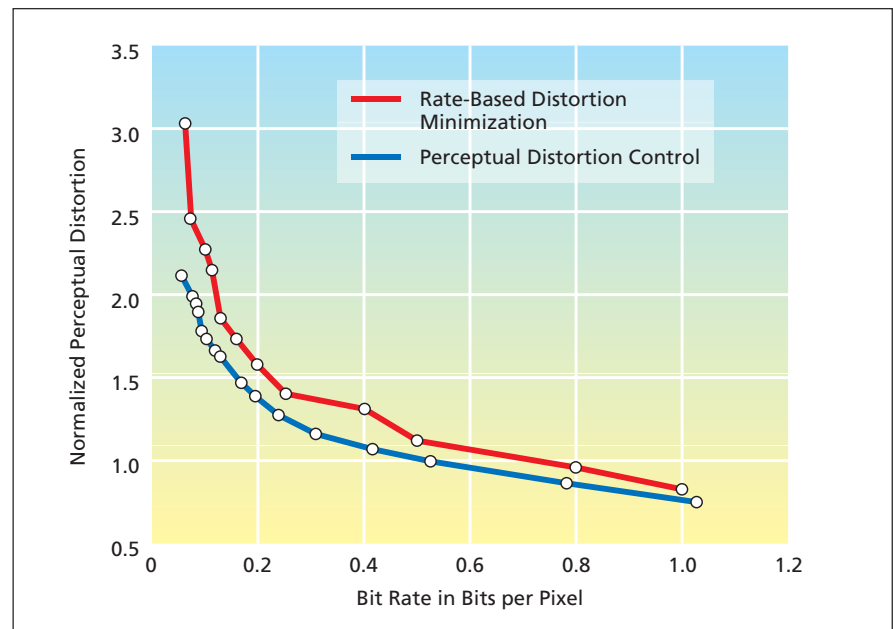
➤ JPEG 2000 Encoding With Perceptual Distortion Control

The bit rate for a given level of perceptual distortion is minimized.

Ames Research Center, Moffett Field, California

An alternative approach has been devised for encoding image data in compliance with JPEG 2000, the most recent still-image data-compression standard of the Joint Photographic Experts Group. Heretofore, JPEG 2000 encoding has been implemented by several related schemes classified as rate-based distortion-minimization encoding. In each of these schemes, the end user specifies a desired bit rate and the encoding algorithm strives to attain that rate while minimizing a mean squared error (MSE). While rate-based distortion minimization is appropriate for transmitting data over a limited-bandwidth channel, it is not the best approach for applications in which the perceptual quality of reconstructed images is a major consideration. A better approach for such applications is the present alternative one, denoted perceptual distortion control, in which the encoding algorithm strives to compress data to the lowest bit rate that yields at least a specified level of perceptual image quality.

Some additional background information on JPEG 2000 is prerequisite to a meaningful summary of JPEG encoding with perceptual distortion control. The JPEG 2000 encoding process includes two subprocesses known as tier-1 and



The Normalized Perceptual Distortion in compressed data from a test image were computed for compression by a JPEG 2000 perceptual-distortion-control and a JPEG 2000 rate-based distortion-minimization encoding algorithm.

tier-2 coding. In order to minimize the MSE for the desired bit rate, a rate-distortion-optimization subprocess is introduced between the tier-1 and tier-2 subprocesses. In tier-1 coding, each coding

block is independently bit-plane coded from the most-significant-bit (MSB) plane to the least-significant-bit (LSB) plane, using three coding passes (except for the MSB plane, which is coded using

only one “clean up” coding pass). For M bit planes, this subprocess involves a total number of $(3M - 2)$ coding passes. An embedded bit stream is then generated for each coding block. Information on the reduction in distortion and the increase in the bit rate associated with each coding pass is collected. This information is then used in a rate-control procedure to determine the contribution of each coding block to the output compressed bit stream.

In tier-2 coding, the results of those coding passes for each coding block that have not been discarded are organized into an output compressed bit stream. With a carefully optimized implementation of a discrete wavelength transform, the embedded block coding tends to dominate the whole encoding time; consequently, prior JPEG 2000 encoding algorithms waste computational power and memory on those coding passes that are eventually discarded. This concludes the background information.

A complete description of JPEG encoding with perceptual distortion control would greatly exceed the space available

for this article, making it necessary to summarize briefly: The multiresolution wavelet decomposition and the two-tier coding structure of JPEG 2000 are amenable to incorporation of perceptual distortion control. In the present approach, one strives to determine the number of coding passes needed for each coding block by use of a perceptual model of the human vision system. Then only that number of (and no more) coding passes need be made in the tier-1 encoding.

A basic idea of the use of the perceptual model of the human vision system is to hide the coding distortion beneath detection thresholds, typically by exploiting the masking properties of the human visual system and establishing detection thresholds of just-noticeable distortion and minimally noticeable distortion based on psychophysical experiments. Among the masking properties included in the model are luminance masking [also known as light adaptation (in which the detection threshold varies with background light intensity)] and contrast making (in which the visibility of an image component is affected by

other image components). The model also incorporates a perceptual distortion metric that takes account of spatial and spectral summations of quantization errors.

Experimental data have confirmed the expectation that in addition to yielding consistent image quality, JPEG 2000 encoding with perceptual distortion control makes it possible to do so at bit rates lower than those of JPEG 2000 rate-based distortion-minimization encoding. The figure presents comparative plots of such data, showing that the bit rate for a given level of normalized perceptual distortion is lower for perceptual distortion control.

This work was done by Andrew B. Watson of Ames Research Center and Zhen Liu and Lina J. Karam of Arizona State University. Further information is contained in a TSP (see page 1).

This invention is owned by NASA, and a patent application has been filed. Inquiries concerning rights for the commercial use of this invention should be addressed to the Ames Technology Partnerships Division at (650) 604-2954. Refer to ARC-15522-1.

Intelligent Integrated Health Management for a System of Systems

Intelligent elements exchange information and each determines its own condition.

Stennis Space Center, Mississippi

An intelligent integrated health management system (IIHMS) incorporates major improvements over prior such systems. The particular IIHMS is implemented for any system defined as a hierarchical distributed network of intelligent elements (HDNIE), comprising primarily: (1) an architecture (Figure 1), (2) intelligent elements, (3) a conceptual framework and taxonomy (Figure 2), and (4) and ontology that defines standards and protocols.

Some definitions of terms are prerequisite to a further brief description of this innovation:

- A system-of-systems (SoS) is an engineering system that comprises multiple subsystems (e.g., a system of multiple possibly interacting flow subsystems that include pumps, valves, tanks, ducts, sensors, and the like).
- “Intelligent” is used here in the sense of artificial intelligence. An intelligent element may be physical or virtual, it is network enabled, and it is able to man-

age data, information, and knowledge (DIaK) focused on determining its condition in the context of the entire SoS.

- As used here, “health” signifies the functionality and/or structural integrity of

an engineering system, subsystem, or process (leading to determination of the health of components).

- “Process” can signify either a physical process in the usual sense of the word

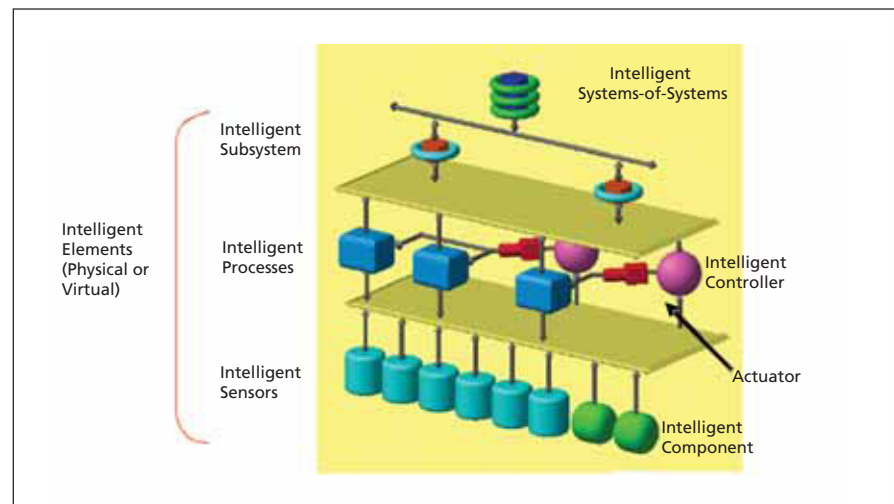


Figure 1. A Hierarchical Network of Distributed Intelligent Elements defines the architecture of the system described in the text.

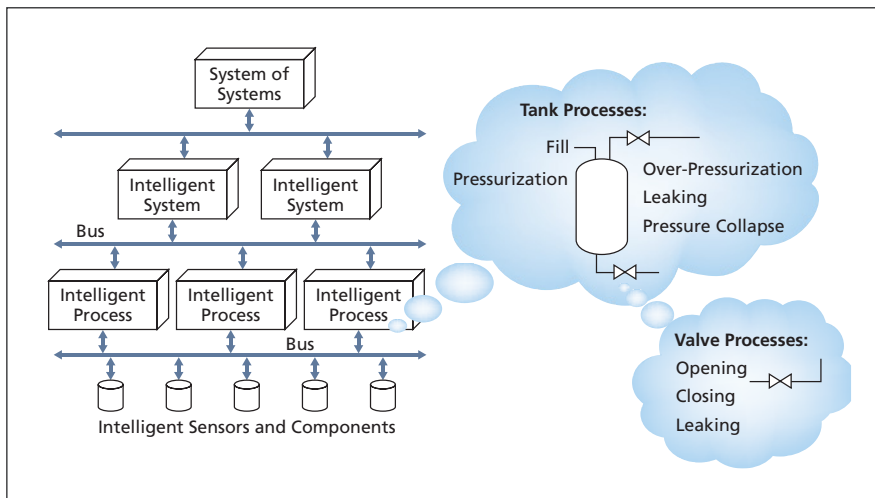


Figure 2. **Multiple Process Models** make possible an effective integrated approach.

or an element into which functionally related sensors are grouped.

- “Element” can signify a component (e.g., an actuator, a valve), a process, a controller, an actuator, a subsystem, or a system.
- The term Integrated System Health Management (ISHM) is used to describe a capability that focuses on determining the condition (health) of every element in a complex system (detect anomalies, diagnose causes, prognosis of future anomalies), and provide data, information, and knowledge (DIaK) — not just data — to control systems for safe and effective operation.

A major novel aspect of the present development is the concept of intelligent integration. The purpose of intelligent integration, as defined and implemented in the present IIHMS, is to enable automated analysis of physical phenomena in imita-

tion of human reasoning, including the use of qualitative methods. Intelligent integration is said to occur in a system in which all elements are intelligent and can acquire, maintain, and share knowledge and information.

In the HDNIE of the present IIHMS, an SoS is represented as being operationally organized in a hierarchical-distributed format. The elements of the SoS are considered to be intelligent in that they determine their own conditions within an integrated scheme that involves consideration of data, information, knowledge bases, and methods that reside in all elements of the system.

The conceptual framework of the HDNIE and the methodologies of implementing it enable the flow of information and knowledge among the elements so as to make possible the determination of the condition of each element. The necessary information and knowledge is

made available to each affected element at the desired time, satisfying a need to prevent information overload while providing context-sensitive information at the proper level of detail.

Provision of high-quality data is a central goal in designing this or any IIHMS. In pursuit of this goal, functionally related sensors are logically assigned to groups denoted processes. An aggregate of processes is considered to form a system. Alternatively or in addition to what has been said thus far, the HDNIE of this IIHMS can be regarded as consisting of a framework containing object models that encapsulate all elements of the system, their individual and relational knowledge bases, generic methods and procedures based on models of the applicable physics, and communication processes (Figure 2). The framework enables implementation of a paradigm inspired by how expert operators monitor the health of systems with the help of (1) DIaK from various sources, (2) software tools that assist in rapid visualization of the condition of the system, (3) analytical software tools that assist in reasoning about the condition, (4) sharing of information via network communication hardware and software, and (5) software tools that aid in making decisions to remedy unacceptable conditions or improve performance.

This work was done by Fernando Figueroa of Stennis Space Center, John Schmalzel of Rowan University, and Harvey Smith of Jacobs Sverdrup.

Inquiries concerning rights for the commercial use of this invention should be addressed to the Intellectual Property Manager, Stennis Space Center, (228) 688-1929. Refer to SSC-00234.

2 Delay Banking for Managing Air Traffic

Delay credits could be expended to gain partial relief from flow restrictions.

Ames Research Center, Moffett Field, California

Delay banking has been invented to enhance air-traffic management in a way that would increase the degree of fairness in assigning arrival, departure, and en-route delays and trajectory deviations to aircraft impacted by congestion in the national airspace system. In delay banking, an aircraft operator (airline, military, general aviation, etc.) would be assigned a numerical credit when any of their flights are delayed because of an air-traffic flow restriction. The operator could subsequently bid

against other operators competing for access to congested airspace to utilize part or all of its accumulated credit. Operators utilize credits to obtain higher priority for the same flight, or other flights operating at the same time, or later, in the same airspace, or elsewhere. Operators could also trade delay credits, according to market rules that would be determined by stakeholders in the national airspace system.

Delay banking would be administered by an independent third party who would

use delay banking automation to continually monitor flights, allocate delay credits, maintain accounts of delay credits for participating airlines, mediate bidding and the consumption of credits of winning bidders, analyze potential transfers of credits within and between operators, implement accepted transfers, and ensure fair treatment of all participating operators.

A flow restriction can manifest itself in the form of a delay in assigned takeoff time, a reduction in assigned airspace, a

change in the position for the aircraft in a queue of all aircraft in a common stream of traffic (e.g., similar route), a change in the planned altitude profile for an aircraft, or change in the planned route for the aircraft. Flow restrictions are typically imposed to mitigate traffic congestion at an airport or in a region of airspace, particularly congestion due to inclement weather, or the unavailability of a runway or region of airspace.

A delay credit would be allocated to an operator of a flight that has accepted, or upon which was imposed, a flow restriction. The amount of the credit would increase with the amount of delay caused by the flow restriction, the exact amount depending on which of several candidate formulas is eventually chosen. For example, according to one formula, there

would be no credit for a delay smaller than some threshold value (e.g., 30 seconds) and the amount of the credit for a longer delay would be set at the amount of the delay minus the threshold value. Optionally, the value of a delay credit could be made to decay with time according to a suitable formula (e.g., an exponential decay). Also, optionally, a transaction charge could be assessed against the value of a delay credit that an operator used on a flight different from the one for which the delay originated or that was traded with a different operator.

The delay credits accumulated by a given airline could be utilized in various ways. For example, an operator could enter a bid for priority handling in a new flow restriction that impacts one or more of the operator's flights; if the bid

were unsuccessful, all or a portion of the credit would be returned to the bidder. If the bid pertained to a single aircraft that was in a queue, delay credits could be consumed in moving the aircraft to an earlier position within the queue. In the case of a flow restriction involving a choice of alternate routes, planned altitude profile, aircraft spacing, or other non-queue flow restrictions, delay credits could be used to bid for an alternative assignment.

This work was done by Steve Green of Ames Research Center.

This invention is owned by NASA and a patent application has been filed. Inquiries concerning rights for the commercial use of this invention should be addressed to the Ames Technology Partnerships Division at (650) 604-2954. Refer to ARC-15392-1.

Σ Spline-Based Smoothing of Airfoil Curvatures

Spurious curvature oscillations and bumps are suppressed.

Langley Research Center, Hampton, Virginia

Constrained fitting for airfoil curvature smoothing (CFACS) is a spline-based method of interpolating airfoil surface coordinates (and, concomitantly, airfoil thicknesses) between specified discrete design points so as to obtain smoothing of surface-curvature profiles in addition to basic smoothing of surfaces. CFACS was developed in recognition of the fact that the performance of a transonic airfoil is di-

rectly related to both the curvature profile and the smoothness of the airfoil surface.

Older methods of interpolation of airfoil surfaces involve various compromises between smoothing of surfaces and exact fitting of surfaces to specified discrete design points. While some of the older methods take curvature profiles into account, they nevertheless sometimes yield unfavorable results, in-

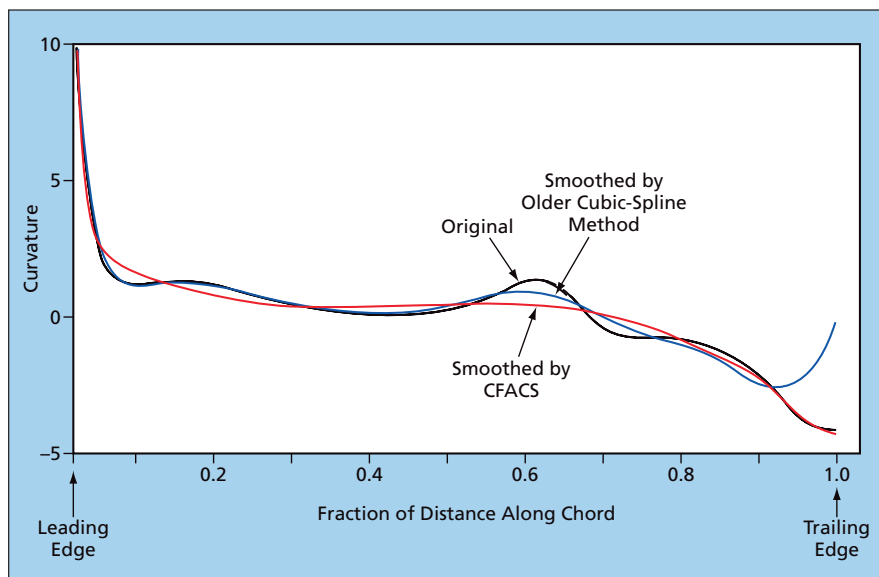
cluding curvature oscillations near end points and substantial deviations from desired leading-edge shapes.

In CFACS as in most of the older methods, one seeks a compromise between smoothing and exact fitting. Unlike in the older methods, the airfoil surface is modified as little as possible from its original specified form and, instead, is smoothed in such a way that the curvature profile becomes a smooth fit of the curvature profile of the original airfoil specification.

CFACS involves a combination of rigorous mathematical modeling and knowledge-based heuristics. Rigorous mathematical formulation provides assurance of removal of undesirable curvature oscillations with minimum modification of the airfoil geometry. Knowledge-based heuristics bridge the gap between theory and designers' best practices.

In CFACS, one of the measures of the deviation of an airfoil surface from smoothness is the sum of squares of the jumps in the third derivatives of a cubic-spline interpolation of the airfoil data. This measure is incorporated into a formulation for minimizing an overall deviation-from-smoothness measure of the airfoil data within a specified fitting error tolerance.

CFACS has been extensively tested on a number of supercritical airfoil data



Curvature Profiles were computed for the lower surface of a supercritical airfoil. The CFACS profile closely fits the original profile at the trailing edge, whereas the profile generated by the older cubic-spline smoothing method exhibits substantial bias away from the original profile at the trailing edge.

sets generated by inverse design and optimization computer programs. All of the smoothing results show that CFACS is able to generate unbiased smooth fits

of curvature profiles, trading small modifications of geometry for increasing curvature smoothness by eliminating curvature oscillations and bumps (see figure).

This work was done by W. Li and S. Krist of Langley Research Center. Further information is contained in a TSP (see page 1). LAR-17227-1

② Reducing Spaceborne-Doppler-Radar Rainfall-Velocity Error

NASA's Jet Propulsion Laboratory, Pasadena, California

A combined frequency-time (CFT) spectral moment estimation technique has been devised for calculating rainfall velocity from measurement data acquired by a nadir-looking spaceborne Doppler weather radar system. Prior spectral moment estimation techniques used for this purpose are based partly on the assumption that the radar resolution volume is uniformly filled with rainfall. The assumption is unrealistic in general but introduces negligible error in application to airborne radar systems. How-

ever, for spaceborne systems, the combination of this assumption and inhomogeneities in rainfall [denoted non-uniform beam filling (NUBF)] can result in velocity measurement errors of several meters per second.

The present CFT spectral moment estimation technique includes coherent processing of a series of Doppler spectra generated in a standard manner from data over measurement volumes that are partially overlapping in the along-track direction. Performance

simulation of this technique using high-resolution data from an airborne rain-mapping radar shows that a spaceborne Ku-band Doppler radar operating at signal-to-noise ratios >10 dB can achieve root-mean-square accuracy between 0.5 and 0.6 m/s in vertical-velocity estimates.

This work was done by Simone Tanelli, Eastwood Im, and Stephen L. Durden of Caltech for NASA's Jet Propulsion Laboratory. For more information, contact iaoffice@jpl.nasa.gov. NPO-40590



Progress in Acoustic Transmission of Power Through Walls

A document presents updated information on implementation of the wireless acoustic-electric feed-through (WAEF) concept, which was reported in "Using Piezoelectric Devices To Transmit Power Through Walls" (NPO-41157), *NASA Tech Briefs*, Vol. 32, No. 6 (June 2008), page 70. To recapitulate: In a basic WAEF setup, a transmitting piezoelectric transducer on one side of a wall is driven at resonance to excite ultrasonic vibrations in the wall. A receiving piezoelectric transducer on the opposite side of the wall converts the vibrations back to an ultrasonic AC electric signal, which is then detected and otherwise processed in a manner that depends on the modulation (if any) applied to the signal and whether the signal is used to transmit power, data, or both.

The present document expands upon the previous information concerning underlying physical principles, advantages, and potential applications of WAEF. It discusses the design and construction of breadboard prototype piezoelectric transducers for WAEF. It goes on to present results of computational simulations of performance and results of laboratory tests of the prototypes. In one notable test, a 100-W light bulb was lit by WAEF to demonstrate the feasibility of powering a realistic load.

This work was done by Stewart Sherrit, Benjamin Doty, Xiaoqi Bao, Yoseph Bar-Cohen, Mircea Badescu, and Zensheu Chang of Caltech for NASA's Jet Propulsion Laboratory. Further information is contained in a TSP (see page 1).

In accordance with Public Law 96-517, the contractor has elected to retain title to this invention. Inquiries concerning rights for its commercial use should be addressed to:

*Innovative Technology Assets Management
JPL*

Mail Stop 202-233

4800 Oak Grove Drive

Pasadena, CA 91109-8099

E-mail: iaoffice@jpl.nasa.gov

Refer to NPO-44928, volume and number of this NASA Tech Briefs issue, and the page number.

Lightweight Carbon-Carbon High-Temperature Space Radiator

A document summarizes the development of a carbon-carbon composite radiator for dissipating waste heat from a spacecraft nuclear reactor. The radiator is to be bonded to metal heat pipes and to operate in conjunction with them at a temperature approximately between 500 and 1,000 K. A goal of this development is to reduce the average areal mass density of a radiator to about 2 kg/m² from the current value of ≈10 kg/m² characteristic of spacecraft radiators made largely of metals.

Accomplishments thus far include: (1) bonding of metal tubes to carbon-carbon material by a carbonization process that includes heating to a temperature of 620 °C; (2) verification of the thermal and mechanical integrity of the bonds through pressure-cycling, axial-shear, and bending tests; and (3) construction and testing of two prototype heat-pipe/carbon-carbon-radiator units having different radiator areas, numbers of heat pipes, and areal mass densities. On the basis of the results achieved thus far, it is estimated that optimization of design could yield an areal mass density of 2.2 kg/m² — close to the goal of 2 kg/m².

This work was done by W. O. Miller and Wei Shih of Allcomp Corp. for Glenn Research Center.

Inquiries concerning rights for the commercial use of this invention should be addressed to NASA Glenn Research Center, Innovative Partnerships Office, Attn: Steve Fedor, Mail Stop 4-8, 21000 Brookpark

Road, Cleveland, Ohio 44135. Refer to LEW-18210-1.

Stochastic Analysis of Orbital Lifetimes of Spacecraft

A document discusses (1) a Monte-Carlo-based methodology for probabilistic prediction and analysis of orbital lifetimes of spacecraft and (2) Orbital Lifetime Monte Carlo (OLMC) — a Fortran computer program, consisting of a previously developed long-term orbit-propagator integrated with a Monte Carlo engine.

OLMC enables modeling of variances of key physical parameters that affect orbital lifetimes through the use of probability distributions. These parameters include altitude, speed, and flight-path angle at insertion into orbit; solar flux; and launch delays. The products of OLMC are predicted lifetimes (durations above specified minimum altitudes) for the number of user-specified cases. Histograms generated from such predictions can be used to determine the probabilities that spacecraft will satisfy lifetime requirements.

The document discusses uncertainties that affect modeling of orbital lifetimes. Issues of repeatability, smoothness of distributions, and code run time are considered for the purpose of establishing values of code-specific parameters and number of Monte Carlo runs. Results from test cases are interpreted as demonstrating that solar-flux predictions are primary sources of variations in predicted lifetimes. Therefore, it is concluded, multiple sets of predictions should be utilized to fully characterize the lifetime range of a spacecraft.

This work was done by Washito Sasamoto of Langley Research Center and Kandyce Goodliff and David Cornelius of Analytical Mechanics Associates, Inc. Further information is contained in a TSP (see page 1). LAR-17498-1



▶ **Displaying CFD Solution Parameters on Arbitrary Cut Planes**

Langley Research Center, Hampton, Virginia

USMC6 is a Fortran 90 computer program for post-processing in support of visualization of flows simulated by computational fluid dynamics (CFD). The name "USMC6" is partly an abbreviation of "TetrUSS — USM3D Solution Cutter," reflecting its origin as a post-processor for use with USM3D — a CFD program that is a component of the Tetrahedral Unstructured Software System and that solves the Navier-Stokes equations on tetrahedral un-

structured grids. "Cutter" here refers to a capability to acquire and process solution data on (1) arbitrary planes that cut through grid volumes, or (2) user-selected spheroidal, conical, cylindrical, and/or prismatic domains cut from within grids. Cutting saves time by enabling concentration of post-processing and visualization efforts on smaller solution domains of interest.

The user can select from among more than 40 flow functions. The cut planes

can be trimmed to circular or rectangular shape. The user specifies cuts and functions in a free-format input file using simple and easy-to-remember keywords. The USMC6 command line is simple enough that the slicing process can readily be embedded in a shell script for assembly-line post-processing. The output of USMC6 is a data file ready for plotting.

This program was written by S. Paul Pao of Langley Research Center. LAR-17527-1

▶ **Flow Solver for Incompressible 2-D Drive Cavity**

Goddard Space Flight Center, Greenbelt, Maryland

This software solves the Navier-Stokes equations for the incompressible driven cavity flow problem. The code uses second-order finite differencing on a staggered grid using the Chorin projection method. The resulting intermediate Poisson equation is

efficiently solved using the fast Fourier transform.

Time stepping is done using fourth-order Runge-Kutta for stability at high Reynolds numbers. Features include check-pointing, periodic field snapshots, ongoing reporting of kinetic energy and changes between time

steps, time histories at selected points, and optional streakline generation.

This program was written by Virginia Kalb of Goddard Space Flight Center. For further information, contact the Goddard Innovative Partnerships Office at (301) 286-5810. GSC-15107-1

▶ **Flow Solver for Incompressible Rectangular Domains**

Goddard Space Flight Center, Greenbelt, Maryland

This is an extension of the Flow Solver for Incompressible 2-D Drive Cavity software described in the preceding article. It solves the Navier-Stokes equations for incompressible flow using finite differencing on a uniform, staggered grid. There is a runtime choice of either central differencing or modified upwinding for the convective term. The domain must be rectangular, but may have a rectangular walled region within it. Currently, the position of the interior region and exterior

boundary conditions are changed by modifying parameters in the code and recompiling. These features make it possible to solve a variety of classical fluid flow problems such as an L-shaped cavity, channel flow, or wake flow past a square cylinder. The code uses fourth-order Runge-Kutta time-stepping and overall second-order spatial accuracy.

This software permits the walled region to be positioned such that flow past a square cylinder, an L-shaped cavity, and

the flow over a back-facing step can all be solved by reconfiguration. Also, this extension has an automatic detection of periodicity, as well as use of specialized data structure for ease of configuring domain decomposition and computing convergence in overlap regions.

This program was written by Virginia L. Kalb of Goddard Space Flight Center. For further information, contact the Goddard Innovative Partnerships Office at (301) 286-5810. GSC-15111-1

▶ **Simulating Avionics Upgrades to the Space Shuttles**

Lyndon B. Johnson Space Center, Houston, Texas

Cockpit Avionics Prototyping Environment (CAPE) is a computer program that simulates the functions of proposed

upgraded avionics for a space shuttle. In CAPE, pre-existing space-shuttle-simulation programs are merged with a

commercial-off-the-shelf (COTS) display-development program, yielding a package of software that enables high-fi-

delity simulation while making it possible to rapidly change avionic displays and the underlying model algorithms. The pre-existing simulation programs are Shuttle Engineering Simulation, Shuttle Engineering Simulation II, Interactive Control and Docking Simulation, and Shuttle Mission Simulator playback.

The COTS program — Virtual Application Prototyping System (VAPS) —

not only enables the development of displays but also makes it possible to move data about, capture and process events, and connect to a simulation. VAPS also enables the user to write code in the C or C++ programming language and compile that code into the end-product simulation software. As many as ten different avionic-upgrade ideas can be incorporated in a single compilation

and, thus, tested in a single simulation run. CAPE can be run in conjunction with any or all of four simulations, each representing a different phase of a space-shuttle flight.

This program was written by Daniel Deger and Kenneth Hill of Johnson Space Center and Karsten E. Braaten of United Space Alliance. Further information is contained in a TSP (see page 1). MSC-23453-1/15-1

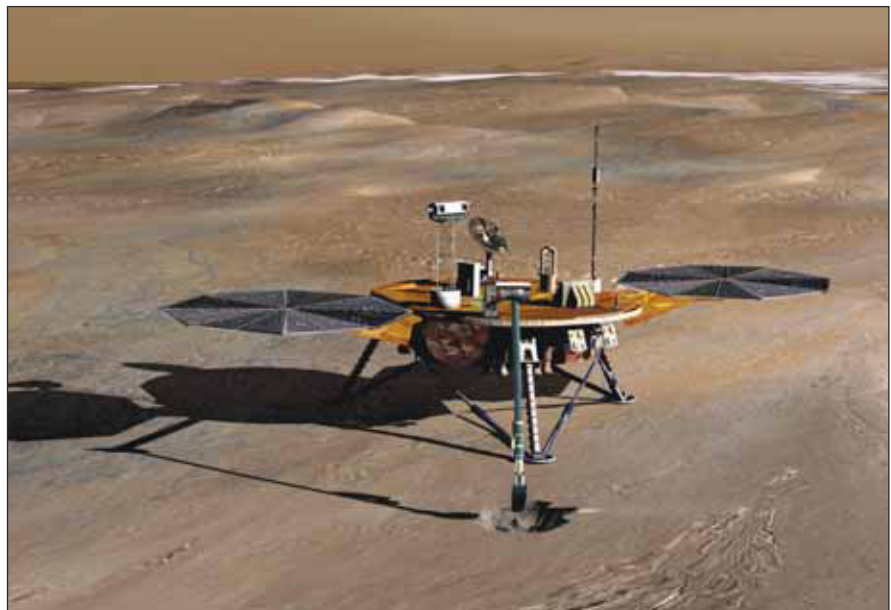
Simulating the Phoenix Landing Radar System

NASA's Jet Propulsion Laboratory, Pasadena, California

A computer program called “phxlr-sim” simulates the behavior of the radar system used as an altimeter and velocimeter during the entry, descent, and landing phases of the Phoenix lander spacecraft. The simulation includes modeling of internal functions of the radar system, the spacecraft trajectory, and the terrain. The computational models incorporate representations of nonideal hardware effects in the radar system and effects of radar speckle (coherent scatter of radar signals from terrain).

This program was written by Curtis W. Chen of Caltech for NASA's Jet Propulsion Laboratory. Further information is contained in a TSP (see page 1).

This software is available for commercial licensing. Please contact Karina Edmonds of the California Institute of Technology at (626) 395-2322. Refer to NPO-44431.



Phoenix Mission Lander on Mars, artist's concept.

Injecting Artificial Memory Errors Into a Running Computer Program

NASA's Jet Propulsion Laboratory, Pasadena, California

Single-event upsets (SEUs) or “bit-flips” are computer memory errors caused by radiation. BITFLIPS (Basic Instrumentation Tool for Fault Localized Injection of Probabilistic SEUs) is a computer program that deliberately injects SEUs into another computer program, while the latter is running, for the purpose of evaluating the fault tolerance of that program. BITFLIPS was written as a plug-in extension of the open-source Valgrind debugging and profiling software. BITFLIPS can inject SEUs into any program that can

be run on the Linux operating system, without needing to modify the program's source code. Further, if access to the original program source code is available, BITFLIPS offers fine-grained control over exactly when and which areas of memory (as specified via program variables) will be subjected to SEUs.

The rate of injection of SEUs is controlled by specifying either a fault probability or a fault rate based on memory size and radiation exposure time, in units of SEUs per byte per

second. BITFLIPS can also log each SEU that it injects and, if program source code is available, report the magnitude of effect of the SEU on a floating-point value or other program variable.

This program was written Benjamin J. Bornstein, Robert A. Granat, and Kiri L. Wagstaff of Caltech for NASA's Jet Propulsion Laboratory.

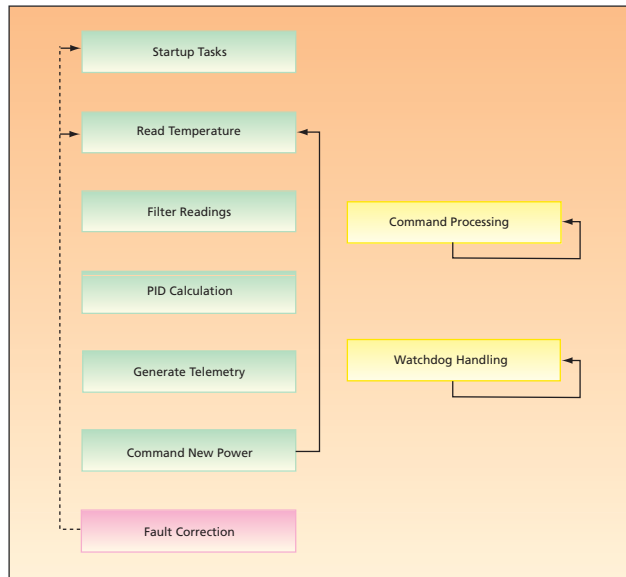
This software is available for commercial licensing. Please contact Karina Edmonds of the California Institute of Technology at (626) 395-2322. Refer to NPO-45368.

Fault-Tolerant, Multiple-Zone Temperature Control

NASA's Jet Propulsion Laboratory, Pasadena, California

A computer program has been written as an essential part of an electronic temperature control system for a spaceborne instrument that contains several zones. The system was developed because the temperature and the rate of change of temperature in each zone are required to be maintained to within limits that amount to degrees of precision thought to be unattainable by use of simple bimetallic thermostats.

The software collects temperature readings from six platinum resistance thermometers, calculates temperature errors from the readings, and implements a proportional + integral + de-



Logical Architecture of the active thermal control software.

rivative (PID) control algorithm that adjusts heater power levels. The software accepts, via a serial port, commands to change its operational parameters. The software attempts to detect and mitigate a host of potential faults. It is robust to many kinds of faults in that it can maintain PID control in the presence of those faults (see figure).

This program was written by James Granger, Brian Franklin, Martin Michalik, Phillip Yates, Erik Peterson, and James Borders of Caltech for NASA's Jet Propulsion Laboratory.

This software is available for commercial licensing. Please contact Karina Edmonds of the California Institute of Technology at (626) 395-2322. Refer to NPO-45230.

Implementing a Digital Phasemeter in an FPGA

NASA's Jet Propulsion Laboratory, Pasadena, California

Firmware for implementing a digital phasemeter within a field-programmable gate array (FPGA) has been devised. In the original application of this firmware, the phase that one seeks to measure is

the difference between the phases of two nominally-equal-frequency heterodyne signals generated by two interferometers. In that application, zero-crossing detectors convert the heterodyne signals to

trains of rectangular pulses (see figure), the two pulse trains are fed to a fringe counter (the major part of the phasemeter) controlled by a clock signal having a frequency greater than the heterodyne frequency, and the fringe counter computes a time-averaged estimate of the difference between the phases of the two pulse trains.

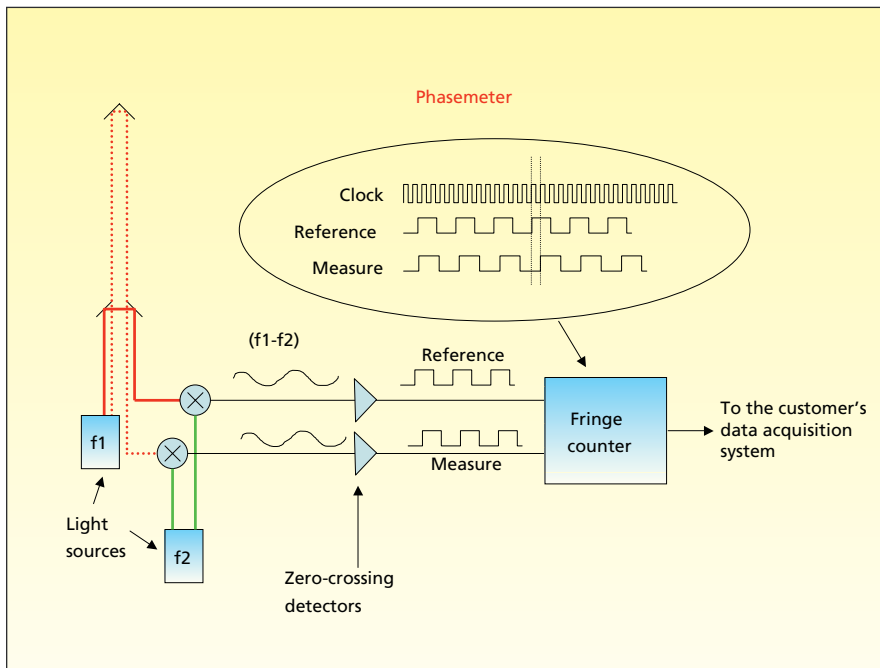
The firmware also does the following:

- Causes the FPGA to compute the frequencies of the input signals;
- Causes the FPGA to implement an Ethernet (or equivalent) transmitter for readout of phase and frequency values; and
- Provides data for use in diagnosis of communication failures.

The readout rate can be set, by programming, to a value between 250 Hz and 1 kHz. Network addresses can be programmed by the user.

This program was written by Shanti R. Rao of Caltech for NASA's Jet Propulsion Laboratory. Further information is contained in a TSP (see page 1).

The software used in this innovation is available for commercial licensing. Please contact Karina Edmonds of the California Institute of Technology at (626) 395-2322. Refer to NPO-45575.



The Firmware Code converts two inputs (reference and measure) into a time-averaged estimate of the phase difference between the two signals.

⚙️ Post-Flight Estimation of Motion of Space Structures: Part 1

NASA's Jet Propulsion Laboratory, Pasadena, California

A computer program estimates the relative positions and orientations of two space structures from data on the angular positions and distances of fiducial objects on one structure as measured by a target-tracking electronic camera and laser range finders on another structure. The program is written specifically for determining the relative alignments of two antennas, connected by a long truss, deployed in outer space from a space shuttle.

The program is based partly on transformations among the various coordi-

nate systems involved in the measurements and on a nonlinear mathematical model of vibrations of the truss. The program implements a Kalman filter that blends the measurement data with data from the model. Using time series of measurement data from the tracking camera and range finders, the program generates time series of data on the relative position and orientation of the antennas. A similar program described in a prior *NASA Tech Briefs* article was used onboard for monitoring the structures

during flight. The present program is more precise and designed for use on Earth in post-flight processing of the measurement data to enable correction, for antenna motions, of scientific data acquired by use of the antennas.

This program was written by Paul Brugarolas and William Breckenridge of Caltech for NASA's Jet Propulsion Laboratory.

This software is available for commercial licensing. Please contact Karina Edmonds of the California Institute of Technology at (626) 395-2322. Refer to NPO-45072.

⚙️ Post-Flight Estimation of Motion of Space Structures: Part 2

NASA's Jet Propulsion Laboratory, Pasadena, California

A computer program related to the one described in the immediately preceding article estimates the relative position of two space structures that are hinged to each other. The input to the program consists of time-series data on distances, measured by two range finders at different positions on one structure, to a corner-cube retroreflector on the other structure. Given a Cartesian (x, y, z) coordinate system and the known x coordinate of the retroreflector rela-

tive to the y, z plane that contains the range finders, the program estimates the y and z coordinates of the retroreflector.

The estimation process involves solving for the y, z coordinates of the intersection between (1) the y, z plane that contains the retroreflector and (2) spheres, centered on the range finders, having radii equal to the measured distances. In general, there are two such solutions and the program chooses the one consistent with the de-

sign of the structures. The program implements a Kalman filter. The output of the program is a time series of estimates of the relative position of the structures.

This program was written by Paul Brugarolas and William Breckenridge of Caltech for NASA's Jet Propulsion Laboratory.

This software is available for commercial licensing. Please contact Karina Edmonds of the California Institute of Technology at (626) 395-2322. Refer to NPO-45074.

⚙️ Simulating Operation of a Large Turbofan Engine

John H. Glenn Research Center, Cleveland, Ohio

The Commercial Modular Aero-Propulsion System Simulation (C-MAPSS) is a computer program for simulating transient operation of a commercial turbofan engine that can generate as much as 90,000 lb (≈ 0.4 MN) of thrust. It includes a power-management system that enables simulation of open- or closed-loop engine operation over a wide range of thrust levels throughout the full range of flight conditions.

C-MAPSS runs in the Simulink (The Mathworks, Inc.) block-diagram language, providing a graphical simulation environment in which advanced control and diagnostics algorithms can be implemented and tested. The software has a graphical user interface (GUI) that makes engine "health" data and control and engine parameters easily accessible. It can run user-specified transient simu-

lations and generate state-space linear models of a nonlinear engine model at an operating point.

C-MAPSS produces GUI screens that enable point-and-click operation and include editable fields for user-specified input. The software includes an atmospheric model for simulating operation at altitudes from sea level to 40,000 ft (≈ 12 km), Mach numbers from 0 to 0.90, and sea-level ambient temperatures from -60 to $+103$ °F (≈ -51 to $+39$ °C). CMAPSS has a comprehensive control system consisting of a gain-scheduled fan-speed controller and several limit regulators, integrated in a manner similar to that used in real engine controllers to avoid integrator windup. The simulation code itself operates several times faster than real time, giving it the potential to be deployed (all or in part) as machine code

for hardware-in-the-loop applications such as flight simulators and real-time controller/diagnostic system validation.

Overall, C-MAPSS provides the user with a set of tools for performing open- and closed-loop transient simulations and comparison of linear and non-linear models throughout its operating envelope, in an easy-to-use graphical environment.

This program was written by Jonathan S. Litt of Glenn Research Center; Dean K. Frederick of Saratoga Control Systems, Inc.; and Jonathan A. DeCastro of ASRC Aerospace Corp. Further information is contained in a TSP (see page 1).

Inquiries concerning rights for the commercial use of this invention should be addressed to NASA Glenn Research Center, Innovative Partnerships Office, Attn: Steve Fedor, Mail Stop 4-8, 21000 Brookpark Road, Cleveland, Ohio 44135. Refer to LEW-18315-1.

Automated Assistance for Designing Active Magnetic Bearings

Stennis Space Center, Mississippi

MagBear12 is a computer code (see figure) that assists in the design of radial, heteropolar active magnetic bearings (AMBs). MagBear12 was developed to help in designing the system described in "Advanced Active-Magnetic-Bearing Thrust-Measurement System" (SSC-00177-1), which appears in *NASA Tech Briefs*, Vol. 32, No. 9 (September 2008), p. 61.. (See the Mechanics/Machinery section in the accompanying issue of *NASA Tech Briefs*). Beyond this initial application, MagBear12 is expected to be useful for designing AMBs for a variety of rotating machinery. This program incorporates design rules and governing equations that are also implemented in other, proprietary design software used by AMB manufacturers. In addition, this program incorporates an advanced unpublished fringing-magnetic-field model that increases accuracy beyond that offered by the other AMB-design software.

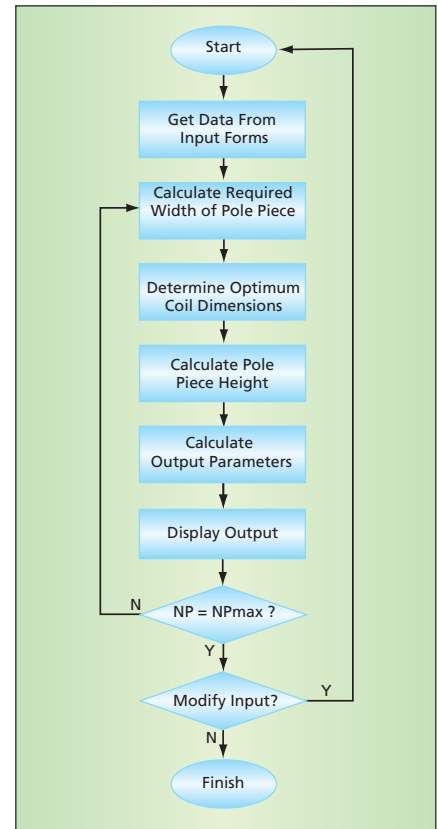
MagBear12 accepts input from the user in the form of parameters that specify the envelope, performance, and acceptable ranges of geometric features other than the envelope. The program then calculates optimized designs within those ranges. A series of designs are presented to the designer for review. The designer can accept one of the designs or can modify the input parameters to refine the designs. The program can also be used to analyze pre-existing AMB designs.

This work was done by Joseph Imlach of Innovative Concepts In Engineering LLC for Stennis Space Center.

Inquiries concerning rights for the commercial use of this invention should be addressed to:

*Innovative Concepts In Engineering LLC
2142 Tributary Circle
Anchorage, AK 99516
(907) 337-8954*

Refer to SSC-00176-1, volume and number of this NASA Tech Briefs issue, and the page number.



MagBear12 Flowchart

Computational Simulation of a Water-Cooled Heat Pump

Lyndon B. Johnson Space Center, Houston, Texas

A Fortran-language computer program for simulating the operation of a water-cooled vapor-compression heat pump in any orientation with respect to gravity has been developed by modifying a prior general-purpose heat-pump design code used at Oak Ridge National Laboratory (ORNL). Although it is specific to the design of a high-temperature-lift heat pump for the International Space Station, this program could serve as a basis for development of general-purpose computational software for de-

signing and analyzing liquid-cooled heat-pumps. The ORNL program contained models of refrigerant-fluid-to-air heat exchangers; the main modification consisted in replacing those models with models of plate-type heat exchangers utilizing water as both the cooling and the heating source liquid.

The present program incorporates a Fortran implementation of the American Society of Mechanical Engineers water-properties tables. Semi-empirical models of the heat transfer coefficients

for these heat exchangers were developed from vendor and laboratory test data, inasmuch as applicable published correlations were not available. The program produces estimates of evaporator and condenser capacities, coefficients of performance, and operating temperatures over a range of compressor speeds.

This work was done by Duane Bozarth of H and R Technical Associates for Johnson Space Center. Further information is contained in a TSP (see page 1). MSC-23375-1

Computational Model of Heat Transfer on the ISS

Lyndon B. Johnson Space Center, Houston, Texas

SCRAM Lite ("SCRAM" signifies "Station Compact Radiator Analysis Model") is a computer program for analyzing convective and radiative heat-transfer and heat-rejection performance of coolant loops and radiators, respectively, in the active thermal-control systems of

the International Space Station (ISS). SCRAM Lite is a derivative of prior versions of SCRAM but is more robust.

SCRAM Lite computes thermal operating characteristics of active heat-transport and heat-rejection subsystems for the major ISS configurations from Flight 5A

through completion of assembly. The program performs integrated analysis of both internal and external coolant loops of the various ISS modules and of an external active thermal control system, which includes radiators and the coolant loops that transfer heat to the radiators.

The SCRAM Lite run time is of the order of one minute per day of mission time. The overall objective of the SCRAM Lite simulation is to process input profiles of equipment-rack, crew-metabolic, and other heat loads to determine flow rates,

coolant supply temperatures, and available radiator heat-rejection capabilities. Analyses are performed for timelines of activities, orbital parameters, and attitudes for mission times ranging from a few hours to several months.

This program was written by John G. Torian and Michael L. Rischar of United Space Alliance for Johnson Space Center. Further information is contained in a TSP (see page 1). MSC-23622-1

Optimization of Angular-Momentum Biases of Reaction Wheels

NASA's Jet Propulsion Laboratory, Pasadena, California

RBOT [RWA Bias Optimization Tool (wherein "RWA" signifies "Reaction Wheel Assembly")] is a computer program designed for computing angular-momentum biases for reaction wheels used for providing spacecraft pointing in various directions as required for scientific observations. RBOT is currently deployed to support the Cassini mission to prevent operation of reaction wheels at unsafely high speeds while minimizing time in undesirable low-speed range, where elasto-hydrodynamic lubrication films in bearings become ineffective, lead-

ing to premature bearing failure. The problem is formulated as a constrained optimization problem in which maximum wheel speed limit is a hard constraint and a cost functional that increases as speed decreases below a low-speed threshold.

The optimization problem is solved using a parametric search routine known as the Nelder-Mead simplex algorithm. To increase computational efficiency for extended operation involving large quantity of data, the algorithm is designed to (1) use large time increments during intervals when spacecraft

attitudes or rates of rotation are nearly stationary, (2) use sinusoidal-approximation sampling to model repeated long periods of Earth-point rolling maneuvers to reduce computational loads, and (3) utilize an efficient equation to obtain wheel-rate profiles as functions of initial wheel biases based on conservation of angular momentum (in an inertial frame) using pre-computed terms.

This work was done by Clifford Lee and Allan Lee of Caltech for NASA's Jet Propulsion Laboratory. Further information is contained in a TSP (see page 1). NPO-42011

Short- and Long-Term Propagation of Spacecraft Orbits

NASA's Jet Propulsion Laboratory, Pasadena, California

The Planetary Observer Planning Software (POPS) comprises four computer programs for use in designing orbits of spacecraft about planets. These programs are the Planetary Observer High Precision Orbit Propagator (POHOP), the Planetary Observer Long-Term Orbit Predictor (POLOP), the Planetary Observer Post Processor (POPP), and the Planetary Observer Plotting (POPLOT) program.

POHOP and POLOP integrate the equations of motion to propagate an initial set of classical orbit elements to a future epoch. POHOP models short-term (one revolution) orbital motion;

POLOP averages out the short-term behavior but requires far less processing time than do older programs that perform long-term orbit propagations.

POPP postprocesses the spacecraft ephemeris created by POHOP or POLOP (or optionally can use a less-accurate internal ephemeris) to search for trajectory-related geometric events including, for example, rising or setting of a spacecraft as observed from a ground site. For each such event, POPP puts out such user-specified data as the time, elevation, and azimuth.

POPLOT is a graphics program that plots data generated by POPP. POPLOT can plot orbit ground tracks on a world map and can produce a variety of summaries and generic ordinate-vs.-abscissa plots of any POPP data.

This program was written by John C. Smith, Jr., Theodore Sweetser, Min-Kun Chung, Chen-Wan L. Yen, Ralph B. Roncoli, and Johnny H. Kwok of Caltech, and Mark A. Vincent of Raytheon for NASA's Jet Propulsion Laboratory.

This software is available for commercial licensing. Please contact Karina Edmonds of the California Institute of Technology at (626) 395-2322. Refer to NPO-45418.

Monte Carlo Simulation To Estimate Likelihood of Direct Lightning Strikes

John F. Kennedy Space Center, Florida

A software tool has been designed to quantify the lightning exposure at launch sites of the stack at the pads under different configurations. In order to predict lightning strikes to generic

structures, this model uses leaders whose origins (in the x - y plane) are obtained from a 2D random, normal distribution. The striking distance is a function of the stroke peak current, which is obtained

from a random state machine that extracts the stroke peak current from a log-normal distribution. The height in which the leaders are originated is fixed and chosen to be several "strike dis-

tances” greater than the tallest object under study.

The Monte Carlo simulation tool uses several random state machines to generate x - y origin of leaders and peak stroke currents. The structures under study are entered in text files whose names are used as descriptors for report purposes. So, “External_tank.txt” could be the text file that contains all the vertices of the external tank. The lines of the text files contain three points (x , y , and z) that define “points” of lines or “vertices” of

polygons. A line composed of three zeros (0 0 0) is used to indicate the end of a line or polygon.

Imaginary spheres (whose diameters are the striking distances) are drawn as the leader descends vertically to ground, and the first object intersected is considered to be struck. Therefore, the last step of the leader can be in any direction. The leaders can move in the z direction only, or in a random xyz direction (software selectable). The leader steps can be either fixed or variable. The

length of the study is also software selectable, so the user can perform a study of “ n ” number of years. A summary report generated by the software indicates the frequency at which objects under study will be struck by lightning.

This work was done by Carlos Mata and Pedro Medelius of ASRC Aerospace Corporation for Kennedy Space Center. For more information, contact Pedro Medelius at Pedro.J.Medelius@nasa.gov, (321) 867-6335, Mail Code: ASRC-19, Kennedy Space Center, FL 32899. KSC-12882

Adaptive MGS Phase Retrieval

NASA's Jet Propulsion Laboratory, Pasadena, California

Adaptive MGS Phase Retrieval software uses the Modified Gerchberg-Saxton (MGS) algorithm, an image-based sensing method that can turn any focal plane science instrument into a wavefront sensor, avoiding the need to use external metrology equipment. Knowledge of the wavefront enables intelligent control of active optical systems.

The software calculates the optical path difference (wavefront) errors in the exit pupil of an optical system using only intensity images of a point of light. The light input may be a star, laser, or any point source measured at symmetric positions about focus and at the pupil. As such, the software is a key enabling technology for space telescopes. With only a basic understanding of the optical system parameters (e.g. imaging wavelength, f /number, measurement positions, etc.), the software evolves an internal model of the optical system to best match the data ensemble. Once optimized, the software proceeds to accurately estimate the wavefront of light as it travels through the optical system.

The MGS software is highly adaptable to a large range of optical systems

and includes many innovative features. This version does not require an extensive and complete understanding of the system under test. Instead, using Automatic Model Adaptation, only the most basic system characteristics must be known. The algorithm adapts these parameters to best fit the data ensemble. These steps are crucial in achieving extremely high accuracy in the wavefront solution at the system exit-pupil. In addition, a convergence-monitoring feature allows the algorithm to stop when the wavefront solution has been reached to within a specified error tolerance level.

The software also facilitates the application of prior system knowledge to better deal with high-dynamic range wavefront errors. This is especially important where the error magnitude is much greater than the imaging wavelength (a significant problem in wavefront sensing). The software can use wavefront models based on previous runs or optical measurements, or predictions from external models, to initiate a prior phase estimate, through its Prior Phase Builder Graphical User In-

terface. The prior phase is treated by the software as a Numerical Nulling Reference, which is evolved in an outer-outer loop during computation, until it contains the full solution. The innermost iteration then has the simpler job of estimating the low-dynamic range residual difference of the true wavefront error from the Nulling Reference model. This allows the inner loop to operate around null, where it is most accurate and robust.

In addition to the wavefront solution, the software can provide an improved set of system parameters. For example, the result can report the true position of best focus and true f /number in the optical system.

This program was written by Scott A. Basinger, Siddarayappa Bikkannavar, David Cohen, Joseph J. Green, John Lou, Catherine Ohara, David Redding, and Fang Shi of Caltech for NASA's Jet Propulsion Laboratory. Further information is contained in a TSP (see page 1).

This software is available for commercial licensing. Please contact Karina Edmonds of the California Institute of Technology at (626) 395-2322. Refer to NPO-43857.

Simulating the Gradually Deteriorating Performance of an RTG

NASA's Jet Propulsion Laboratory, Pasadena, California

Degra (now in version 3) is a computer program that simulates the performance of a radioisotope thermoelectric generator (RTG) over its lifetime. Degra is provided with a graphical user interface that is used to edit input parameters that describe the initial state of the RTG and the time-

varying loads and environment to which it will be exposed. Performance is computed by modeling the flows of heat from the radioactive source and through the thermocouples, also allowing for losses, to determine the temperature drop across the thermocouples. This temperature drop is used to deter-

mine the open-circuit voltage, electrical resistance, and thermal conductance of the thermocouples. Output power can then be computed by relating the open-circuit voltage and the electrical resistance of the thermocouples to a specified time-varying load voltage.

Degra accounts for the gradual deterioration of performance attributable primarily to decay of the radioactive source and secondarily to gradual deterioration of the thermoelectric material. To provide guidance to an RTG designer, given a minimum of input,

Degra computes the dimensions, masses, and thermal conductances of important internal structures as well as the overall external dimensions and total mass.

This program was written by Eric G. Wood, Richard C. Ewell, Jagdish Patel, David R.

Hanks, Juan A. Lozano, G. Jeffrey Snyder, and Larry Noon of Caltech for NASA's Jet Propulsion Laboratory.

This software is available for commercial licensing. Please contact Karina Edmonds of the California Institute of Technology at (626) 395-2322. Refer to NPO-45252.

Calculations for Calibration of a Mass Spectrometer

NASA's Jet Propulsion Laboratory, Pasadena, California

A computer program performs calculations to calibrate a quadrupole mass spectrometer in an instrumentation system for identifying trace amounts of organic chemicals in air. In the operation of the mass spectrometer, the mass-to-charge ratio (m/z) of ions being counted at a given instant of time is a function of the instantaneous value of a repeating ramp voltage waveform applied to electrodes. The count rate as a function of time can be converted to an m/z spectrum (equivalent to a mass spectrum for singly

charged ions), provided that a calibration of m/z is available.

The present computer program can perform the calibration in either or both of two ways: (1) Following a data-based approach, it can utilize the count-rate peaks and the times thereof measured when fed with air containing known organic compounds. (2) It can utilize a theoretical proportionality between the instantaneous m/z and the instantaneous value of an oscillating applied voltage. The program can also

estimate the error of the calibration performed by the data-based approach. If calibrations are performed in both ways, then the results can be compared to obtain further estimates of errors.

This program was written by Seungwon Lee of Caltech for NASA's Jet Propulsion Laboratory. Further information is contained in a TSP (see page 1).

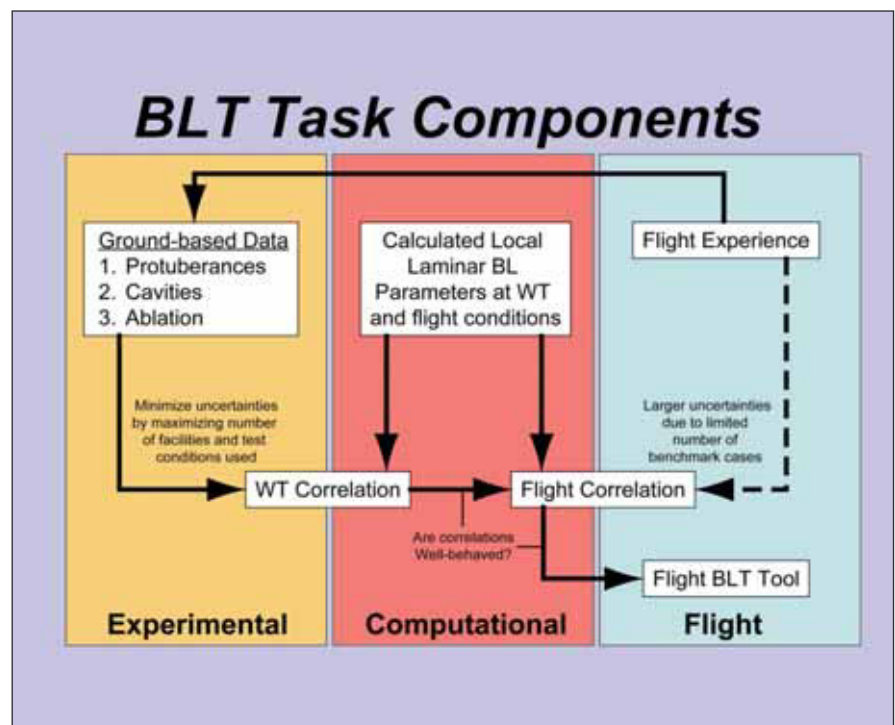
This software is available for commercial licensing. Please contact Karina Edmonds of the California Institute of Technology at (626) 395-2322. Refer to NPO-45181.

Predicting Boundary-Layer Transition on Space-Shuttle Re-Entry

Langley Research Center, Hampton, Virginia

The BLT Prediction Tool ("BLT" signifies "Boundary Layer Transition") is provided as part of the Damage Assessment Team analysis package, which is utilized for analyzing local aerothermodynamics environments of damaged or repaired space-shuttle thermal protection tiles. Such analyses are helpful in deciding whether to repair launch-induced damage before re-entering the terrestrial atmosphere. Given inputs that include re-entry trajectory and attitude parameters, air density, air temperature, and details of each damage or repair site, the BLT Prediction Tool calculates expected times of laminar-to-turbulent transition onset of the boundary-layer flow during re-entry. (These times help to define the proper aerothermodynamic environment to use in subsequent thermal and stress analyses of local structural components.)

The BLT Prediction Tool includes a database of computed boundary-layer parameters that cover a range of nominal re-entry trajectories and uses an interpolation program for estimating local boundary-layer properties during flight



Critical Elements for development of new BLT tool for on-orbit assessments.



Space Shuttle Model in wind tunnel tests.

along a specific trajectory. Boundary-layer-transition criteria used in the BLT Prediction Tool were developed from ground-based measurements to account for effects of both protuberances and cavities, and have been calibrated against flight data. Version 1 of this BLT prediction tool was developed in time for the first Return-to-Flight mission STS-114.

This work was done by Scott Berry, Tom Horvath, Ron Merski, Derek Liechty, Frank Greene, Karen Bibb, and Greg Buck of Langley Research Center; Harris Hamilton and Jim Weilmuenster, Contractors with Langley Research Center; Chuck Campbell, Stan Bouslog, Ben Kirk, Garry Bourland, Amy Casady, and Brian Anderson of Johnson Space Center; Dan Reda and James Reuther of Ames Research Center; Gerry Kinder, Dennis Chao, Jay Hyatt, Maria Barnwell, and K. C. Wang of The Boeing Co.; and Steve Schneider of Purdue University. For more information, contact the Langley Innovative Partnerships office at (757) 864-4015. LAR-17337-1

2D/3D Synthetic Vision Navigation Display

Langley Research Center, Hampton, Virginia

Flight-deck display software was designed and developed at NASA Langley Research Center to provide two-dimensional (2D) and three-dimensional (3D) terrain, obstacle, and flight-path perspectives on a single navigation display. The objective was to optimize the presentation of synthetic vision (SV) system technology that permits pilots to view multiple perspectives of flight-deck display symbology and 3D terrain information. Research was conducted to evaluate the efficacy of the concept. The concept has numerous unique implementation features that would permit enhanced operational concepts and efficiencies in both current and future aircraft.

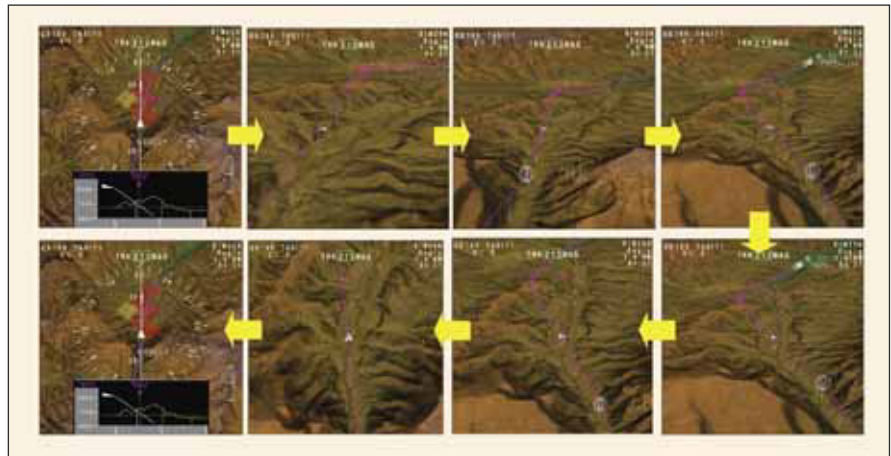
One innovative feature, shown in the figure, was the ability of the flight crew to select among several modes that present a dynamic 3D perspective of aircraft within the flight environment. The study focus was to uncover the developments and benefits of using the 2D and 3D exocentric SV information with regard to primary flight displays (PFDs) and navigational displays (NDs) for reducing accidents and damage for commercial aircraft. The investigated technologies aim toward elimi-

nating low visibility conditions as a causal factor in civil aircraft accidents, while replicating the operational benefits of clear-day flight operations, regardless of actual outside visibility conditions. The concepts also form the basis of revolutionary electronic flight bag applications that utilize these technological enhancements.

The results showed that SV on the PFD was pivotal for pilot use in terrain avoidance and situation awareness,

while SV terrain on the 2D co-planar navigational display was not found to provide much benefit. However, pilots noted that the 3D exocentric display of synthetic terrain, with key implementation features, added significantly to flight-crew situation awareness and substantially enhanced the pilot's ability to detect and avoid controlled-flight-into-terrain situations.

Conclusions reached indicate that SV depicted on PFD is essential for terrain



Dynamic 3D Exocentric Navigation Display: Examples show several available display modes selected by pilots that dynamically present an immersed moving 3D perspective of the aircraft in relation to terrain, flight path, and aviation hazards (represented here as static images).

awareness. The situational awareness ratings for the SV PFD were largely due to the egocentric view that gave pilots an immersed sense of terrain around them. Pilot awareness and the capability for avoiding hazardous conditions were significantly enhanced with the addition of

3D exocentric navigation display modes that allowed for a greater field-of-regard to confirm the presence of hazards along their planned routing. The combination of SV primary flight and navigation display concepts allowed pilots to make the best and quickest decisions re-

garding safety of their aircraft.

This work was done by Lawrence J. Prinzel III, Lynda J. Kramer, J.J. Arthur III, and Randall E. Bailey of Langley Research Center and Jason L. Sweeters of NCI Information Systems, Inc. Further information is contained in a TSP (see page 1). LAR-17354

Automated Camera Array Fine Calibration

NASA's Jet Propulsion Laboratory, Pasadena, California

Using aerial imagery, the JPL FineCalibration (JPL FineCal) software automatically tunes a set of existing CAHVOR camera models for an array of cameras. The software finds matching features in the overlap region between images from adjacent cameras, and uses these features to refine the camera models. It is not necessary to take special imagery of a known target and no surveying is required.

JPL FineCal was developed for use with an aerial, persistent surveillance platform. Synchronized images from an array of cameras are captured and stitched together into a single, very high-resolution image that is projected onto an elevation map of the ground. A GUI

(graphical user interface) tool allows the user to play a movie of any part of the imaged surface from any perspective.

JPL FineCal requires, as input, a set of CAHVOR camera models for the camera array. These models are typically developed on the ground using a calibration procedure requiring a known target at a short distance. JPL FineCal corrects the inaccuracy of the camera model extrinsic parameters resulting from the short target distance by using imagery, taken during flight, at an effective distance of infinity. It also makes small improvements to the intrinsic parameters.

JPL FineCal is an automated process that does not require the use of any

special targets, and which may be applied during normal flight operations. Thus, it makes it simple to retune the camera models to correct for small misalignments that occur due to changes in aperture settings, vibration, or thermal changes.

This work was done by Daniel Clouse, Curtis Padgett, Adnan Ansar, and Yang Cheng of Caltech for NASA's Jet Propulsion Laboratory. Further information is contained in a TSP (see page 1).

The software used in this innovation is available for commercial licensing. Please contact Karina Edmonds of the California Institute of Technology at (626) 395-2322. Refer to NPO-45715.

Multichannel Networked Phasemeter Readout and Analysis

NASA's Jet Propulsion Laboratory, Pasadena, California

Netmeter software reads a data stream from up to 250 networked phasemeters, synchronizes the data, saves the reduced data to disk (after applying a low-pass filter), and provides a Web server interface for remote control. Unlike older phasemeter software that requires a special, real-time operating system, this program can run on any general-purpose computer. It needs about five percent of the CPU (central processing unit) to process 20 channels because it adds built-in data logging and network-based

GUIs (graphical user interfaces) that are implemented in Scalable Vector Graphics (SVG).

Netmeter runs on Linux and Windows. It displays the instantaneous displacements measured by several phasemeters at a user-selectable rate, up to 1 kHz. The program monitors the measure and reference channel frequencies. For ease of use, levels of status in Netmeter are color coded: green for normal operation, yellow for network errors, and red for optical misalignment problems. Netmeter in-

cludes user-selectable filters up to 4 k samples, and user-selectable averaging windows (after filtering). Before filtering, the program saves raw data to disk using a burst-write technique.

This work was done by Shanti Rao of Caltech for NASA's Jet Propulsion Laboratory. Further information is contained in a TSP (see page 1).

This software is available for commercial licensing. Please contact Karina Edmonds of the California Institute of Technology at (626) 395-2322. Refer to NPO-45505.

MISR Instrument Data Visualization

NASA's Jet Propulsion Laboratory, Pasadena, California

The MISR Interactive eXplorer (MINX) software functions both as a general-purpose tool to visualize Multi-angle Imaging SpectroRadiometer (MISR) instrument data, and as a spe-

cialized tool to analyze properties of smoke, dust, and volcanic plumes. It includes high-level options to create map views of MISR orbit locations; scrollable, single-camera RGB (red-green-

blue) images of MISR level 1B2 (L1B2) radiance data; and animations of the nine MISR camera images that provide a 3D perspective of the scenes that MISR has acquired.

The plume height capability provides an accurate estimate of the injection height of plumes that is needed by air quality and climate modelers. MISR provides global high-quality stereo height information, and this program uses that information to perform detailed height retrievals of aerosol plumes. Users can interactively digitize smoke, dust, or volcanic plumes and automatically retrieve heights and winds, and can also archive MISR albedos and aerosol properties, as well as fire power and brightness temperatures associated with smoke plumes derived from Moderate Resolution Imaging Spectroradiometer (MODIS) data.

Some of the specialized options in MINX enable the user to do other tasks. Users can display plots of top-of-atmosphere bidirectional reflectance factors (BRFs) versus camera-angle for selected pixels. Images and animations can be saved to disk in various formats. Also, users can apply a geometric registration correction to warp camera images when the standard processing correction is inadequate. It is possible to difference the images of two MISR orbits that share a path (identical ground track), as well as to construct pseudo-color images by assigning different combinations of MISR channels

(angle or spectral band) to the RGB display channels.

This software is an interactive application written in IDL and compiled into an IDL Virtual Machine (VM) ".sav" file.

This work was done by David Nelson of Columbus Technologies and Services Inc.; Michael Garay of Raytheon; David Diner, Charles Thompson, Jeffrey Hall, Brian Rheingans, and Dominic Mazzoni of Caltech for NASA's Jet Propulsion Laboratory. Further information is contained in a TSP (see page 1).

This software is available for commercial licensing. Please contact Karina Edmonds of the California Institute of Technology at (626) 395-2322. Refer to NPO-45744.

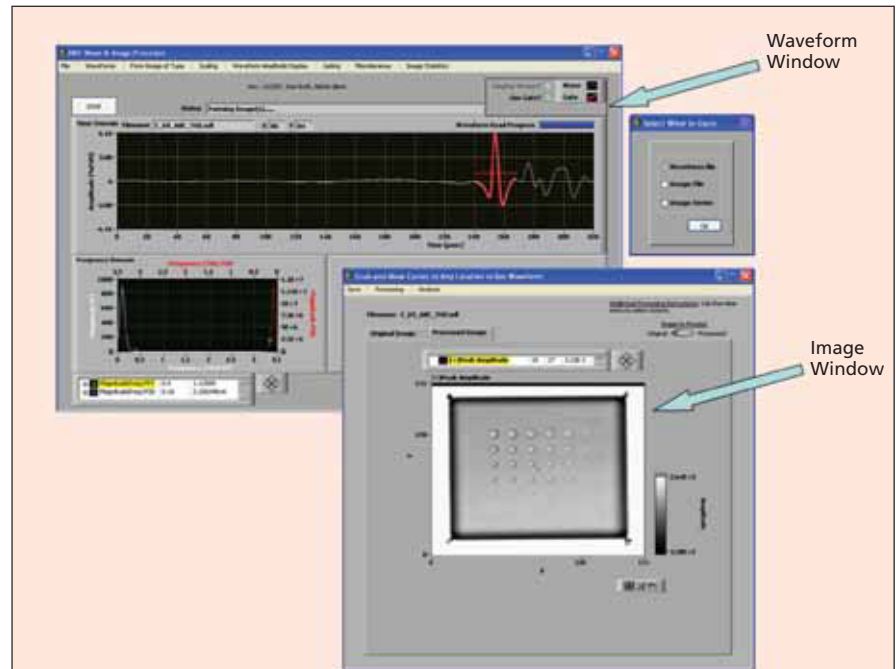
Platform for Postprocessing Waveform-Based NDE

John H. Glenn Research Center, Cleveland, Ohio

Taking advantage of the similarities that exist among all waveform-based non-destructive evaluation (NDE) methods, a common software platform has been developed containing multiple-signal and image-processing techniques for waveforms and images. The NASA NDE Signal and Image Processing software has been developed using the latest versions of LabVIEW, and its associated Advanced Signal Processing and Vision Toolkits. The software is useable on a PC with Windows XP and Windows Vista.

The software has been designed with a commercial grade interface in which two main windows, Waveform Window and Image Window, are displayed if the user chooses a "waveform file" to display. Within these two main windows (see figure), most actions are chosen through logically conceived run-time menus. The Waveform Window has plots for both the raw time-domain waves and their frequency-domain transformations (fast Fourier transform and power spectral density). The Image Window shows the C-scan image formed from information of the time-domain waveform (such as peak amplitude) or its frequency-domain transformation at each scan location. The user also has the ability to open an image, or series of images, or a simple set of X-Y paired data set in text format. Each of the Waveform and Image Windows contains menus from which to perform many user actions.

An option exists to use raw waves obtained directly from scan, or waves after deconvolution if system wave response is provided. Two types of deconvolution,



Graphical-User-Interface Windows are shown for NASA NDE wave and image processor.

time-based subtraction or inverse-filter, can be performed to arrive at a deconvolved wave set. Additionally, the menu on the Waveform Window allows preprocessing of waveforms prior to image formation, scaling and display of waveforms, formation of different types of images (including non-standard types such as velocity), gating of portions of waves prior to image formation, and several other miscellaneous and specialized operations.

The menu available on the Image Window allows many further image processing and analysis operations, some of which are found in commercially-avail-

able image-processing software programs (such as Adobe Photoshop), and some that are not (removing outliers, B-scan information, region-of-interest analysis, line profiles, and precision feature measurements).

This work was done by Don Roth for Glenn Research Center. Further information is contained in a TSP (see page 1). Inquiries concerning rights for the commercial use of this invention should be addressed to NASA Glenn Research Center, Innovative Partnerships Office, Attn: Steve Fedor, Mail Stop 4-8, 21000 Brookpark Road, Cleveland, Ohio 44135. Refer to LEW-18261-1.

Automatic Rock Detection and Mapping from HiRISE Imagery

NASA's Jet Propulsion Laboratory, Pasadena, California

This system includes a C-code software program and a set of MATLAB software tools for statistical analysis and rock distribution mapping. The major functions include rock detection and rock detection validation. The rock detection code has been evolved into a production tool that can be used by engineers and geologists with minor training.

The software takes as an input an image of a scene containing rocks and produces as output a description of the rock population and associated statistics. Each rock is described in terms of location, dimensions, and confidence of detection. The input parameters are the image resolution (ground sampling dis-

tance, or the size of a pixel in centimeters), the Sun incidence and azimuth angles for analysis of the shadows cast by rocks to derive individual rock models, and a parameter that can be adjusted to accommodate variations in image contrast.

The software is able to process very large reconnaissance imagery using a standard desktop computer by automatically processing image blocks and collecting all output in a single rock population description file (RPDF). Processing time is in the order of minutes for nominal HiRISE images covering 6x12 km areas at 30 cm/pixel.

The test option allows small portions of the large images to be selected and

processed. Alternatively, a specific image window can be processed by indicating its coordinates and size. In this mode, visual results (detections overlaid on the images) are provided in addition to the rock population file (RPDF). This option is useful to quickly allow verification of parameter settings, and the quality of the detection results.

This work was done by Andres Huertas, Douglas S. Adams, and Yang Cheng of Caltech for NASA's Jet Propulsion Laboratory.

This software is available for commercial licensing. Please contact Karina Edmonds of the California Institute of Technology at (626) 395-2322. Refer to NPO-45752.

Parallel Computing for the Computed-Tomography Imaging Spectrometer

NASA's Jet Propulsion Laboratory, Pasadena, California

This software computes the tomographic reconstruction of spatial-spectral data from raw detector images of the Computed-Tomography Imaging Spectrometer (CTIS), which enables transient-level, multi-spectral imaging by capturing spatial and spectral information in a single snapshot. The CTIS can be used for surveying planetary landscapes through spectral imaging. It can also be used for battlefield surveillance

and the spectral imaging of live tissues for disease detection.

A Message Passing Interface Library (MPI) is used to parallelize the original serial version of the code without modifying its initial structure. By parallelizing the code, a speedup of up to 20 is reached by using 32 processors. The software does not use any third-party libraries that require licenses. It is written in Fortran and MPI, and the storage of

matrix elements is efficient, thus reducing memory requirements.

This work was done by Seungwon Lee of Caltech for NASA's Jet Propulsion Laboratory. Further information is contained in a TSP (see page 1).

This software is available for commercial licensing. Please contact Karina Edmonds of the California Institute of Technology at (626) 395-2322. Refer to NPO-45831.

Rock Segmentation Through Edge Regrouping

NASA's Jet Propulsion Laboratory, Pasadena, California

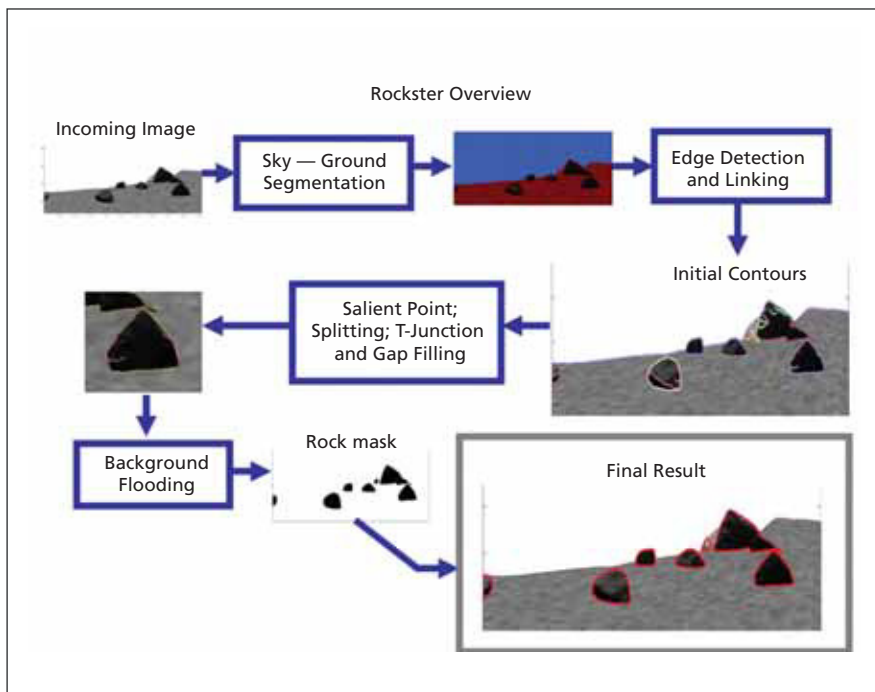
Rockster is an algorithm that automatically identifies the locations and boundaries of rocks imaged by the rover hazard cameras (hazcams), navigation cameras (navcams), or panoramic cameras (pancams). The software uses edge detection and edge regrouping to identify closed contours that separate the rocks from the background (see figure). The algorithm has applications both in ground-based data analysis, for example, to examine large quantities of images returned by the Mars Exploration Rovers, and in onboard (on-rover) opportunistic science applica-

tions such as construction of rock maps during traverse, identification of unusual or otherwise high-value science targets that warrant additional investigation, and detection of certain types of geologic contact zones.

The software uses gray-level intensity gradients to identify raw contours; these raw contours are then split into shorter, low-curvature fragments. New fragments are created where necessary to bridge areas of poor gradient information or poor image quality. The algorithm uses a flooding step to regroup the various

fragments into closed contours. The algorithm is very fast with the C implementation able to process (768x1024) images containing hundreds to thousands of rocks in approximately one second on a desktop workstation.

The algorithm is particularly efficient at quickly detecting small- to medium-sized rocks with sufficient contrast (positive or negative) relative to the background. Full quantitative performance comparisons are not yet available; however, preliminary tests show that Rockster appears to detect a significantly larger fraction of rocks



An Overview of the Rockster rock segmentation algorithm.

present in a scene (higher recall) than previous rock detection schemes, while maintaining a high precision rate (objects identified as rocks, truly are rocks).

Rockster has been integrated successfully into a number of recent, high-level demonstrations, including the SOOPS (Science Operations on Planetary Surfaces) demo, which used a rock exploration scenario to let scientists gain hands-on experience with an autonomous science capability in a simulated environment, and live exercises of the OASIS (Onboard Autonomous Science Investigation System)/CLARAty (Coupled Layer Architecture for Robotic Autonomy) software which were carried out in real-time in the JPL Mars Yard onboard the FIDO Rover (a close relative of the twin Mars Exploration Rovers).

This program was written by Michael Burl of Caltech for NASA's Jet Propulsion Laboratory.

This software is available for commercial licensing. Please contact Karina Edmonds of the California Institute of Technology at (626) 395-2322. Refer to NPO-44417.

System for Continuous Delivery of MODIS Imagery to Internet Mapping Applications

NASA's Jet Propulsion Laboratory, Pasadena, California

This software represents a complete, unsupervised processing chain that generates a continuously updating global image of the Earth from the most recent available MODIS Level 1B scenes.

The software constantly updates a global image of the Earth at 250 m per pixel. It uses an event-driven scheduler to manage asynchronous image generation tasks on a cluster of computers. The output composite image is tightly integrated in the JPL OnEarth WMS server, which offers direct access to the global image to any Web Mapping Service (WMS) compatible client, and also supports KML generation for Google Earth. The resulting Earth image composite is permanently available as an Internet service to WMS compatible mapping applications. This application can handle the throughput of the MODIS satellite, processing more than 80GB of Level 1B input data each day.

There are two main components to this software package: DailyHarvest and DailyPlanet. The first component is a scene harvester that manages a

local copy of available MODIS scenes for the past few days. When active, the DailyHarvest module checks the current state of the MODIS source repository (LAADS) against the local state. Any new scene is downloaded, and the local copy state is altered to reflect the availability of the new scene. The second component, DailyPlanet, is then made aware of the change in the archive state. Once the remote and local scenes are synchronized, the DailyHarvest module reschedules itself, effectively running every few minutes.

The DailyPlanet module functions as an event-driven scheduler that manages the scene transitions from raw scenes to the global composite. There are three separate scene queues: a raw scene queue, a confirmed scene queue, and an image fragment queue. Each scene makes the transition to the next queue based on the result of an external process. The transition from raw-to-confirmed is done by extracting the scene metadata and applying a suitability test, confirming that the scene is not

a night scene, and that the latitude range is within the S72-N72. The transition from the confirmed scene queue to the image fragment queue is the result of the successful completion of an external task that produces a visual image in geographical coordinates from a MODIS Level 1B scene. This processing is done using the HDFLook MODIS software package, running on a remote computer.

The final task is the integration of the image fragments into the global composite, handled by a custom written external task. If an error is detected during any of the transitions, the error is logged and the scene is dropped from the processing queues. Most of the remote processing resources can be configured and are used in parallel for greater efficiency.

This work was done by Lucian Plesea of Caltech for NASA's Jet Propulsion Laboratory.

This software is available for commercial licensing. Please contact Karina Edmonds of the California Institute of Technology at (626) 395-2322. Refer to NPO-45778.

Processing LiDAR Data To Predict Natural Hazards

Stennis Space Center, Mississippi

ELF-Base and ELF-Hazards (wherein “ELF” signifies “Extract LiDAR Features” and “LiDAR” signifies “light detection and ranging”) are developmental software modules for processing remote-sensing LiDAR data to identify past natural hazards (principally, landslides) and predict future ones. ELF-Base processes raw LiDAR data, including LiDAR intensity data that are often ignored in other software, to create digital terrain models (DTMs) and digital feature models (DFMs) with sub-meter accuracy.

ELF-Hazards fuses raw LiDAR data, data from multispectral and hyperspectral optical images, and DTMs and DFMs generated by ELF-Base to generate hazard risk maps. Advanced algo-

rithms in these software modules include line-enhancement and edge-detection algorithms, surface-characterization algorithms, and algorithms that implement innovative data-fusion techniques. The line-extraction and edge-detection algorithms enable users to locate such features as faults and landslide headwall scarps.

Also implemented in this software are improved methodologies for identification and mapping of past landslide events by use of (1) accurate, ELF-derived surface characterizations and (2) three LiDAR/optical-data-fusion techniques: post-classification data fusion, maximum-likelihood estimation modeling, and hierarchical within-class discrimination. This software is expected to

enable faster, more accurate forecasting of natural hazards than has previously been possible.

This program was written by Ian Fairweather and Robert Crabtree of HyPerspectives Inc. and Stacey Hager of Yellowstone Ecological Research Center for Stennis Space Center.

Inquiries concerning rights for its commercial use should be addressed to:

Robert Crabtree

HyPerspectives Inc.

2048 Analysis Drive Suite C

Bozeman, MT 59718

E-mail: crabtree@hyperspectives.net

Phone No.: (406) 556-9880

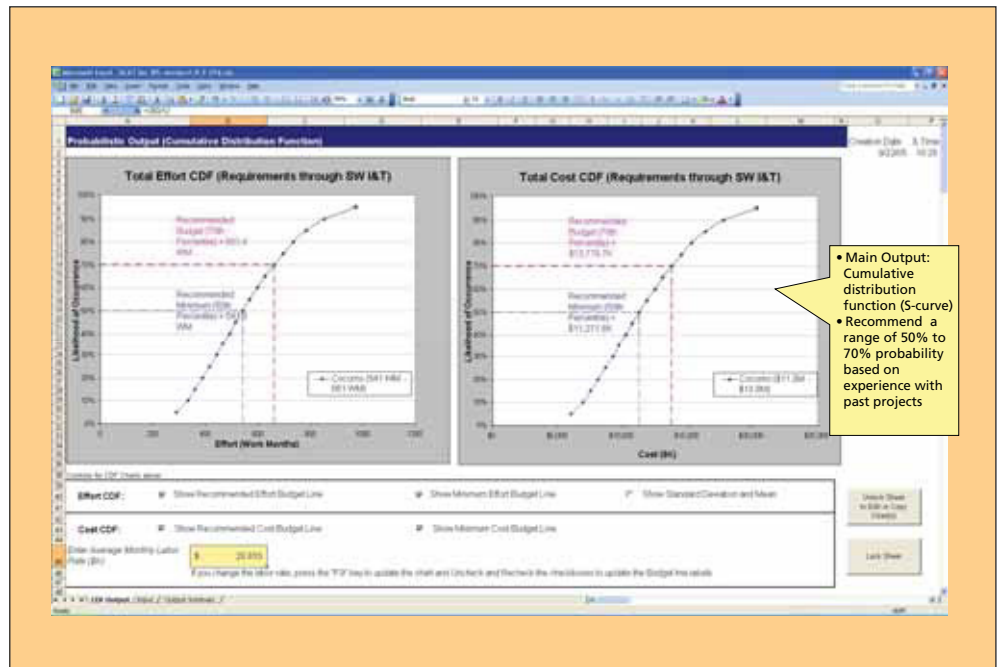
Refer to SSC-00279, volume and number of this NASA Tech Briefs issue, and the page number.

Estimating Software-Development Costs With Greater Accuracy

NASA's Jet Propulsion Laboratory, Pasadena, California

COCOMOST is a computer program for use in estimating software development costs. The goal in the development of COCOMOST was to increase estimation accuracy in three ways: (1) develop a set of sensitivity software tools that return not only estimates of costs but also the estimation error; (2) using the sensitivity software tools, precisely define the quantities of data needed to adequately tune cost estimation models; and (3) build a repository of software-cost-estimation information that NASA managers can retrieve to improve the estimates of costs of developing software for their project (see figure).

COCOMOST implements a methodology, called “2cee,” in which a unique combination of well-known pre-existing data-mining and software-development-effort-estimation techniques are used to increase the accuracy of estimates. COCOMOST utilizes multiple models to analyze historical data pertaining to software-development projects and performs an exhaustive data-mining search over the space of model parameters to improve the perform-



Example Model Output

ances of effort-estimation models. Thus, it is possible to both calibrate and generate estimates at the same time. COCOMOST is written in the C language for execution in the UNIX operating system.

This program was written by Tim Menzies and Dan Baker of West Virginia University

and Jairus Hihn and Karen Lum of Caltech for NASA's Jet Propulsion Laboratory. Further information is contained in a TSP (see page 1).

This software is available for commercial licensing. Please contact Karina Edmonds of the California Institute of Technology at (626) 395-2322. Refer to NPO-44858.

DSN Array Simulator

NASA's Jet Propulsion Laboratory, Pasadena, California

The DSN Array Simulator (wherein "DSN" signifies NASA's Deep Space Network) is an updated version of software previously denoted the DSN Receive Array Technology Assessment Simulation. This software (see figure) is used for computational modeling of a proposed DSN facility comprising user-defined arrays of antennas and trans-

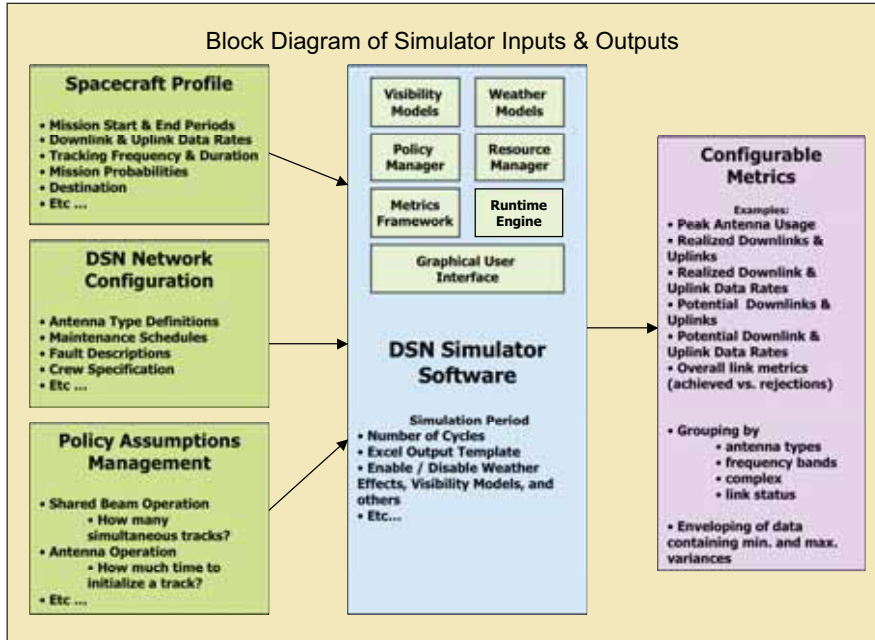
mitting and receiving equipment for microwave communication with spacecraft on interplanetary missions. The simulation includes variations in spacecraft tracked and communication demand changes for up to several decades of future operation. Such modeling is performed to estimate facility performance, evaluate requirements that gov-

ern facility design, and evaluate proposed improvements in hardware and/or software.

The updated version of this software affords enhanced capability for characterizing facility performance against user-defined mission sets. The software includes a Monte Carlo simulation component that enables rapid generation of key mission-set metrics (e.g., numbers of links, data rates, and data volumes), and statistical distributions thereof as functions of time. The updated version also offers expanded capability for mixed-asset network modeling — for example, for running scenarios that involve user-definable mixtures of antennas having different diameters (in contradistinction to a fixed number of antennas having the same fixed diameter). The improved version also affords greater simulation fidelity, sufficient for validation by comparison with actual DSN operations and analytically predictable performance metrics.

This program was written by Raffi Tikidjian and Ryan Mackey of Caltech for NASA's Jet Propulsion Laboratory. Further information is contained in a TSP (see page 1).

This software is available for commercial licensing. Please contact Karina Edmonds of the California Institute of Technology at (626) 395-2322. Refer to NPO-44506.

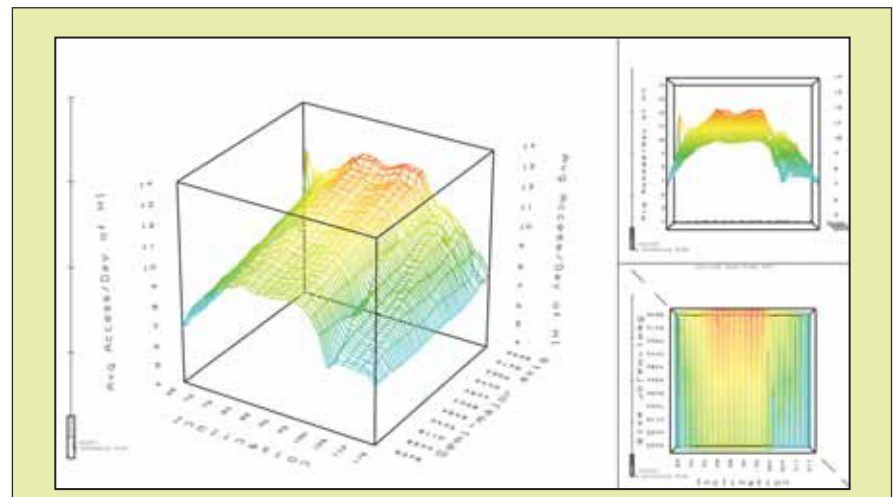


DSN Array Simulator Overview

Parametric-Studies and Data-Plotting Modules for the SOAP

NASA's Jet Propulsion Laboratory, Pasadena, California

"Parametric Studies" and "Data Table Plot View" are the names of software modules in the Satellite Orbit Analysis Program (SOAP). Parametric Studies enables parameterization of as many as three satellite or ground-station attributes across a range of values and computes the average, minimum, and maximum of a specified metric, the revisit time, or 21 other functions at each point in the parameter space. This computation produces a one-, two-, or three-dimensional table of data representing statistical results across the parameter space. Inasmuch as the output of a parametric study in three dimensions can be a very large data set, visualization is a paramount means of discovering trends in the data (see figure).



Sample Output

Data Table Plot View enables visualization of the data table created by Parametric Studies or by another data source: this module quickly generates a display of the data in the form of a rotatable three-dimensional-appearing plot, making it unnecessary to load the SOAP output data into a separate plotting pro-

gram. The rotatable three-dimensional-appearing plot makes it easy to determine which points in the parameter space are most desirable. Both modules provide intuitive user interfaces for ease of use.

This work was done by Robert Carnright, Adam Loverro, and Robert Oberto of Caltech

and David Stodden and John Coggi of The Aerospace Corporation for NASA's Jet Propulsion Laboratory. Further information is contained in a TSP (see page 1).

This software is available for commercial licensing. Please contact Karina Edmonds of the California Institute of Technology at (626) 395-2322. Refer to NPO-45059.

Testing of Error-Correcting Sparse Permutation Channel Codes

NASA's Jet Propulsion Laboratory, Pasadena, California

A computer program performs Monte Carlo direct numerical simulations for testing sparse permutation channel codes, which offer strong error-correction capabilities at high code rates and are considered especially suitable for storage of digital data in holographic and volume memories. A word in a code of this type is characterized by, among other things, a sparseness parameter (M) and a fixed number (K) of 1 or "on" bits in a

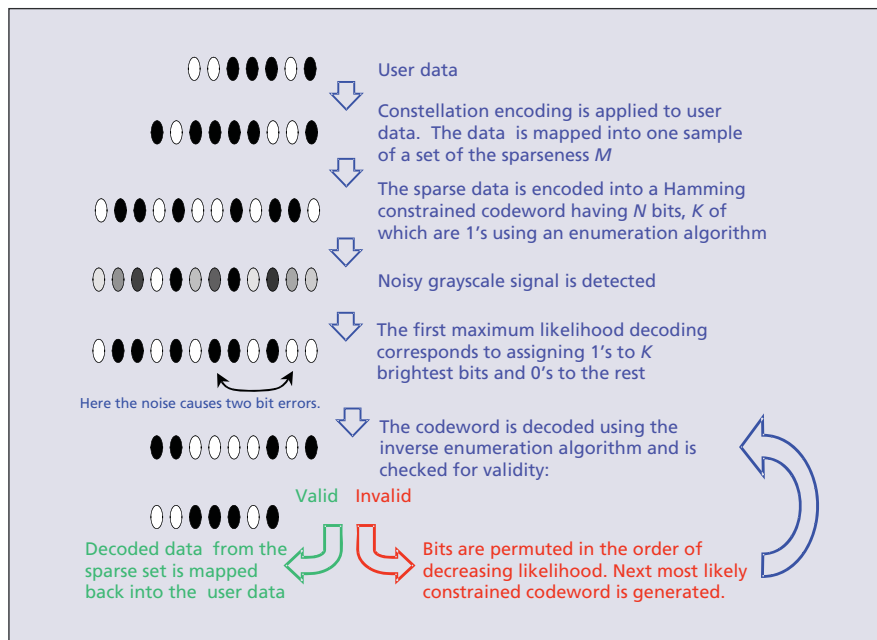
channel block length of N (see figure).

In a test, random user data words are generated and mapped into code words. Transmission of the words through a noisy channel is simulated by adding simulated white Gaussian noise whose amplitude is determined by the signal-to-noise ratio. Detection of each word is performed via strict Maximum Likelihood detection algorithm starting with the initially detected codeword, which is

produced by sorting the resulting bit values and assigning a value of 1 to the highest K of them and 0 to the rest. A newly developed permutation sorting algorithm is further applied to determine the maximum weight valid code word. The maximum likelihood valid sparse codeword is decoded, by means of an inverse of an enumerative scheme used in generating code words, to obtain the original use data. From the results of this simulation, block error rates (BERs) and other statistics that characterize the performance of the code are calculated. Sparse permutation channel codes satisfy the balanced channel coding constraint and, as determined from the direct numerical simulation, also simultaneously provide high error correction with use of BER as low as 10^{-10} and less even for fairly large raw bit error rates. Channel codes of sufficiently large block size ($N > 100$) asymptotically approach the information theoretic limits for communications channel capacity.

This program was written by Kirill V. Shcheglov and Sergei S. Orlov of Stanford and was tested numerically by Hongtao Liu and Snezhana I. Abarzhi of Illinois Institute of Technology for NASA's Jet Propulsion Laboratory.

This software is available for commercial licensing. Please contact Karina Edmonds of the California Institute of Technology at (626) 395-2322. Refer to NPO-45196.



An Outline of the Code used for numerical simulation of the error-correction performance.

Visual Target Tracking on the Mars Exploration Rovers

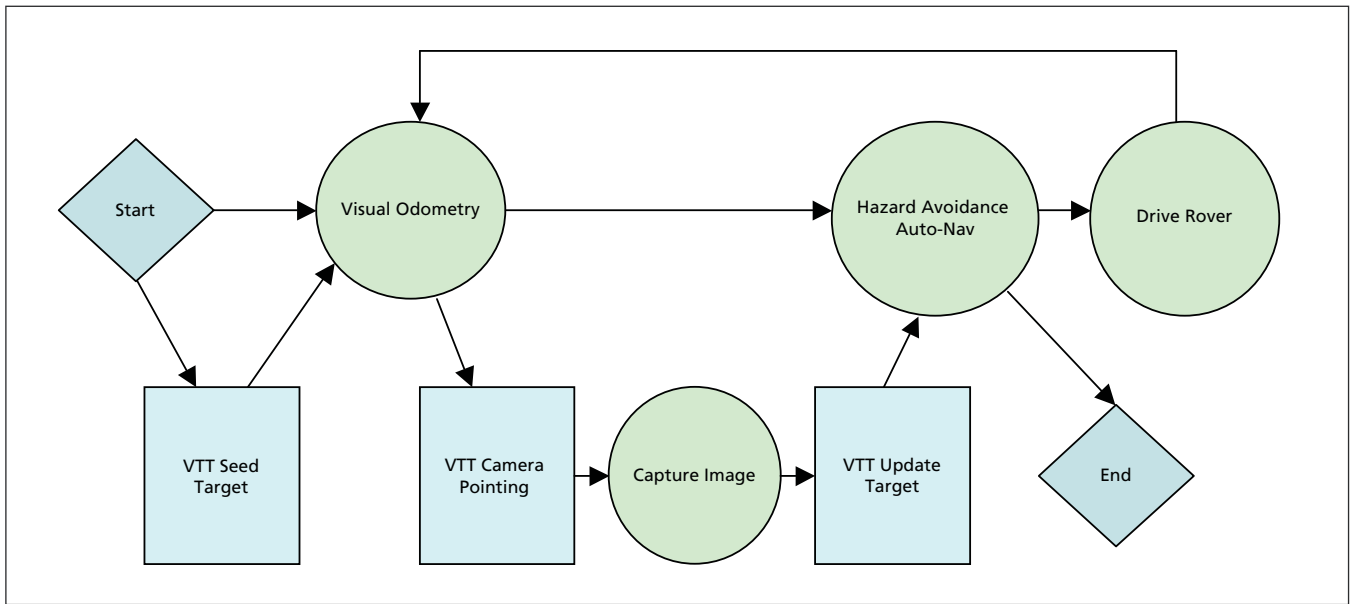
NASA's Jet Propulsion Laboratory, Pasadena, California

Visual target tracking (VTT) software has been incorporated into Release 9.2 of the Mars Exploration Rover (MER) flight software, now running aboard the rovers Spirit and Opportunity. In the VTT operation (see figure), the rover is driven in short steps between stops and,

at each stop, still images are acquired by actively aimed navigation cameras (navcams) on a mast on the rover (see artistic rendition). The VTT software processes the digitized navcam images so as to track a target reliably and to make it possible to approach the target

accurately to within a few centimeters over a 10-m traverse.

The operations on the digitized images include a normalized cross-correlation algorithm along with template-image-magnification and template-image-roll-compensation algorithms.



Functional Flow of VTT integrated into MER flight software. VTT module functions (square boxes) are additions to the existing MER flight software (circles).



Artistic Rendition of MER.

Each VTT update takes about 50 seconds. VTT has helped to make it possible to approach a target over a 10-m traverse and place an instrument on the target during a single sol, whereas previously, such approach and placement took 3 sols. Alternatively, VTT can be used to simply image a target as the rover passes it. VTT can be used in conjunction with any combination of blind driving, autonomous navigation with hazard avoidance, and/or visual odometry.

This program was written by Won Kim, Jeffrey Biesiadecki, and Khaled Ali of Caltech for NASA's Jet Propulsion Laboratory.

This software is available for commercial licensing. Please contact Karina Edmonds of the California Institute of Technology at (626) 395-2322. Refer to NPO-45019.

SPICE Module for the Satellite Orbit Analysis Program (SOAP)

NASA's Jet Propulsion Laboratory, Pasadena, California

A SPICE module for the Satellite Orbit Analysis Program (SOAP) precisely represents complex motion and maneuvers in an interactive, 3D animated environment with support for user-defined quantitative outputs. ("SPICE" stands for Spacecraft, Planet, Instrument, Camera-matrix, and Events). This module enables the SOAP software to exploit NASA mission ephemeris represented in the JPL Ancillary Information Facility (NAIF) SPICE formats. Ephemeris

types supported include position, velocity, and orientation for spacecraft and planetary bodies including the Sun, planets, natural satellites, comets, and asteroids. Entire missions can now be imported into SOAP for 3D visualization, playback, and analysis.

The SOAP analysis and display features can now leverage detailed mission files to offer the analyst both a numerically correct and aesthetically pleasing combination of results that can be var-

ied to study many hypothetical scenarios. The software provides a modeling and simulation environment that can encompass a broad variety of problems using orbital prediction. For example, ground coverage analysis, communications analysis, power and thermal analysis, and 3D visualization that provide the user with insight into complex geometric relations are included.

The SOAP SPICE module allows distributed science and engineering teams to share common mission models of

known pedigree, which greatly reduces duplication of effort and the potential for error. The use of the software spans all phases of the space system lifecycle, from the study of future concepts to operations and anomaly analysis. It allows SOAP software to correctly position and orient all of the principal bodies of the

Solar System within a single simulation session along with multiple spacecraft trajectories and the orientation of mission payloads. In addition to the 3D visualization, the user can define numeric variables and x - y plots to quantitatively assess metrics of interest.

This work was done by Robert Carnright

and Claude Hildebrand of Caltech and David Stodden and John Coggi of The Aerospace Corporation for NASA's Jet Propulsion Laboratory.

This software is available for commercial licensing. Please contact Karina Edmonds of the California Institute of Technology at (626) 395-2322. Refer to NPO-45057.

Facilitating Analysis of Multiple Partial Data Streams

NASA's Jet Propulsion Laboratory, Pasadena, California

Robotic Operations Automation: Mechanisms, Imaging, Navigation report Generation (ROAMING) is a set of computer programs that facilitates and accelerates both tactical and strategic analysis of time-sampled data — especially the disparate and often incomplete streams of Mars Explorer Rover (MER) telemetry data described in the immediately preceding article. As used here, “tactical” refers to the activities over a relatively short time (one Martian day in the original MER application) and “strategic” refers to a longer time (the entire multi-year MER missions in the original application).

Prior to installation, ROAMING must be configured with the types of data of interest, and parsers must be modified to understand the format of the input data (many example parsers are provided, including for general CSV files). Thereafter, new data from multiple disparate sources are automatically resampled into a single common annotated spreadsheet stored in a readable space-separated format, and these data can be processed or plotted at any time scale. Such processing or plotting makes it possible to study not only the details of a particular activity spanning only a few seconds,

[e.g., vehicle tilt as in Figure 1(a), motor current, numbers of images] that, heretofore could be found only in thousands of separate files.

ROAMING also supports automatic annotation of both images and graphs. In the MER application, labels given to terrain features by rover scientists and engineers are automatically plotted in all received images based on their associated camera models (see Figure 2), times measured in seconds are mapped to Mars local time, and command names or arbitrary time-labeled events can be used to label engineering plots, as in Figure 1(b).

This work was done by Mark W. Maimone and Robert R. Liebersbach of Caltech for NASA's Jet Propulsion Laboratory.

This software is available for commercial licensing. Please contact Karina Edmonds of the California Institute of Technology at (626) 395-2322. Refer to NPO-45367.

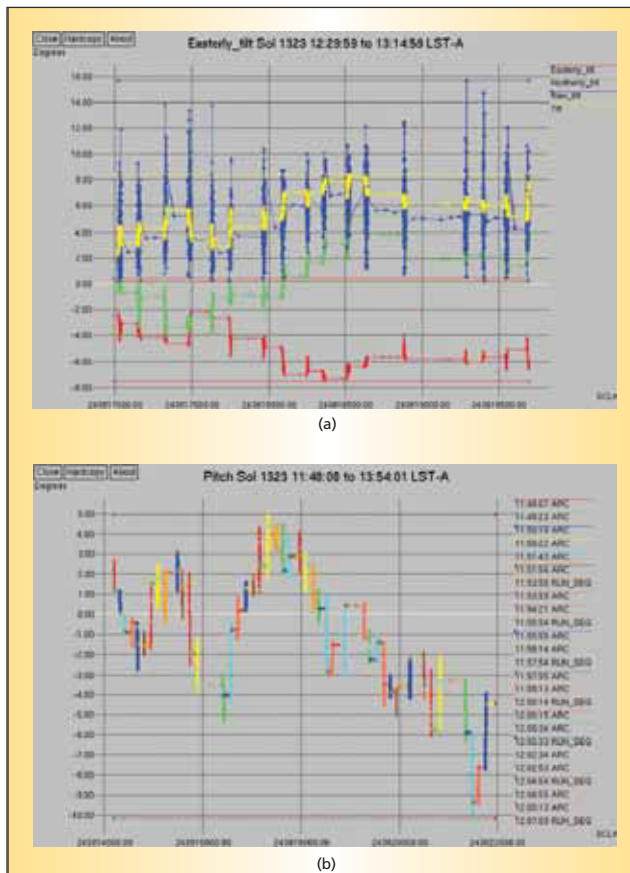


Figure 1. Plots may include (a) multiple fields or (b) event-based color coding, and support interactive zooming.

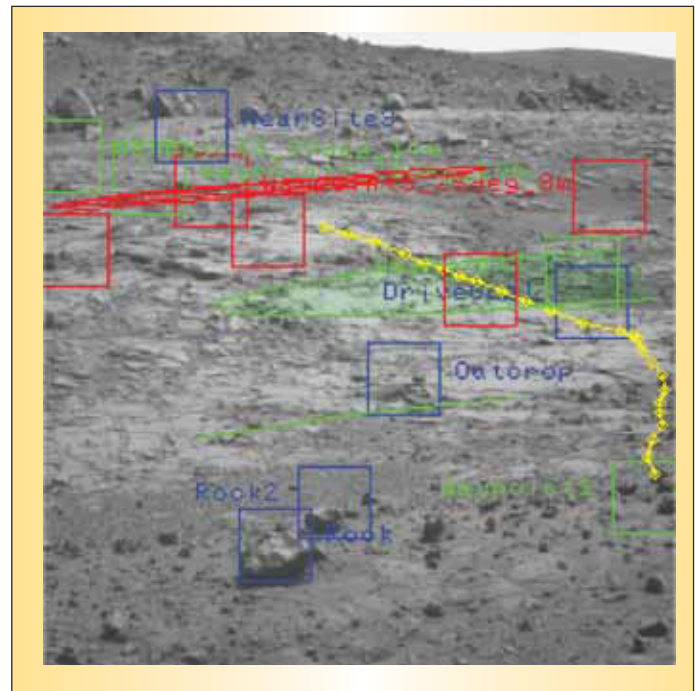


Figure 2. Images are automatically annotated with detailed drive information.

Σ Mars Reconnaissance Orbiter Wrapper Script

NASA's Jet Propulsion Laboratory, Pasadena, California

The MRO OLVM wrapper script software allows Mars Reconnaissance Orbiter (MRO) sequence and spacecraft engineers to rapidly simulate a spacecraft command product through a tool that simulates the onboard sequence management software (OLVM). This script parses sequence files to determine the appropriate time boundaries for the sequence, and constructs the script file to be executed by OLVM to span the entirety of the designated sequence. It then constructs script files to be executed by OLVM, constructs the appropriate file directories, populates these directories with needed input files, initi-

ates OLVM to simulate the actual command product that will be sent to the spacecraft, and captures the results of the simulation run to an external file for later review. Additionally, the tool allows a user to manually construct the script, if desired, and then execute the script with a simple command line.

This work was done by Roy Gladden, Forest Fisher, and Teerapat Khanapornpan of Caltech for NASA's Jet Propulsion Laboratory.

This software is available for commercial licensing. Please contact Karina Edmonds of the California Institute of Technology at (626) 395-2322. Refer to NPO-45242.



Mars Reconnaissance Orbiter on the launch pad.

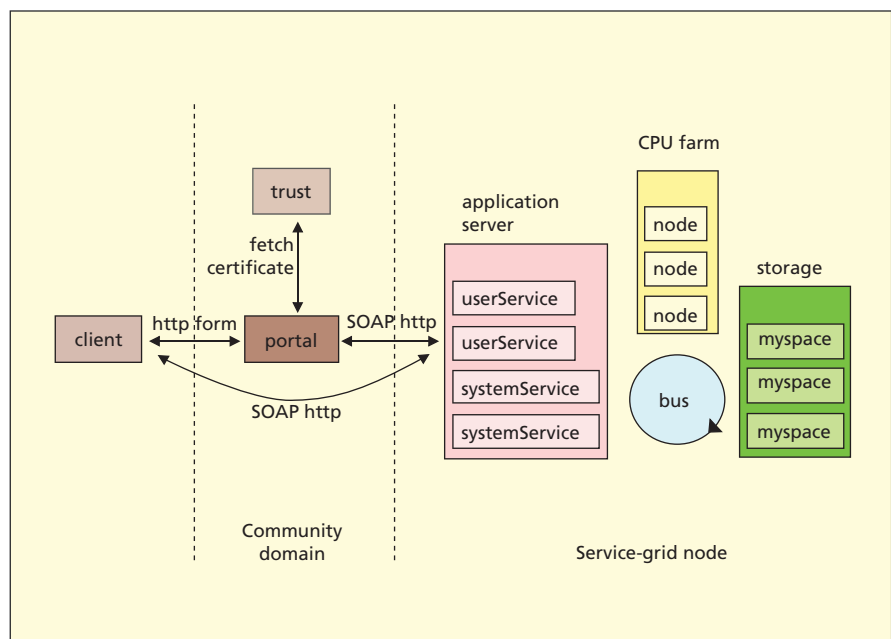
Σ Service-Oriented Architecture for NVO and TeraGrid Computing

NASA's Jet Propulsion Laboratory, Pasadena, California

The National Virtual Observatory (NVO) Extensible Secure Scalable Service Infrastructure (NESSSI) is a Web service architecture and software framework (see figure) that enables Web-based astronomical data publishing and processing on grid computers such as the National Science Foundation's TeraGrid. Characteristics of this architecture include the following:

- Services are created, managed, and upgraded by their developers, who are trusted users of computing platforms on which the services are deployed.
- Service jobs can be initiated by means of Java or Python client programs run on a command line or with Web portals.
- Access is granted within a graduated security scheme in which the size of a job that can be initiated depends on the level of authentication of the user.

A "small" service request may be submitted anonymously. A "medium" request may be submitted with a "weak" certificate issued by the NVO or another certificate authority not associated with an official grid computing organization like TeraGrid or the Department of Energy (DOE). A "large" request must be accompanied by a "strong" certificate is-



In this **Model**, the application server is Web-service container that accepts HTTP connections that may be SOAP messages and may have a certificate attached.

sued by the TeraGrid or DOE certificate authority. User certificates are managed by the Clarens Grid-Enabled Web Services Framework (<http://clarens.sourceforge.net/>).

This work was done by Joseph Jacob, Craig Miller, Roy Williams, Conrad Steenberg, and

Matthew Graham of Caltech for NASA's Jet Propulsion Laboratory. Further information is contained in a TSP (see page 1).

This software is available for commercial licensing. Please contact Karina Edmonds of the California Institute of Technology at (626) 395-2322. Refer to NPO-45067.

Enhanced Reporting of Mars Exploration Rover Telemetry

NASA's Jet Propulsion Laboratory, Pasadena, California

Mars Exploration Rover Enhanced Telemetry Extraction and Reporting System (METERS) is software that generates a human-readable representation of the state of the mobility and arm-related systems of the Mars Exploration Rover (MER) vehicles on each Martian solar day (sol). Data are received from the MER spacecraft in multiple streams having various formats including text messages, sparsely-sampled engineering quantities, images, and individual motor-command histories. Typically, only parts of this data generated on Mars are received the same day they were created, so the summary report tools have to work

well even when data is missing. All information is grouped by type into easily-browsable Web pages (see Figure 1).

METERS is the first software to provide an integrated view of the mobility and arm operations even when data are missing. METERS combines the data received in the various telemetry streams during an entire sol, making clear what has occurred and annotating what data are missing. METERS comprises a set of software tools (primarily in C, C++) and Perl language scripts for robustly combining these data into a concise, human-readable format. Raw data products are converted into Hypertext Markup Lan-

guage files, compatible with Web-browser software, that include thumbnail images (see Figure 2), summaries of motions, and plots of engineering data. Automatically generated reports also summarize the classes of mobility and arm activities that occur during each sol.

This work was done by Mark W. Maimone, Jeffrey J. Biesiadecki, Robert R. Liebersbach, Joseph L. Carsten, and Chris Leger of Caltech for NASA's Jet Propulsion Laboratory.

This software is available for commercial licensing. Please contact Karina Edmonds of the California Institute of Technology at (626) 395-2322. Refer to NPO-45366.

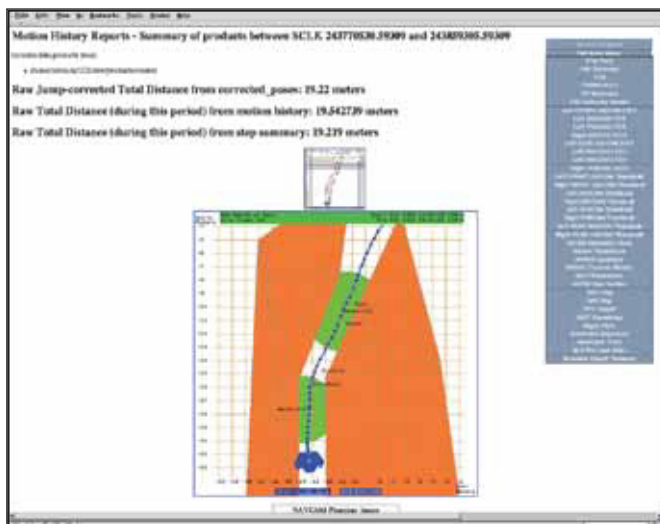


Figure 1. This top view of a METERS Auto-Generated Main Web Page includes a motion summary in plain text, graphical course plot, and a pull-down menu to select individual reports.

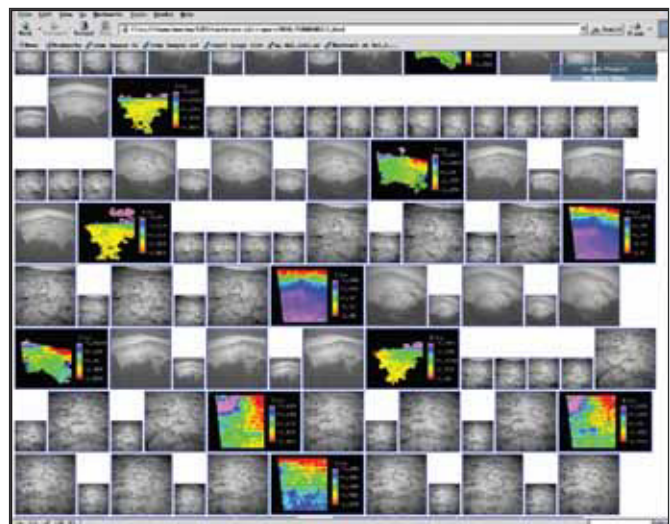
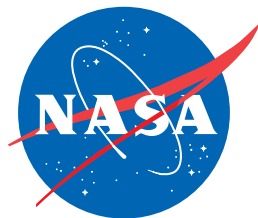


Figure 2. Another page includes Thumbnail Views of All Images, including thumbnail-sized elevation data automatically extracted from stereo pairs of images.



National Aeronautics and
Space Administration